Analysis of the QUENCH-12 bundle experiment with the ATHLET-CD2.2A code

Yoto G. Georgiev, Juri Stuckert

KIT Scientific Publishing

Yoto G. Georgiev, Juri Stuckert

**Analysis of the QUENCH-12 bundle experiment
with the ATHLET-CD2.2A code**

Karlsruhe Institute of Technology

KIT SCIENTIFIC REPORTS 7622

Analysis of the QUENCH-12 bundle experiment with the ATHLET-CD2.2A code

by
Yoto G. Georgiev*
Juri Stuckert

* Delegated Researcher from Energy Institute JSC, Sofia, Bulgaria

KIT Scientific Publishing

Report-Nr. KIT-SR 7622

Karlsruhe Institute of Technology

Report-Nr. **KIT-SR 7622**

Analysis of the QUENCH-12 bundle experiment with ATHLET-CD v.2.2A code

Yoto G. Georgiev*, Juri Stuckert

*Delegated Researcher from Energy Institute JSC, Sofia, Bulgaria

Karlsruhe

2012

Abstract

Simulation of the QUENCH-12 experiment (reflood of a VVER test bundle) was performed by means of the computer code ATHLET-CD. The calculated results were compared with the ones measured during the experiment. Sensitivity analysis was performed for such parameters as gas flow rates, electrical parameters, breakaway onset etc. Influence of different nodalization schemes on the simulation results was examined.

Zusammenfassung

Mittels des Computer-Codes ATHLET-CD wurde eine Simulation des Versuchs QUENCH-12 (Abschrecken eines WWER-Testbündels) durchgeführt. Die berechneten Ergebnisse wurden mit experimentellen Daten verglichen. Der Einfluss durch Variierung der experimentellen Parameter auf die Ergebnisse wurde analysiert. Eine Studie mit verschiedenen Bündel-Diskretisierungsstufen wurde durchgeführt.

Contents

List of tables

List of figures

1 Introduction

The report describes post-test simulation results of the QUENCH-12 bundle experiment with E110 cladding material pre-oxidized, overheated and quenched at the QUENCH/KIT facility. For that purpose an input deck for the ATHLET-CD2.2A computer code was prepared which describes the QUENCH test facility and the VVER test bundle.

The QUENCH-12 test involved preoxidation to a maximum value of about 150 µm oxide thickness at a temperature of about 1180°C, followed by a power ramp until a temperature of 1780°C was reached, then reflood with water at room temperature was initiated.

The reflooding of overheated (above 1200°C) but still relatively intact fuel rods may result in sharp increases of the temperatures of the fuel rods and surrounding core regions, as well as in hydrogen production, fission product release and melting. This behaviour occurs as a direct consequence of strongly exothermic oxidation of cladding in steam. This process can be accelerated due to the cracking and spalling of protective oxide layers and the oxidation of freshly exposed zirconium layers as well as due to oxidation of melt, which can be formed already at 1200°C in presence of absorber materials [1, 2, 3].

The simulation results are compared with the experimental data. The analysis is aimed to support the activities related to verification and validation of models included into the ATHLET-CD code package for description of the high temperature behaviour of the E110 material and simulation of thermohydraulic processes. The ability to predict the overall thermo-hydraulic response of the plant and generated hydrogen during a severe accident is one of the most significant contributors to a good analysis.

2 General features of ATHLET and ATHLET-CD

The thermal-hydraulic system code ATHLET (Analysis of THermal-hydraulics of LEaks and Transients) is being developed by GRS (Gesellschaft fur Anlagen- und Reaktorsicherheit) for the analysis of the whole spectrum of leaks and transients in PWRs and BWRs. The code is applicable for western reactor designs as well as for Russian VVER and RBMK reactors. The main code features are advanced thermal-hydraulics, modular code architecture, the separation between physical models and numerical methods, and the availability of pre- and post-processing tools [4].

ATHLET is composed of several basic modules for the simulation of the different phenomena involved in the operation of light water reactors, including thermal-fluiddynamics (TFD), heat transfer and heat conduction (HECU), neutron kinetics (NEUKIN) and control and balance-of-plant (GCSM), together with the fully implicit numerical time integration method FEBE. Other independent modules (e.g. 3D neutron kinetics or containment modules) can be coupled by means of a general interface [4]. ATHLET is being used by more than 40 organizations, both in Germany and abroad, for the safety demonstration in supervisory and licensing procedures [5].

The code ATHLET-CD (ATHLET with Core Degradation) is developed with the aim to simulate severe accidents in the reactor cooling system and was applied for different

benchmarks (e.g. [6]). It is being developed since 1990 by GRS in cooperation with the Institut für Kernenergetik und Energiesysteme (IKE) of the University of Stuttgart (Germany) and with the French Institut de Radioprotection et de Sûreté Nucléaire (IRSN) at Cadarache [2].

The code consists of the ATHLET part, which describes the circuit thermohydraulics, the non-condensable gases, thermal behaviour of the structures, neutron kinetics, typical reactor control systems, and the CD part, which allows to simulate behaviour of the core (PWR and BWR) in the case of a severe accident. The CD part, which is based on selected models of the KESS-III (KErnschmelz-Simulations-System) code (developed by IKE - Institut für Kernenergetik und Energiesysteme), simulates the following phenomena: structure heat-up, cladding and crust oxidation, hydrogen production, ballooning, mechanical rod failure, UO_2 dissolution, melting and relocation of metallic and ceramic materials, fission product release and transport [2]. ATHLET-CD includes also the aerosol and fission product transport code SOPHAEROS which has been developed by IRSN.

3 Description of the test facility, the QUENCH-12 bundle and the test scenario

The purpose of the QUENCH program running at the KIT (Germany) is to investigate the hydrogen source term resulting from the water or steam injection into an uncovered core of a light water reactor (LWR), to examine the physicochemical behaviour of overheated fuel elements under different flooding/cooling conditions, and to create a database for model development and code improvement in the field of severe accident simulation [7, 8].

The QUENCH-12 bundle experiment was carried out on September 27, 2006 in the electrically heated out-of-pile QUENCH facility at KIT (Figure 3.1) to investigate the effects of VVER materials (niobium-bearing alloys E110 and E125) and the hexagonal bundle geometry on reflood from the bottom, in comparison with bundle test QUENCH-06 using western PWR materials (Zircaloy-4) and rectangular geometry [8, 9].

The Russian abbreviation VVER (ВВЭР) stands for water-cooled water-moderated energy reactor. It is a pressurized water reactor with hexahedral fuel assemblies (due to triangular lattice of the fuel rods) and horizontal steam generators. VVER-1000 is a pressurized water reactor with thermal power of 3000 MW and electrical output of 1000 MW. The reactor core of VVER-1000 (version V320) consists of 163 fuel assemblies: thereof 61 fuel assemblies have control rods [10]. The unit consists of two circuits – the primary and secondary circuit.

For the QUENCH-12 bundle the core geometry of the VVER-1000 version is used: the fuel rod pitch is 12.75 mm and the outer diameter of the rods is 9.1 mm (Figure 3.2). The test section is enclosed by safety containment with a wall thickness of 5.6 mm and an inner diameter of 801.8 mm. The system pressure in the test section is around 0.2 MPa. The argon, steam, and hydrogen produced in the zirconium-steam reaction flow upwards inside the bundle and from the outlet at the top through a water-cooled off-gas pipe to the condenser where the steam not consumed is separated from the non-condensable gases, usually argon and hydrogen. The water cooling circuits for bundle head and off-gas pipe are

temperature-controlled to guarantee that the temperature of the steam/gas mixture is high enough so that condensation at the test section outlet and inside the off-gas pipe can be avoided. The temperature at the bundle head is kept at 348 K, and the flow rate of the cooling water is ~250 g/s. The off-gas pipe consists of a water-cooled inner pipe with a counter-current flow and a flow rate of ~370 g/s. The water inlet temperature is controlled at 393 K. There is stagnant gas between the off-gas pipe and inner cooling jacket.

The test bundle is made up of 18 heated and 13 unheated fuel rod simulators, each with a length of approximately 2.5 m. Heating is electric performed by 4 mm diameter tungsten heaters installed in the rod center. The heated length is 1024 mm. Electrodes of molybdenum/copper are connected to the tungsten heaters at one end and with cables leading to the DC electrical power supply at the other end. The total heating power is distributed between two groups of heated rods as follows: 33 % of the power is released in the six inner fuel rod simulators, 67 % in the twelve outer fuel rod simulators [9].

The fuel rod simulators are held in position by seven grid spacers, all made of Zr1%Nb. Their length is 20 mm. Furthermore, the thickness of the spacer is 0.25 mm and the mass of one grid spacer was measured to be 46.5 g.

The tungsten heaters of 4 mm diameter are installed in the centre of the rods surrounded by annular ZrO_2 pellets (bore size 4.15 mm). The unheated fuel rods are filled with ZrO_2 pellets (bore size 2.5 mm).

The tungsten heaters are connected to electrodes made of molybdenum and copper at each end of the heater. The molybdenum and copper electrodes were joined by high frequency/high-temperature brazing under vacuum ($2x10^{-3}$ mbar) using an AuNi 18 powder (particle size <105 µm). The surfaces of both types of electrodes were plasma-coated with 0.2 mm ZrO_2 for electrical insulation. To protect the copper electrodes and the O-ring-sealed wall lead-through adapters against excessive heat water-cooling is performed (lower and upper cooling chambers are filled with circulated demineralized water). The copper electrodes are connected to the DC electric power supply by means of special sliding contacts both at the top and bottom.

The rod claddings of the heated and unheated fuel rod simulators are identical to those used in reactors of type VVER both with respect to material and dimensions (Zr1%Nb, 9.13 mm outside diameter, 0.7 mm wall thickness). The heated rods were filled with a gas mixture Ar5%Kr and unheated test rods, including the central one, were filled with He, each rod at a pressure of approx. 0.22 MPa. The different fill gases allow the observation of a first cladding failure for heated and unheated rods separately.

Six Zr1%Nb corner rods were installed in the bundle. Three of them, i.e. rods "A", "C", and "E" were made of a solid Zr1%Nb rod at the upper part and a Zr1%Nb tube at the lower part and were used for thermocouple instrumentation whereas the other three corner rods, i.e. rods "B", "D", and "F", were made of solid Zr1%Nb rods of 6 mm diameter being able to be withdrawn from the bundle for checks of the ZrO_2 oxidation degree and the hydrogen uptake at pre-defined times.

The test bundle was surrounded by a shroud of Zr2.5%Nb (E 125) with a 35 mm thick ZrO_2 fiber insulation extending from the bottom to the upper end of the heated zone and a double walled cooling jacket of stainless steel over the entire length. The annulus between shroud and cooling jacket was purged (after several cycles of evacuation) and then filled with stagnant argon of 0.22 MPa. The annulus was connected to a flow- and pressure-controlled argon feeding system in order to keep the pressure constant at the target of 0.22 MPa (beyond this pressure gas is released) and to prevent an access of steam to the annulus after shroud failure (argon feeding below the target value). The 6.7 mm annulus of the cooling jacket was cooled by an argon flow. Both the absence of ZrO_2 insulation above the heated region and the water cooling of the bundle head helps to avoid overheating in that bundle region.
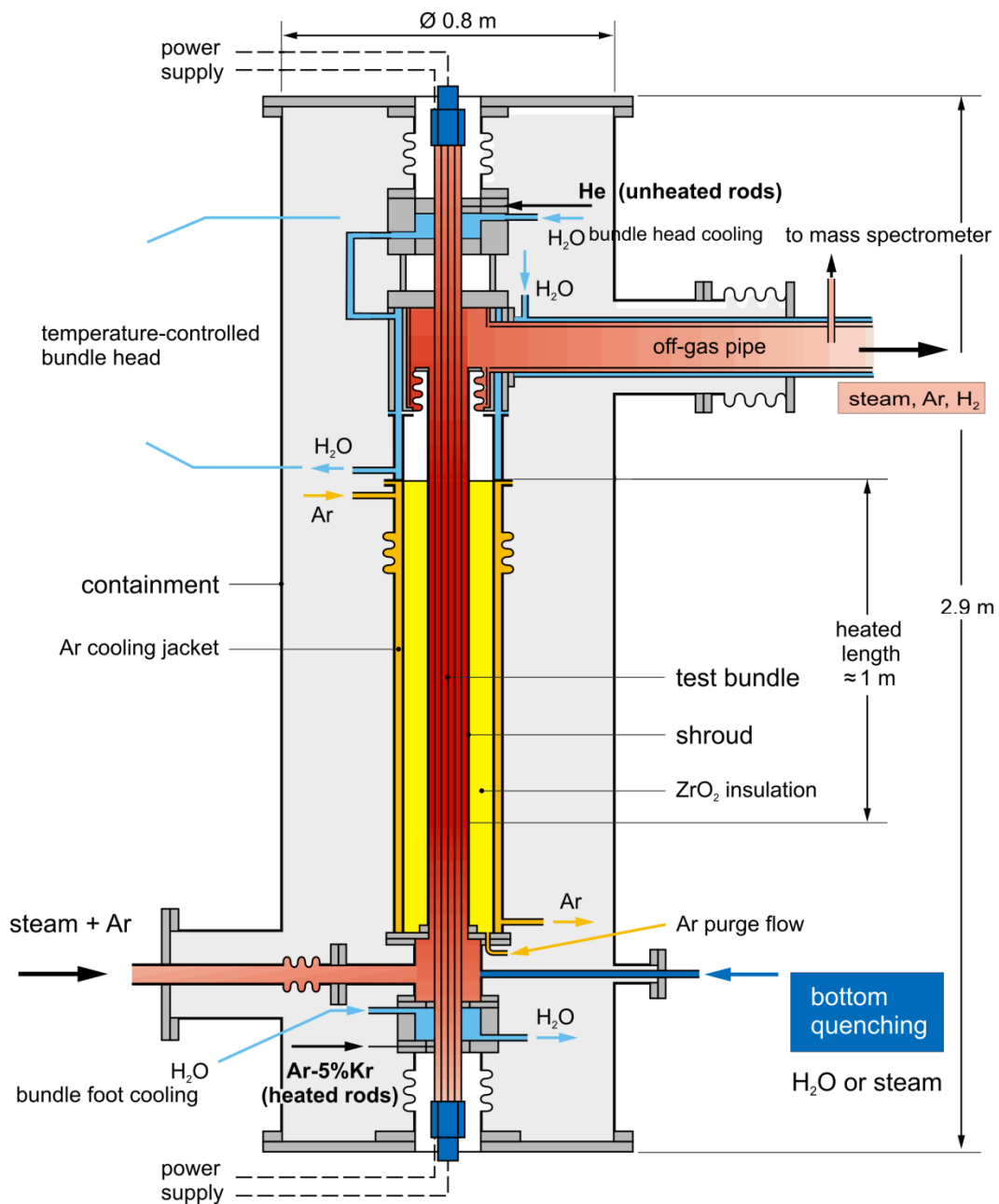
Figure 3.1: QUENCH-12 test facility [9]
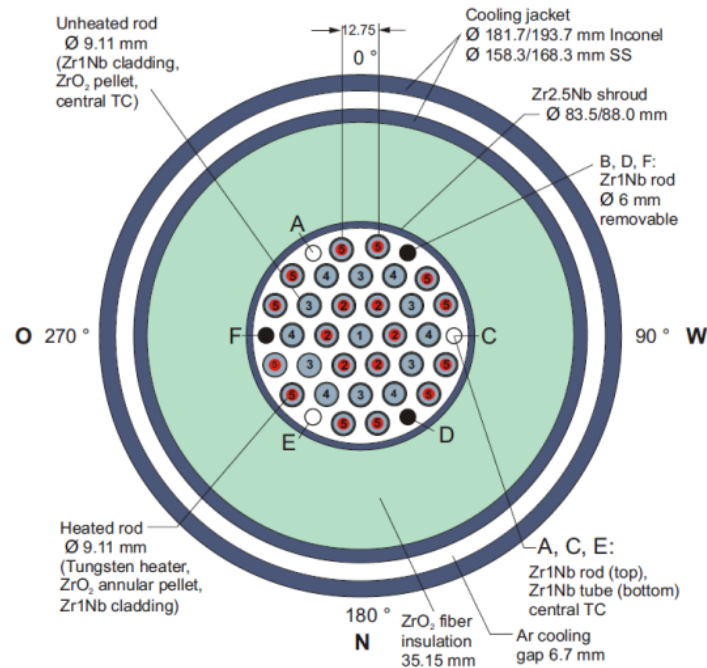
Figure 3.2: Cross section of the QUENCH-12 bundle [9]

The experiment started with an application of an electrical bundle power of ca. 3.5 kW, which was ramped stepwise to 9.9 kW over approx. 2300 s to achieve the desired preoxidation temperature at bundle peak position of 1473 K, in a flow of 3.3 g/s argon and 3.3 g/s steam. Preoxidation continued to the test time of 6000 s. At this time corner rod D was withdrawn to check the oxidation degree. The power was then ramped at a rate of 5.1 W/s to ensure a temperature increase until the desired maximum temperature before quench of 2073 K was reached. Corner rod F was withdrawn after about 900 s from the start of the transient phase, when the bundle temperature was about 1823 K at the 950 mm level.

Reflood with 48 g/s of water (at room temperature) was initiated with the help of a fast injection system. The electrical power was reduced to 4 kW during the reflood phase, approximating effective decay heat levels.

4 Model of the test facility QUENCH-12 built by computer code ATHLET-CD2.2A

A nodalization scheme was developed and tested for the QUENCH-12 test facility using the computer code ATHLET-CD2.2A. The test facility is simulated by the application of standard thermo-fluiddynamic objects, heat conduction objects and GCSM (General Control Simulation Module) signals. Only the modules of ATHLET (thermal-hydraulics, heat conduction) and ECORE (core heat-up, cladding oxidation, and core degradation processes) have been applied in the model. The thermal behaviour of debris bed and the molten pool, the fission product release from the fuel rods and the transport and deposition of radionuclides are not considered in the input deck of the quench facility.

The annular lower plenum *RV-LP* is simulated as one branch to which the inlet pipe for steam and argon injection, the inlet pipe for quench water injection and the bundle with rods

are connected. The steam, argon and quenching water flows are represented by a *fill* in a combination with related GCSM signals. The *fill* simulation model is a junction related model. The mass flows and the specific enthalpies are specified via GCSM control signals.

The core bundle is represented by a thermo-fluiddynamic object type *pipe RV-CC* consisting of 19 control volumes with a collapse level track. Within the pipe, the active core is represented through its corresponding geometric data and the coupling of heat conduction objects simulating 31 fuel rods and 7 grid spacers. In addition 6 corner rods are simulated too. The coolant channel area is 32.8 cm^2, the hydraulic diameter is 10.4 mm and the bundle diameter is 83.5 mm. The thermal impact of the bundle wall is considered in such way, that the bundle channel is coupled on the right side with heat conduction objects (module HECU) *H-SHROUD1* and *H-SHROUD2* to take into account the heat losses in the shroud. The heat exchange between the rods and shroud is affected by radiation and the convective heat transfer to the gas mixture (steam/argon/hydrogen). The shroud failure cannot be calculated by ATHLET module HECU, and oxidation of the outer surface of the shroud cannot be simulated. Also melt oxidation of these HECU structures is not calculable.

The annular outer part of the upper plenum nozzle section is represented by the *branch RV-UP*. It is nodalized into one control volume. As in the test facility at the beginning of the quench initiation of water flooding, the argon injection switches from the bottom to the top of the bundle, a pipe coupled to upper plenum is modeled for the argon top injection. The off-gas pipe is modelled by the pipe object *OUT-L*, the heat conduction objects *H-OFF-GAS1* and *H-OFF-GAS2*, and the pipe *OGP-WC*.

For heatup, cladding oxidation, and the core degradation processes the ECORE module of ATHLET-CD is used. The total number of fuel rods in the core is 31. Fuel rod outer radius is 4.555x10^{-3} m, the inner radius of the cladding is 3.875x10^{-3} m, the outer radius of fuel pellet is 3.785x10^{-3} m and the inner is 1.175x10^{-3} m. In axial direction each one of the rod is divided into 19 nodes. The distance between fuel rod centers (pitch) is 12.75x10^{-3} m. The bundle geometry is triangular. For the internal fuel rod the pressure input is 0.7 MPa (at peak cladding temperature PCT=600°C). No absorber rods are described in the input deck. Power generation in the rods is controlled by an electrical heater model in ATHLET-CD (KfK fuel rod simulator). The external resistance per heated rod is set to 4.65 mΩ.

Fuel rod cladding oxidation is one of the most important processes during the accident progress [11]. The correct simulation of this process is very significant for the simulation results. This reaction is exothermal and accompanied by hydrogen release. The oxidation model *IOXMOD* = 18 was applied, which uses correlation of Sokolov for the VVER cladding type. The initial oxide thickness is set to 0.3x10^{-6} m.

The test bundle is divided into four radial core sections (HEAT objects): *ROD1*, *ROD2*, *ROD3* and *ROD4*. They are coupled with thermo−fluid object *RV-CC* which is the core channel itself. Since in ATHLET-CD different geometries of fuel rods cannot be considered, for all rods the geometric data of the general ECORE module input are adopted the geometric data of the heated rods. The only difference is, that unheated rods are without any power generation. In the first radial core section *ROD1*, there is one unheated rod. This *HEAT*

object represents the central unheated rod. In the second radial core section *ROD2*, there are 6 heated rods. The radius of the center line of the outermost rods in this section is 12.75×10^{-3} m. In the third radial core section *ROD3*, there are 12 unheated rods. The radius of the center line of the outermost rods in this section is 26.0×10^{-3} m. In the fourth radial core section *ROD4*, there are 12 heated rods. The radius of the center line of the outermost rods in this section is 36.0×10^{-3} m. The emissivity of rod surface is set to 0.8. The six corner rods are not modelled in ATHLET-CD, but were considered as heat conducting objects in module HECU of ATHLET. In contrast to the modelled fuel rods defined as HEAT objects, the melting of corner rods cannot be considered.

The quench front model is used in the input model. One quench region for four radial core sections of the model is predefined. A quench region consists of vertically staggered heat conduction volumes which belong to corresponding group of rods. For each quench region, the model calculates the position and the movement both of the bottom and the top quench front. The Semeria-Martinet correlation [12] is selected for calculation of quench front velocity. The quench front model is activated by the GCSM signal *QUENCHST* at 7270.0 s.

The standard multi-component model is applied for all control volumes in the thermohydraulic system. The presence of a build-in hydrogen and user-defined argon in the bundle is specified. The properties of argon are given via the input data: the specific heat capacity at constant pressure and the specific enthalpy as a function of related temperatures. Input *ICK00*=3 is set to enforce steam in the control volumes for initial conditions. The model includes external cooling channels with argon *CO-JC* and water in the upper electrode zone *HEAD-COOL* and considers the absence of the fibre insulation (ZrO_2) in the shroud above 1.024 m.

The nodalization scheme of ATHLET-CD2.2A input deck prepared for the test facility QUENCH-12 is depicted in Figure 4.1.
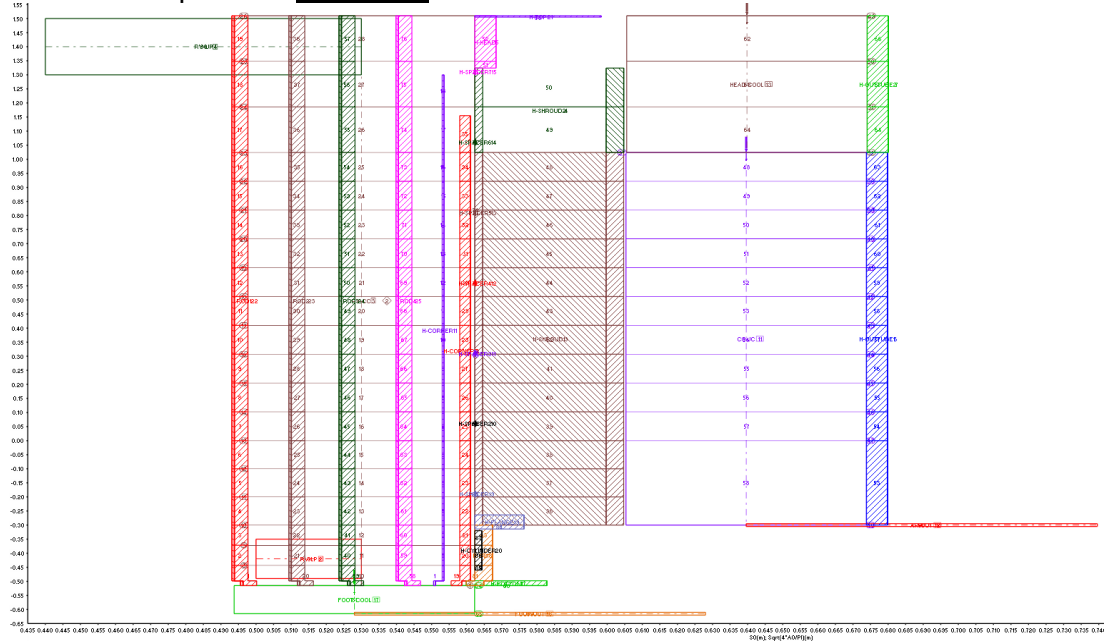
Figure 4.1: Nodalization of the QUENCH-12 facility

5 Results

5.1 Round-off error with ATHLET-CD2.2A

During the calculations an additional error arises due to the error in the floating point arithmetic. Because computers can only store numbers to a certain precision, some accuracy is lost every time a computation is performed. The error due to this is called round-off error. The total integration error is both due to truncation and round-off error.

ATHLET-CD is written in FORTRAN 90 (ANSI Standard). The declaration *IMPLICIT DOUBLE PRECISION (A-H, O-Z)* at the beginning of each subprogram of the source code is inserted to ensure double-precision (64 bit) real arithmetic in ATHLET-CD. Double precision is a binary format that occupies 64 bits (8 bytes): one bit for sign, eleven bits for the exponent and 52 bits for the fraction (about 16 decimal digits). The executable file of ATHLET-CD has been compiled with the INTEL FORTRAN Compiler Version 9.0.

The machine epsilon is defined as the smallest positive number which, when added to one, yields a result other than one (it gives the difference between 1.0 and the next-nearest number representable as a machine-precision number) [13]. This value characterizes computer arithmetic and is used to study the effects of the rounding error – it measures the limitations of exact arithmetic using computers. Machine epsilon varies from machine to machine: higher precision computers will have a smaller epsilon. The correctness of the results depends on the machine epsilon value. The following value does not actually determine the machine epsilon, rather it determines a number within a factor of two: $\varepsilon = 2.220446049250313 \times 10^{-16}$ for double precision variable type on the computer used for the simulation of QUENCH-12 with the computer code ATHLET-CD2.2.A.

5.2 Validation of the model for QUENCH-12

There is a regulatory requirement that codes should be validated in relation to relevant experimental data for the major phenomena expected to occur. The validation relates to the confidence that can be placed on the accuracy of the values predicted by the code. The code validation is an assessment of the accuracy of values predicted by the code against relevant experimental data for the important phenomena expected to occur [1]. As the calculation with ATHLET-CD2.2A has been completed, the results are checked by comparison with the results measured during the QUENCH-12 test in KIT. The calculations were performed up to 9000 s.

The comparison of the central rod temperatures measured during the QUENCH-12 experiment and the calculated values referring to elevation 950 mm are depicted in Figure 5.1. The black line is the temperature measured by the thermocouple in the center line of the central rod and the red line is the temperature measured by the thermocouple mounted at the outer rod surface.
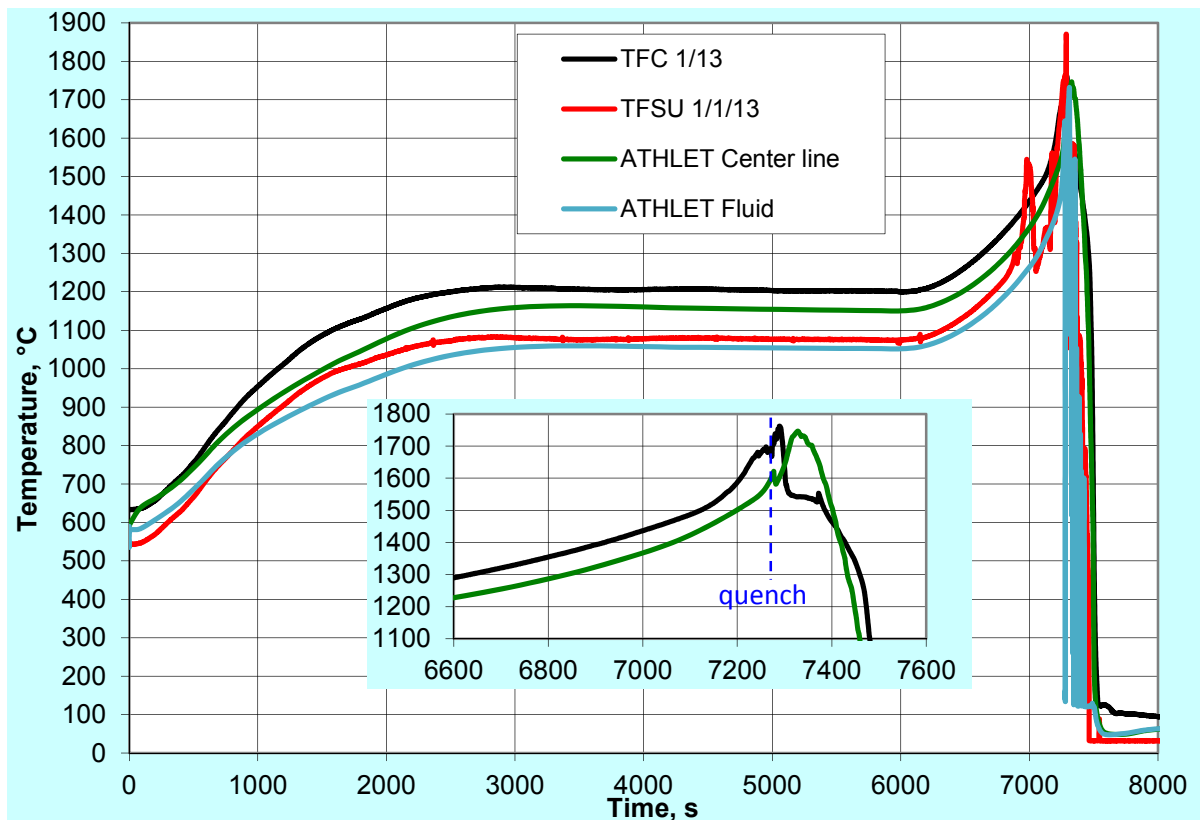
Figure 5.1: Bundle temperatures at the elevation 950 mm measured by thermocouples TFC 1/13, TFSU 1/13 and temperatures calculated by ATHLET-CD

Results for the temperatures calculated by ATHLET-CD2.2A for the pre-oxidation and transient phases are not significant underestimated in comparison to the experimental results. The calculated temperatures are varying within a range of about 100°C. The temperature peak is observed between 7300 s and 7310 s. The main deviations between the calculated and measured temperatures are observed at about 2000 s. During the quench phase the temperatures are in good agreement with the experimental data. After 7500 s the temperatures move to the values between 32÷100°C.

A possible reason for deviations occurring before quenching is the uncertainty in the properties of the materials (the thermal conductivities and the specific heat capacities). Other reason for the deviations is the fact that the electrical power, which is released into the test bundle, is not well known due to the estimated value of the external resistance. Instead of that the total electrical power of the heaters and the external resistance are used in the ATHLET-CD2.2A modelling; the last parameter can be a reason for deviations in the calculations. The temperatures refer to the electrical power release in the bundle and the electrical resistances of the tungsten heaters depend on the temperatures. Also nodalization effects (discretization errors) and some limitations in ATHLET-CD2.2A (different geometries of fuel rods cannot be considered) may result in deviations in calculated temperatures in the test bundle. The proper selection of nodalization for modelling of a quench facility by means of the computer code has a significant beneficial impact on the calculated results. Furthermore, the numerical values of temperatures are also strongly depending on the correct modelling of the zirconium oxidation. The intensive breakaway oxidation was

observed for the QUENCH-12 bundle, but a corresponding model of breakaway effect has not been yet fully developed in ATHLET-CD2.2A. Additionally, the double sided oxidation of cladding (observed at hottest elevations with melt formation) is not considered in the ATHLET-CD2.2A, too.

For the thermocouples mounted at the outer rod surface one have to take into account that this temperature is not the temperature of the cladding itself but a value being affected by the temperature of the fluid near the surface of the rod.

The observed discrepancy could also be explained considering the behaviour of the collapsed water level in the bundle, different axial bundle modelling and not fully correct described heat transfer processes. Additionally, the beginning of heat up is strongly influenced by the corresponding calculated water level too, which in turn is significantly affected by the correctness of the modelling of the heat balance and the axial profile of the linear electrical rod power. The reasons for discrepancies in the values mentioned above are valid for all temperatures in the figures shown below.

<u>Figure 5.2</u> depicts the temperature on the surface of the fuel rod-2 of the test bundle at the elevation of 950 mm (red line) and the corresponding temperature calculated by ATHLET-CD2.2A, for the temperature of the cladding for the second radial core section *ROD2*, which consists of 6 heated rods and the temperature of the fluid in the bundle for this elevation. The green line is the temperature in the middle of the cladding and the blue line is the temperature of the fluid around the fuel rod. The temperature of the thermocouple mounted at the outer rod surface shows good agreement with the fluid temperature calculated by ATHLET-CD2.2A for that elevation. Temperatures of the thermocouple after 7492 s are not correct due to the failure of the thermocouple.
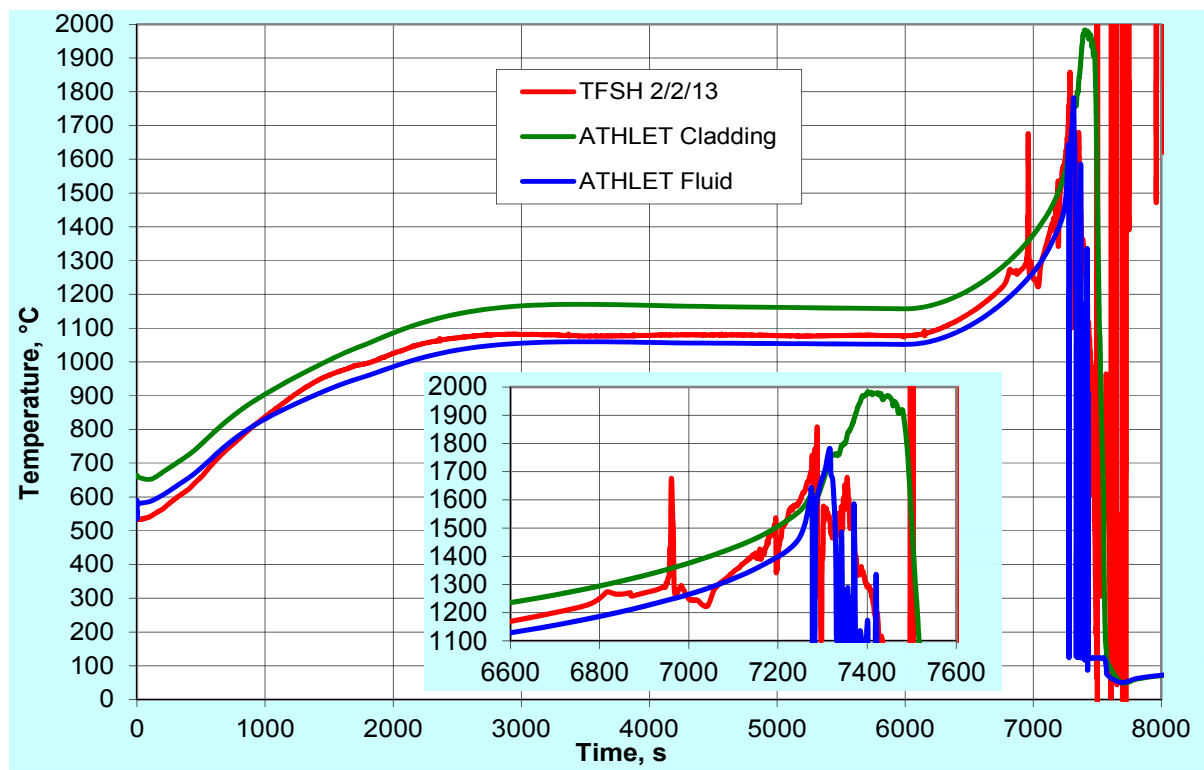
Figure 5.2: Surface temperature of heated rods at 950 mm elevation measured by thermocouples TFSH 2/2/13 and temperatures calculated by ATHLET-CD

Figure 5.3 depicts temperatures calculated by ATHLET-CD2.2A for the third radial core section *ROD3*, which consists of 12 unheated rods. The temperatures are compared with measured ones for this rod group in the test bundle at the elevation 950 mm. The red line is the temperature measured by thermocouple in the centre of fuel rod-11, the light blue line corresponds to the temperature in the centre of fuel rod-14, the purple line is temperature in the centre of fuel rod-8, blue dash line - the temperature on the surface of fuel rod-10 and grey dash line - the temperature on the surface of fuel rod-17. It can be said that before the failure of the thermocouples (about 7500 s) there is no big discrepancy between the calculated temperatures by ATHLET-CD2.2A and the temperature measured in the test facility.
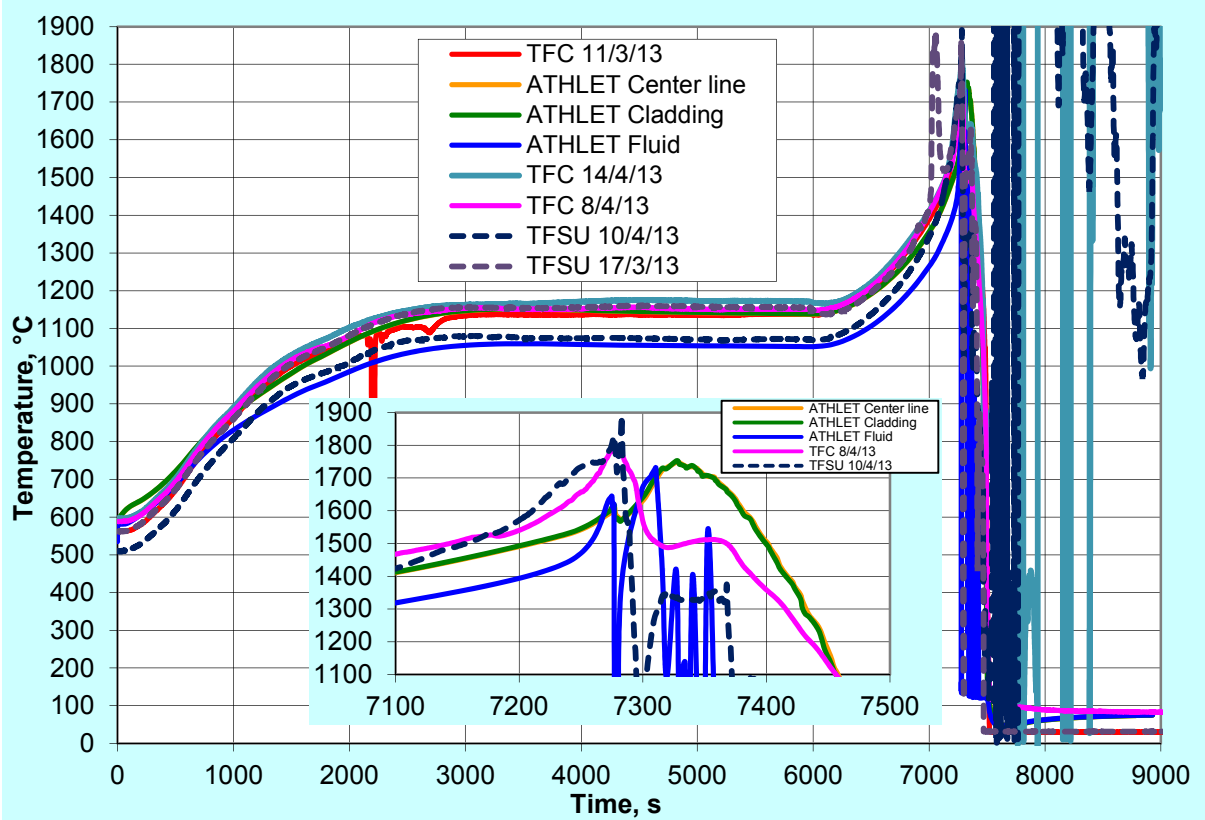
Figure 5.3: Bundle temperatures at the elevation 950 mm measured by thermocouples TFC 11/3/13, TFSU 10/4/13, TFC 14/4/13, TFC8/4/13, TFSU 17/3/13 and temperatures calculated by ATHLET-CD

Figure 5.4 presents the temperatures on surface of fuel rod-29 of the test bundle at elevation 950 mm (red line) and the temperature calculated by ATHLET-CD2.2A for the temperature of the cladding for the fourth radial core section *ROD4*, which consists of 12 heated rods, and the temperature of the fluid in bundle for this elevation. The green line corresponds the temperature in the middle of the cladding and the blue line - to the temperature of the fluid around the fuel rod. The temperature measured by thermocouple is higher during the transient and the quench phases which is because the fact that breakaway phenomena are not considered in the model. Another possible reason for discrepancy during the quench phase is possible oxidation of the shroud outer surface: used version of ATHLET-CD cannot describe the shroud failure. The rods in fourth radial core section are the nearest to the shroud and the corner rods. The oxidation of the outer surface of the shroud (measured oxide thicknesses up to 400 μm at 950 mm) will generate additional heat which increases the

temperature of the peripheral rods. This affects all rods in the bundle, but the biggest influence is on the fourth radial core section.
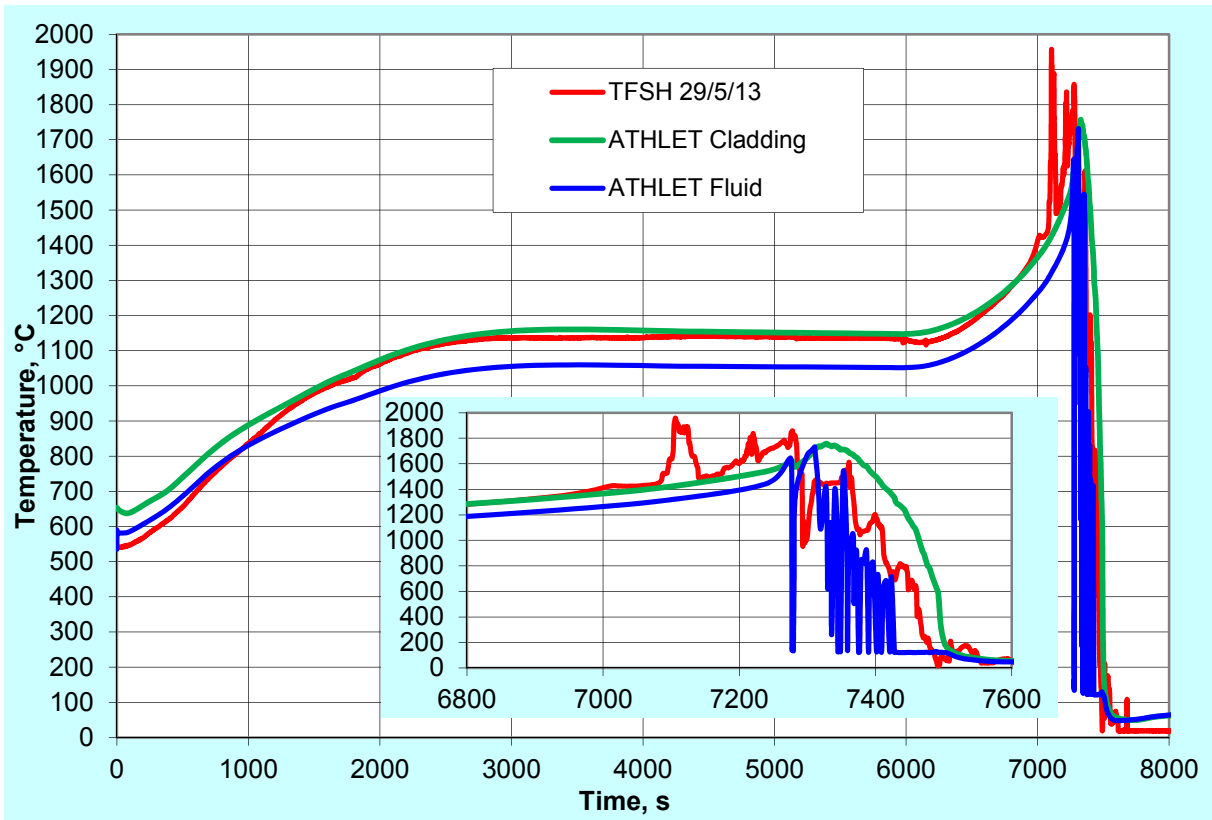
Figure 5.4: Bundle temperatures at the elevation 950 mm measured by thermocouple TFSH 29/5/13 and the temperatures calculated by ATHLET-CD
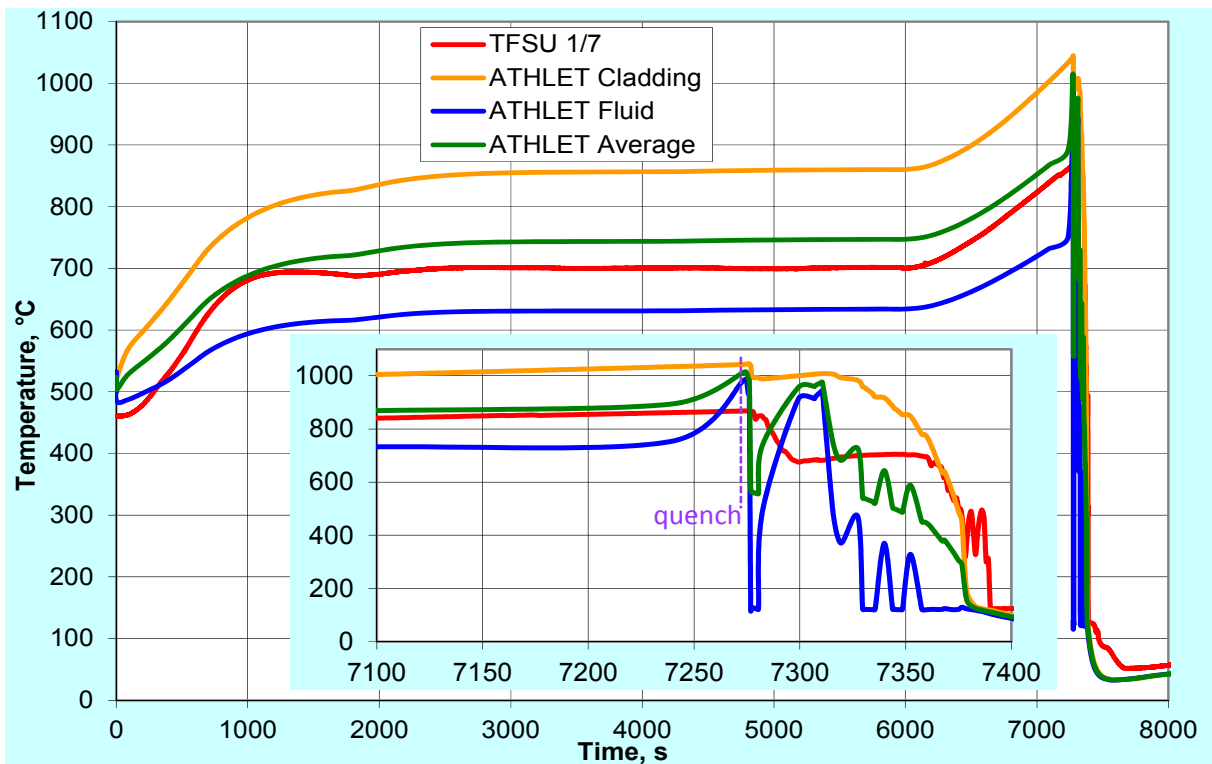
Figure 5.5: Bundle temperatures at the elevation 350 mm measured by thermocouple TFSU 1/7 and temperatures calculated by ATHLET-CD

Figure 5.5 shows the temperature measured by the thermocouple mounted at the surface of the center rod of the test bundle at the elevation 350 mm (red line) and the temperatures calculated by ATHLET-CD2.2A for the temperature of the cladding (orange line) and fluid temperature (blue line). The green line represents an average between temperature of cladding and the fluid temperature. The temperature measured by thermocouple mounted at the surface (TSFU 1/7) during the whole time of experiment is in-between the calculated temperature values for the cladding and for the fluid around the fuel rod. The difference between average temperature calculated by ATHLET-2.2A and the measured one is about 40 degrees, and the temperature in the computer model is higher than the experimental data. A possible reason for this could be the difference in the power distribution between the test bundle values and the according assumptions of the computer model.
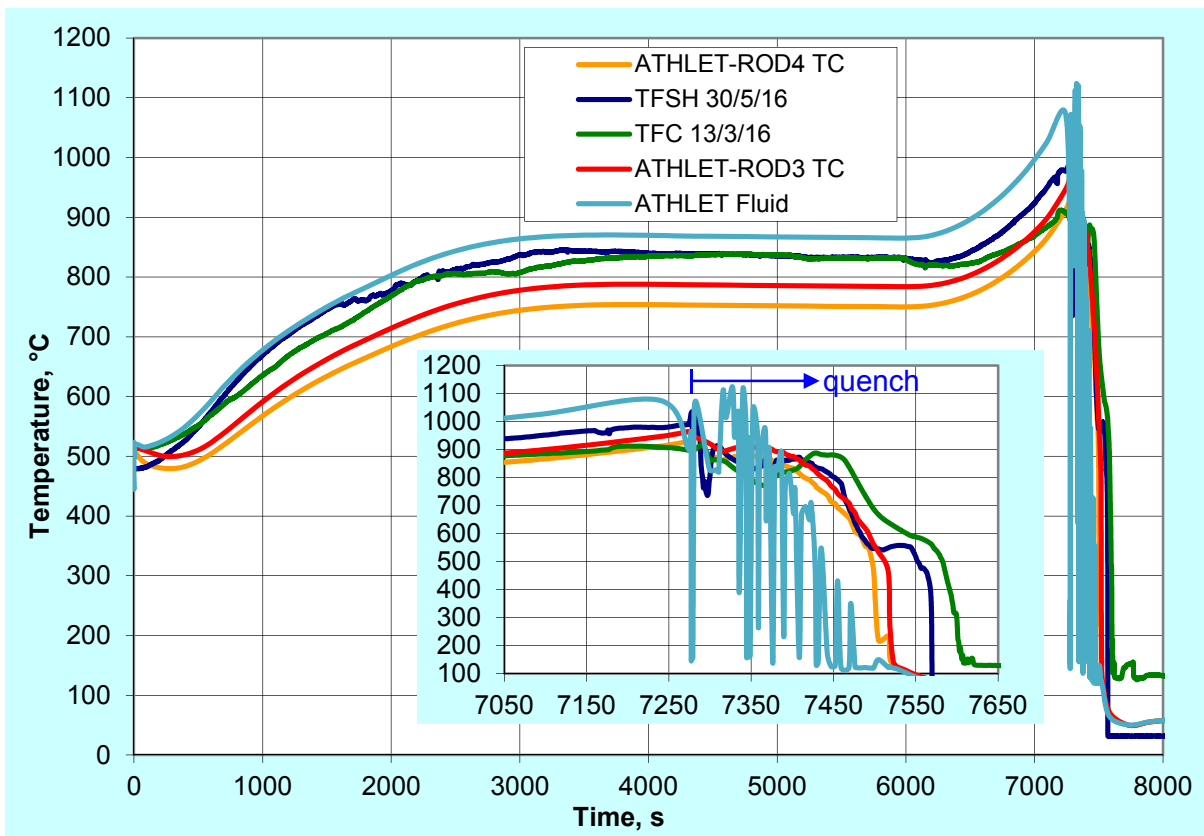
Figure 5.6: Bundle temperatures at the elevation 1250 mm measured by thermocouples TFC 13/3/16, TFSH 30/5/16 and temperatures calculated by ATHLET-CD

Figure 5.6 depicts the temperatures measured by the thermocouple in the centre line of rod-13 (green line) and those measured by the thermocouple mounted at the surface of fuel rod-30 of the test bundle at elevation 1250 mm (dark blue line) as well as the temperatures calculated by ATHLET-CD2.2A for the fluid temperature (light blue line). The orange line corresponds to the temperature of the cladding calculated by ATHLET-CD2.2A for the fourth radial core section rods and red line – accordingly to the temperatures in the centre line of the rods in the third radial core section.

Figure 5.7 presents temperatures on the shroud outer surface at the elevation 950 mm. The blue line corresponds to the temperature of shroud outer surface at the orientation 270°, the green line depicts the orientation 90° and the red line gives the temperature calculated by ATHLET-CD2.2A for this elevation – 950 mm. Evaluated temperature is in good agreement

with the temperatures measured by the two thermocouples. Only in the quench phase there is significant difference between the values of the thermocouples and the value predicted by ATHLET-CD2.2A (underestimation in ATHLET-CD). Possible reason is the breakaway phenomenon which is not considered in this simulation. The other reason was discussed for Figure 5.4: it is not possible to calculate the oxidation of the outer surface of the shroud. After failure of shroud at elevation of about 850 mm shortly before initiation of reflood (shroud failure on 7268 s), the gas mixture from inside can penetrate through the holes in the shroud which raised the temperature outside it. But in the model for ATHLET-CD2.2A heat is transferred to the outer surface of the shroud only by heat conductivity. There is no possibility to calculate the shroud melting followed by its failure.
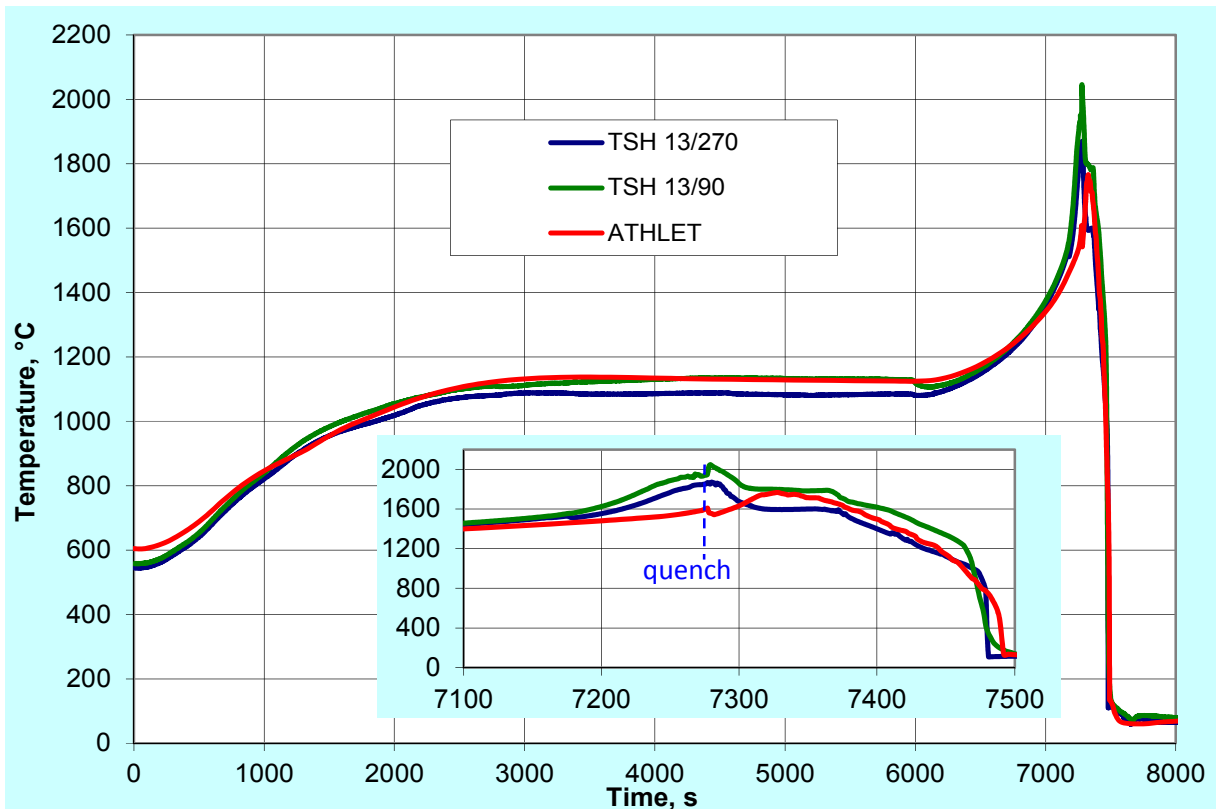
Figure 5.7: Shroud temperature at the elevation 950 mm measured by thermocouples TSH 13/270, TSH 13/90 and temperatures calculated by ATHLET-CD

Additionally, the current version of ATHLET does not consider the influence of growing oxide on the changes of the thermal conductivity and emissivity both of the cladding and the shroud. Oxidized materials have lower heat conductivity in comparison with non-oxidized ones.

In general when overheated core of a nuclear reactor is flooded with water, hydrogen is released due to oxidation of the zirconium cladding by steam. Comparison of experimentally measured and calculated total hydrogen release for QUENCH-12 is shown in Figure 5.8. For the modelling of the rod cladding, the shroud and the spacer grid oxidation correlation according to Sokolov is chosen since this particular correlation is recommended by the developers for the cladding alloy E-110 used for VVER fuel rod claddings [14, 15]. Furthermore, a sensitivity analysis concerning the available correlations in ATHLET-CD2.2A and ATHLET-2.2A to calculate the zirconium-steam reaction has been performed in

section 5.3 to study its impact on the thermal response of the bundle and the amount of hydrogen release.
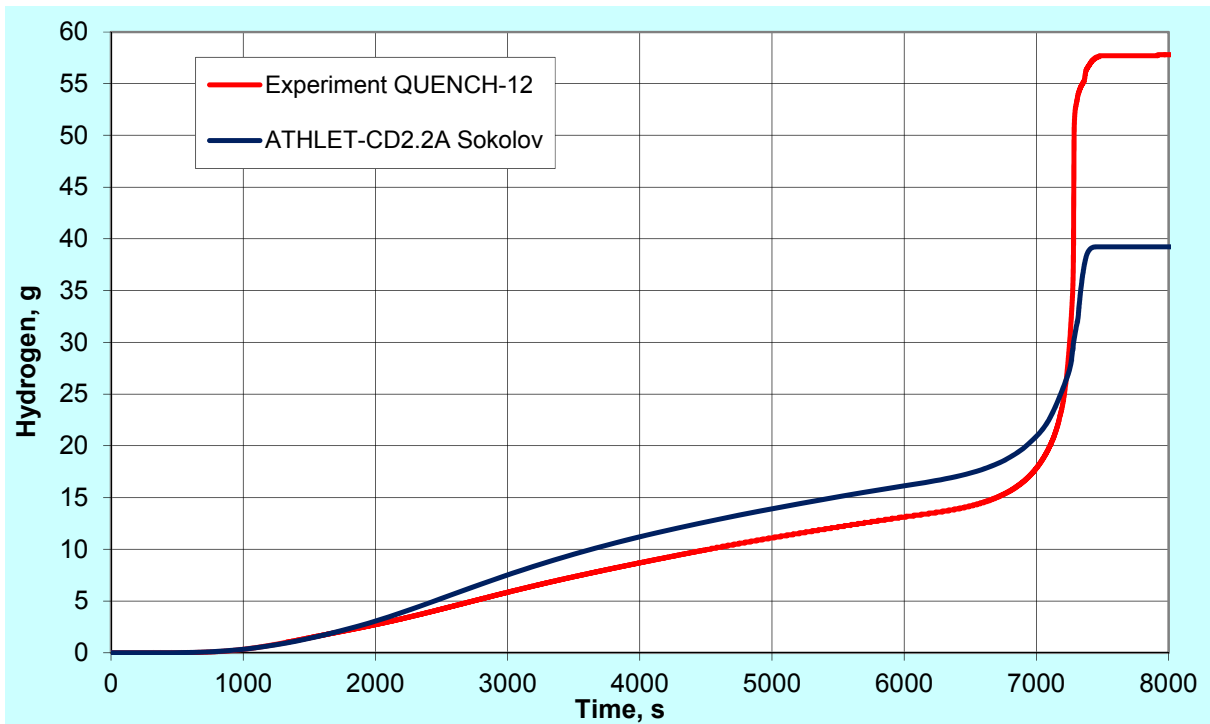
Figure 5.8: Total hydrogen production during the QUENCH-12 experiment

The total hydrogen production in the test was 58 g: 34 g before quenching and 24 g during reflooding. The amount of hydrogen generated during preoxidation calculated by ATHLET-CD is higher compared to the measured hydrogen release. Possible reason could be absorption of hydrogen by metal of claddings, corner rods and shroud. According to [9] it can be estimated that about 25% of the free hydrogen produced in the preoxidation phase was absorbed in the zirconium alloy. In ATHLET-CD2.2A it is not possible to simulate the hydrogen absorption in metal; therefore the amount of hydrogen which was absorbed and released again cannot be calculated.

Nevertheless, the total amount of hydrogen measured in the test facility is larger than the one calculated by ATHLET-CD2.2A. This is due to underestimation of hydrogen generated during reflooding (9 g calculated versus 24 g measured). Four possible sources of additional hydrogen, which cannot be modelled, are: 1) breakaway phenomena; 2) melt oxidation; 3) release of absorbed hydrogen; 4) oxidation of outer shroud surface.

The ATHLET-CD criterion on breakaway is not full: the onset of breakaway is initiated, if some threshold oxide thickness will be reached. But the transition of parabolic to linear oxidation kinetics depends not only on oxide layer thickness but also on the temperature [17].

No specific models for the oxidation of molten zirconium are available in ATHLET-CD2.2A. Instead, the extrapolated relation for oxidation of solid cladding is used, which can also lead to an underestimation of the produced hydrogen. The melt oxidation process is more complicate and must be described appropriately [16].
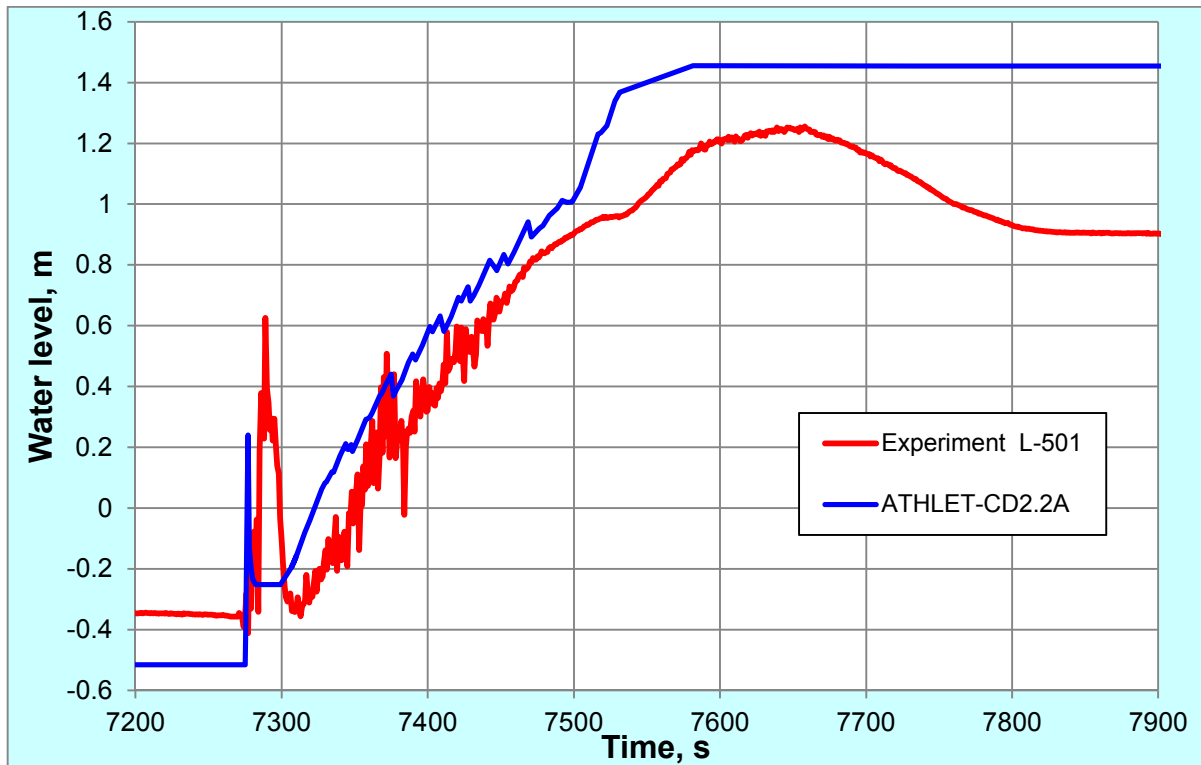
Figure 5.9: Water level in the bundle

The collapsed water level in the test bundle is measured by a differential pressure gauge (L 501) connected to the test section at the -386 mm and +1360 mm bundle elevations. The comparison of measured and calculated collapsed water levels in the bundle is presented in Figure 5.9. The rapid increase of the water level at about 7280 s is due to the fast water injection system filling the lower bundle plenum very fast. During the quench phase the calculated level is slightly above the experimental curve. The reason for the big difference after 7500 s is that the shroud failed at elevation about 850 mm during the quench phase and some water may have left the bundle through the holes in the shroud. Calculated higher level of the water leads to lower temperatures of the bundle in that region compared to the experimental values. There are no code options to model a failure of the shroud because, as it was mentioned above, for ATHLET it is not possible to calculate the shroud failure due to melting. Shroud failure in the test facility was observed shortly before initiation of reflood - at 7268 s (it was proved by decrease of pressure inside the space between shroud and cooling jacket) [9]. The difference in the levels before start of quenching phase is caused by the fact that differential pressure gauge is installed at some distance from the bottom – technically it would be very difficult to put it directly at the bundle bottom.

Finally it can be said that the comparison of the results shows that the general behavior with respect to the main events and thermal-hydraulic phenomena is similar. The calculations adequately reproduce the temperature evolution of the central rod at different elevations during the whole test duration with some discrepancies at the quenching phase. There are some differences due to code limitation or uncertainties for material properties, boundary conditions and used correlations. The deviations could also be explained by differences in the axial power distribution of the bundle. In section 5.3 is discussed sensitivity analysis of some parameters to investigate their influence on the results.

5.3   Sensitivity analysis

The sensitivity analysis defined on the basis of the reference calculation provides additional information about the influence of the computer code input parameters and the modelling options on the simulation of the main phenomena observed experimentally in the test facility. The results from the calculation are depicted in the Appendix in the end of the report. Figures are divided into eight parts – for each of the varied parameter for the according sensitivity analysis.

At first the influence of the steam flow on the process in the bundle was checked. Six values for the mass flow of steam were used in addition to the reference value of 3.3 g/s (Figures A.1 ÷ A.5). From the results one can derive that different steam flows lead to significant discrepancies, mainly in quench phase, in the temperatures and those in hydrogen generations. In cases with mass flow rate 3.0 g/s and 3.1 g/s the difference in temperature for the central rod is about 370°C between these two cases in the quench phase. As the steam flow was stopped with the beginning of quenching, the difference in temperatures in the quench phase can be explained as result of bigger accumulation of heat in the material of the bundle during preoxidation and the transient phase. The biggest influence exhibits the hydrogen release. From Figure A.4 one can see, that decreasing mass flow rate of steam by only 10% (3.0 g/s) results in an increase of the total generated hydrogen of 228%. The effect on the water level is not so big, except the case with the smallest flow rate (3.0 g/s), where a lower value of the water level was detected due to evaporation of greater amount of water as a result of higher temperatures in the bundle.

Changing reflood rates (quench water mass flow) has shown great difference in the quench phase (Figures A.6 ÷ A.10). In cases with smaller mass flow (15 g/s and 20 g/s) the temperatures in the quench phase reach higher value due to the slower cooling of the bundle (Figure A.6 ÷ A.8). Higher temperatures in the bundle result in greater values for the generated hydrogen (Figure A.9). Difference between simulations with 15 g/s and 20 g/s in hydrogen mass produced in the bundle is more than twice as much (while the difference in quench water flow is only 25%).

Examining the influence of argon mass flow rates shows that their effect on the results is very limited in comparison to the influence of steam mass flow rate (Figures A.11 ÷ A.15). Decrease of 330% of argon mass flow has an effect which is comparable with a 10% change of the steam mass flow. It is caused by the differences in the material properties of steam and argon. Indeed, the specific heat capacity of steam is approximately four times higher than the heat capacity of argon. For the calculation of the water level, the Ar flow rate of 1.0 g/s shows a great difference compared with experimental data and data calculated with Ar flow rate of 3.3 g/s. In this case, the water level is lower because higher temperatures in the bundle enhance the evaporation rate.

External electrical resistance per rod in the computer model was ranged within 4.0 mΩ ÷ 5.0 mΩ. External resistance determines what part of the total power is released in the bundle. From the results it can be seen that differences in the external resistance do not lead to significant discrepancies in the results (Figure A.16 ÷ A.20). Temperatures in the bundle (except the peak in the quench phase) deviate within a range of 30°C. All values calculated

by ATHLET-CD2.2A for the total hydrogen generation overestimate moderately the hydrogen release during pre-oxidation and noticeable underestimate it during reflood. There are no significant scattering in the simulations of water level. It can be stated, that external resistance has not a significant effect on the pre-oxidation results. In other words it means that the results are less affected by the power of the electrical heaters in the fuel rods.

With the help of the zirconium oxidation model in ATHLET/ATHLET-CD one can calculate the amount of oxidation, the corresponding energy release, the release of hydrogen and the dissipation of steam. The model consists of several empirical correlations based on a parabolic law derived from the analytical solution of the diffusion equation. A representative part of the available zirconium oxidation models is presented in Table 1.

Table 1: Some of zirconium oxidation models in ATHLET-2.2A/ATHLET-CD2.2A

Model selection key	Temperature region [K]	Correlation
15	1273 – 1800 1800 – 2600 2600 – 2673	Cathcart Transition range Prater / Courtright
16	1273 – 1800 1800 – 1900 1900 – 2100	Cathcart Transition range Urbanic / Heidrick
17	1273 – 1573 1573 – 1800 1800 – 2600 2600 – 2673	Leistikow / Schanz Prater / Courtright Transition range Prater / Courtright
18	1273 – 1800 1800 – 1900 1900 – 1973	Sokolov Transition range Sokolov
19	1273 – 1800 1800 – 2600 2600 – 2673	Leistikow / Schanz Transition range Prater / Courtright

The influence of the applied correlations depicted in Figures A.21 – A-25. One can see that there are significant differences in the temperatures of the bundle and the amount of generated hydrogen. A benchmark of the oxidation correlations (oxidation models 15÷19) shows that during the preoxidation phase the best values for hydrogen generation are reached using the correlations of Leistikow and Prater/Courtright in the oxidation model 17. In the same phase the correlations of Cathcart and Prater/Courtright in oxidation model 15, as well as Cathcart and Urbanic/Heidrick in the oxidation model 16 give values for the mass of generated hydrogen which are about two times higher than the measured ones. Simulation with the oxidation model 15 couldn't finish normally because it was terminated by FEBE – the time integration module.

The results presented in section 5.2 were obtained without the consideration of the breakaway phenomenon which can also lead to an underestimation of the zirconium

oxidation. Additionally, an investigation was made on the influence of the breakaway effect on the results. Breakaway phenomena occur as an accelerated oxidation of the zirconium structures due to the cracking of protective oxide films and the oxidation of freshly exposed zirconium materials. The breakaway oxidation is described in ATHLET-CD by a linear kinetics. The comparison of data calculated with different threshold thicknesses of the oxide layer, which is used as a parameter for the switch from parabolic to linear oxidation, are presented in Figures A-26 ÷ A-30. For the hydrogen generation two figures are presented to show a huge difference between the case with threshold thickness of 50 μm and all the other cases: 100 μm, 150 μm, 200 μm and 300 μm. Switch from parabolic to linear oxidation kinetics is made when a user defined value of the oxide layer thickness is reached – this is true for the both ATHLET-2.2A and the ATHLET-CD2.2A codes. But the transition from parabolic to linear oxidation kinetics in reality depends not only on the oxide layer thickness but also on the temperature and that's why the calculated results with different values for threshold oxide layer thickness (criterion for start of breakaway) exhibits such high deviations in comparison to the measurements. It is the point, where the sensitivity analysis exhibits the greatest deviations in the temperatures and in the generation of hydrogen. All five runs were made with the Sokolov correlation [11]. It can be seen from the results, that the use of the accelerated oxidation kinetics has a very big influence on the hydrogen release. Simulations with 50 μm, 100 μm and 150 μm couldn't finish regularly because they were terminated by FEBE – the time integration module. Calculation with a value for the threshold oxide layer of 300 μm (62 g) gave the nearest value to the experimental one of 58 g released hydrogen. Ratio in generated hydrogen between simulations with 200 μm and 300 μm is more than two. Temperatures corresponding to the case with 50 μm reach about 2300°C after 4000 s, while the measured temperatures are about 1200°C at the same time. After the high value is reached in the case with 50 μm the bundle temperature decreases, although the power of the electrical heaters is not changing until 6035 s. The power was then ramped with rate of 5.1 W/s to cause a temperature increase, but ATHLET-CD2.2A calculates here a decrease of the bundle temperature. Possible reason for the decrease of temperatures is, that most of the zirconium is oxidized – the rate of the reaction has slowed down due to zirconium exhausting. Additionally, the maximum amount of the produced hydrogen at a given location is limited by the amount of zirconium present at that location after melting and relocation of the zirconium.

Increasing the quench water temperature, presented in Figures A.31 ÷ A.35, does not result in significant changes of temperatures. Only in case with 80°C there are higher values (of about 100°C) for temperatures in the bundle. For produced hydrogen, there is only a little difference between the case with 80°C and other cases (about 20 %), but the values are below the measured one. In conclusion, there is noticeable change in the results only in the case with quench water temperatures higher than 80°C.

Fast injection system is used to fill the lower plenum of the bundle at the beginning of quenching. It injects 4 liters of water for the time of 2 seconds. The system consists of a reservoir filled with water under a pressure of 6 bar. The reservoir is connected to the quench line by a pipe supplied with an electromagnetic valve. When the valve opens, the water goes into the lower plenum of the bundle. An investigation has been done on the effect of the flow rate of the fast injection system. A comparison of different cases is presented in Figures A-36

÷ A-40. The calculated cases were: 0 l/2s, 2.0 l/2s, 4.0 l/2s, 6.0 l/2s and 8.0 l/2s. The biggest differences are detected for the water levels in the bundle. In the case without fast water injection (case 0 l/s) the level in the bundle is kept low, what results in a slower cooling of the bundle itself. It causes a larger hydrogen production – 119 g, while in other four cases the total mass of the produced hydrogen is under the measured value (58 g).

Higher cooling speed results in bigger degradation of the core due to the damage caused by thermal shock. Claddings will collapse due to the thermal shock associated with quenching. In the cases of using higher mass flow for fast injecting water, ATHLET-CD predicts less amount of generated hydrogen. It is due to the fact that the code does not consider degradations caused by a high-speed cooling of the core. That is another weak point of the ATHLET-CD2.2A, which should be corrected for simulation of scenarios with quick flooding of overheated core by emergency core cooling systems (ECCS).

Finally, the calculations showed that the correct simulation of the core degradation phenomena is strongly dependent on the choice of the code input parameters like the threshold oxide layer thickness used as a trigger value for initiation of the breakaway oxidation. It was identified that application of correct zirconium oxidation kinetics is very important for appropriate simulation.

5.4   Influence of nodalization parameters on the results

Additionally, in this section an examination on the effect of different nodalization on the accuracy in the simulation of QUENCH-12 was performed. The objective was to check the availability of different nodalization schemes. User effects are any differences in calculations that adopt the same code version and the same initial and boundary conditions for a given plant or facility. The main source of code user effects on the calculated results is the nodalization of the system. It is the responsibility of the user, to develop an adequate nodalization for the given facility. An adequate nodalization for a given plant or facility to be analysed is usually unknown because no general criteria are given. Consequently, the accuracy of a calculation is related to the choices of the user who prepares the input deck.

ATHLET provides a modular network approach for the representation of a thermal-hydraulic system. A given system configuration is simulated just by connecting basic fluiddynamic elements, called thermo-fluiddynamic objects. A benchmark of different nodalization schemes was performed with seven post-test calculations using different nodalizations. Thermo-fluiddynamic object type *pipe RV-CC* which represents the core bundle was divided in different number of control volumes consisting of 8, 14, 19, 26, 31, 38 and 50 nodes, accordingly. Calculations were made to see the influence of the number of control volumes and junctions on the simulation results. The control volume itself represents a spatial zone where the mass and energy balance equations are solved. The thermal-hydraulic properties of each node are considered to be concentrated at the central point of the control volume. The heat conduction objects in ATHLET (shroud, corner rods and grid spacers) and HEAT objects in ATHLET-CD (fuel rods) decompose axially into heat conduction volumes according to the adjacent thermo-fluiddynamic object. The size of the node is important, because when large nodes are used, the difference between the average temperature in the control volume

and the temperature at the node boundary can be considerable. This nodalization error can be reduced by applying finer grids with an increased computational time, but not always smaller nodes result in better simulations.

The results of the corresponding calculations are depicted at the end of the Appendix (Figures A.41 ÷ A.48). All the calculations were made using the Sokolov correlation for the zirconium oxidation and without transition of parabolic to linear oxidation kinetics. For each temperature two pictures are shown. From the results it can be seen that the ATHLET-CD2.2A code calculates similar temperatures for the different nodalization schemes. It can be observed, that reducing of the number of control volumes tends to give higher predictions of the temperatures at the quench phase. The highest values have been predicted by the versions with 8 and 50 control volumes. Using smaller control volumes reduces the thermal inertia (it is very important) in the bundle which consequently allows temperature gradients to be simulated more accurately. Temperatures in the cases with 8 and 14 control volumes exhibit little offset with time (Figures A.41 ÷ A.43). In the preoxidation phase the lowest temperatures are calculated with 19 control volumes and the highest with 8 control volumes. Except the case with 19 control volumes, all other nodalizations predicted higher temperature in the quench phase for the centre line of the central rod than measured by thermocouple in the experiment. It is expected that the peak in the temperatures at the quench phase should be lower in comparison with the measurement due to the fact that following phenomena are not considered in ATHLET-CD: breakaway, failure of the shroud, melting of grid spacers and corner rods. The calculated temperatures are varying within a range of about 250°C. The main deviations between the calculated and the measured temperatures are observed in the cases with 8, 14, 38 and 50 control volumes. It can be summarized that runs with the number of control volumes under 19 and more than 31 give significant deviations in the temperatures and in both cases they are higher than the measured ones.

The next point of interest is the hydrogen production (Figure A.44). The amount of hydrogen generated during the preoxidation calculated by ATHLET-CD for all cases is higher compared to the measured hydrogen release in the test QUENCH-12. The biggest amount of hydrogen is calculated using 8 control volumes. All values, except the case with 8 control volumes, calculated by ATHLET-CD2.2A for total hydrogen generation are lower than the measured ones. The lowest value of the total amount of hydrogen was calculated in the case with 19 control volumes. Further changes in the number of control volumes resulted in bigger mass of generated hydrogen. The reason for overprediction of hydrogen in the case with 8 control volumes is the higher temperature.

The water level is a parameter which also shows some deviations. As it can be seen from the Figure A.45 the mainstream of results is in good agreement with the experimental data except for the simulations with 8 and 14 control volumes. In the case with 8 control volumes water level exhibits significant deviation. It can be considered as the worst case. For other cases no significant trends have been observed with respect to increasing the number of the control volumes.

It can be deduced from all the results that discrepancies in the calculations are the largest at the quench initiation. It can be explained by the fact that this is the time with highly transient

behaviour of the solution variables – it is the time with strongly and rapidly changing physical states. Different nodalization schemes have different thermal inertia which results in significant deviations in highly transient states.

Table 2: CPU time and number of time steps as a function of the control volumes number

Number of control volumes	CPU time [s]	Number of time steps
8	460	25746
14	493	21222
19	822	31119
26	2002	58092
31	1048	23616
38	1419	25985
50	2441	32882

The observed discrepancies in the results could be due to the fact that different nodalizations lead to changes in the time step of integration. It must be kept in mind that not always a lower number of junctions and volumes lead to a faster calculation because in some cases rough nodalization increases the time steps. The time integration module FEBE is a general purpose solver based on an Euler method. The system of ordinary differential equations is integrated numerically as time advancement procedure. In Table 2 results for the CPU time and the number of time steps for the different runs are presented.

The integration error is caused by two types of error. The local truncation error is the difference between the exact solution of the equation and the numerical approximation - which is due to the use of a numerical algorithm. Because of that rounding error in the computing is due to the fact that computers can not represent some numbers exactly. Computers are able to represent exactly only integers in a certain range. Rounding errors are unavoidable in computing. The total integration error is due to both truncation and rounding error. As the time step size is reduced the truncation error decreases however rounding error increases as the step size is reduced because more calculations are made and the numbers are computed with finite accuracy. So, for extremely small values of the time step size the truncation error will be small but the effect of rounding error may be big. Decreasing the time step size does not always result in the increased accuracy of the obtained solution. Very small time step size in some cases may even cause a loss of accuracy leading to unreasonable states.

The biggest differences could be seen in the produced hydrogen. For the other results the deviations between calculations with different nodalizations schemes are relatively small. It is clear, that the nodalization scheme can have a significant impact on the accuracy of the simulations. It is very difficult to define the best size of the control volumes for given model. It

can be concluded that the best nodalization schemes for the test facility QUENCH-12 using computer code ATHLET-CD2.2A, concerning the *pipe RV-CC* which represents the core bundle, is with number of control volumes between 19 and 31. It could be deduced from the results presented in figures that increasing the number of nodes in axial direction lead to approaching the results obtained by models with little number of control volumes (8, 14). The exact reasons for the observed deviations could not be determined.

6   Conclusions

A post-test calculation of the QUENCH-12 experiment, complemented by a sensitivity analysis, was performed with the system code ATHLET-CD2.2A. The calculated results showed a good overall agreement with the experimental results concerning the thermal-hydraulic behaviour of the test bundle. The performed simulations adequately reproduce temperature evolution at different elevations during the whole test with only small discrepancies. In the thermo-hydraulics and the heat conduction no significant model weakness were found.

Calculations show inadequate work of the code with respect to hydrogen production rate. The difference between experimental data and calculation results in QUENCH-12 test is mainly due to breakaway oxidation of the bundle. Model for breakaway oxidation has not been yet fully developed in ATHLET-CD2.2A. By performing sensitivity calculation analysis it was found that the model of zirconium oxidation is significant weakness in the code. Uncertainties on modelling of zirconium oxidation (especially influence of breakaway effect) affect very strong the whole behaviour of the bundle.

Other reason for discrepancy in simulated hydrogen rate production is the fact that the hydrogen absorption by metal and its release actually cannot be simulated.

The oxidation of the heat conducting (HECU) structures (corner rods, shroud and grid spacers) is underestimated due to the fact that the failure of these structures cannot be simulated by ATHLET-CD2.2A. Moreover, the melt oxidation of these HECU structures is not taken into account in the computer code until now.

It can be summarized that further development of oxidation model, the melting model, hydrogen absorption in the metal bulk as well as breakaway effect is necessary to predict the severe accident behaviour of VVER-type reactors in more correct way. Consequently further development of the zirconium oxidation model is strongly recommended to support the ATHLET-CD application for deterministic safety analysis in nuclear power plants. Transition from parabolic to linear oxidation kinetics (criterion to start breakaway) should depend not only on oxide layer thickness but also on the temperature of zirconium. For the user it is very difficult to define the right value for oxide layer thickness in the input deck for the start of accelerated oxidation. Due to that, the calculation in chapter 5.2 was made without considering breakaway (no accelerated oxidation of zirconium in the bundle) which led to underestimation of the produced hydrogen and the temperatures in the bundle.

ATHLET-CD cannot describe different rod types inside the same bundle. Corresponding improvements should be made to describe such structures like unheated rods and corner rods.

Finally, a study was made on the effect of different nodalization on the accuracy in the simulation of QUENCH-12 using ATHLET-CD2.2A. The results of the simulations were significantly affected by the chosen nodalization schemes. The most accurate results were achieved by using a number of control volumes between 19 and 31.

Any testing process of computer codes can only identify and fix the errors encountered in modelling of specific integral experiments. Therefore, it is important to validate the codes on the basis of good instrumented bundle experiments (like QUENCH tests). As it is known, the number of defects in a computer program increases linearly with its size and exponentially with its complexity. Such codes can be correctly validated only with the help of a wide spectrum of experiments.

Acknowledgements

References

[1]   Accident Analysis for Nuclear Power Plants, Safety Report Series No. 23, IAEA, Vienna, Austria, October 2002. http://www-pub.iaea.org/mtcd/publications/pdf/pub1131_scr.pdf

[2]   Approaches and Tools for Severe Accident Analysis for Nuclear Power Plants, Safety Report Series № 56, IAEA, Vienna, Austria, 2008. http://www-pub.iaea.org/MTCD/publications/PDF/Pub1327_web.pdf

[3]   P. Hofmann, "Current knowledge on core degradation phenomena, a review", Journal of Nuclear Materials 270 (1999) 194-211.

[4]   A. Pautz, K. Velkov, H. Glaeser, M. Sonnenkalb, J. Sievers, "Scientific Codes Developed and Used at GRS Volume 1: Reactor Safety", Gesellschaft für Anlagen- und Reaktorsicherheit (GRS) mbH, June 2011. http://www.grs.de/sites/default/files/pdf/GRS_Codes_.pdf

[5]   Gesellschaft für Anlagen- und Reaktorsicherheit, GRS Annual Report 2008, 2008. http://www.grs.de/sites/default/files/pdf/Annual%20Report%202008.pdf

[6]   G. Bandini, H. Austregesilo, M. Buck, O. Marchand, F. Fichot, M. Barnak, P. Matejovic, L. Humphries, K. Suh, S. Paci, "Ability of current advanced codes to predict core degradation, melt progression and reflooding. Benchmark exercise on an alternative TMI-2 accident scenario", NUCLEAR ENERGY AGENCY COMMITTEE ON THE SAFETY OF NUCLEAR INSTALLATIONS, NEA/CSNI/R(2009)3. http://www.oecd-nea.org/nsd/docs/2009/csni-r2009-3.pdf

[7]   L. Sepold, W. Hering, G. Schanz, W. Scholtyssek, M. Steinbrück, J. Stuckert, Severe fuel damage experiments performed in the QUENCH facility with 21-rod bundles of LWR-type. Nuclear Engineering and Design 237 (22), 2007.

[8]   J. Stuckert, J. Birchley, M. Große, T. Haste, L. Sepold, M. Steinbrück, Experimental and post-test calculation results of the integral reflood test QUENCH-12 with a VVER-type bundle, Annals of Nuclear Energy 36 (2009) 183–192.

[9]   J. Stuckert, A. Goryachev, M. Große, M. Heck, I. Ivanova, G. Schanz, L. Sepold,U. Stegmaier, M. Steinbrück, Results of the QUENCH-12 Experiment on Reflood of a VVER-type Bundle, Scientific Report FZKA-7307, Karlsruhe, 2008. http://bibliothek.fzk.de/zb/berichte/FZKA7307.pdf.

[10]   В.Д. Шмелев, Драгунов Ю.Г., Денисов В.П., Васильченко И.Н., Активные зоны ВВЭР для атомных электростанций, ИКЦ "Академкнига", 2004. (in Russian)

[11]   M. Steinbrück, Birchley J., Boldyrev A.V., Goryachev A.V., Grosse M., Haste T.J., Hozer Z., Kisselev A.E., Nalivaev V.I., Semishkin V.P., Sepold L., Stuckert J., Ver N., Veshchunov M.S., High-temperature oxidation and quench behaviour of Zircaloy-4 and E110 cladding alloys, Progress in Nuclear Energy 52 (2010) 19–36.

[12]   R. Semeria and B. Martinet, "Calefaction Spots on a Heated Wall, Temperature Distribution and Resorption," presented at IME Symposium on Boiling Heat Transfer in Steam Generating Units and Heat Exchangers, Manchester, England, September 15-16, 1965.

[13]   G. Forsythe, Malcolm M., Moler C., Computer Methods for Mathematical Computations, PRENTICE-HALL, 1977.

[14]   K. Trambauer, Bals C., Schubert J., Austregesilo H., ATHLET-CD Mod- 2.2 Cycle A – User's Manual, Gesellschaft für Anlagen- und Reaktorsicherheit (GRS) mbH, 2009.

[15]   G. Lerchl, Austregesilo H., ATHLET Mod 2.2 Cycle A – User's Manual, Gesellschaft für Anlagen- und Reaktorsicherheit (GRS) mbH, 2009.

[16]   M. S. Veshchunov, J. Stuckert, A.V. Berdyshev. „Modelling of Zr-O and U-Zr-O melts oxidation and new crucible tests ". Scientific report FZKA-7373. Karlsruhe, April, 2008. http://bibliothek.fzk.de/zb/berichte/FZKA6792.pdf

[17]   M. Steinbrück, N. Ver, M. Große. "Oxidation of Advanced Zirconium Cladding Alloys in Steam at Temperatures in the Range of 600–1200 °C". Oxid Met (2011) 76:215–232.

Appendix (diagrams from sensitivity analysis)

A 1. Steam flow rates
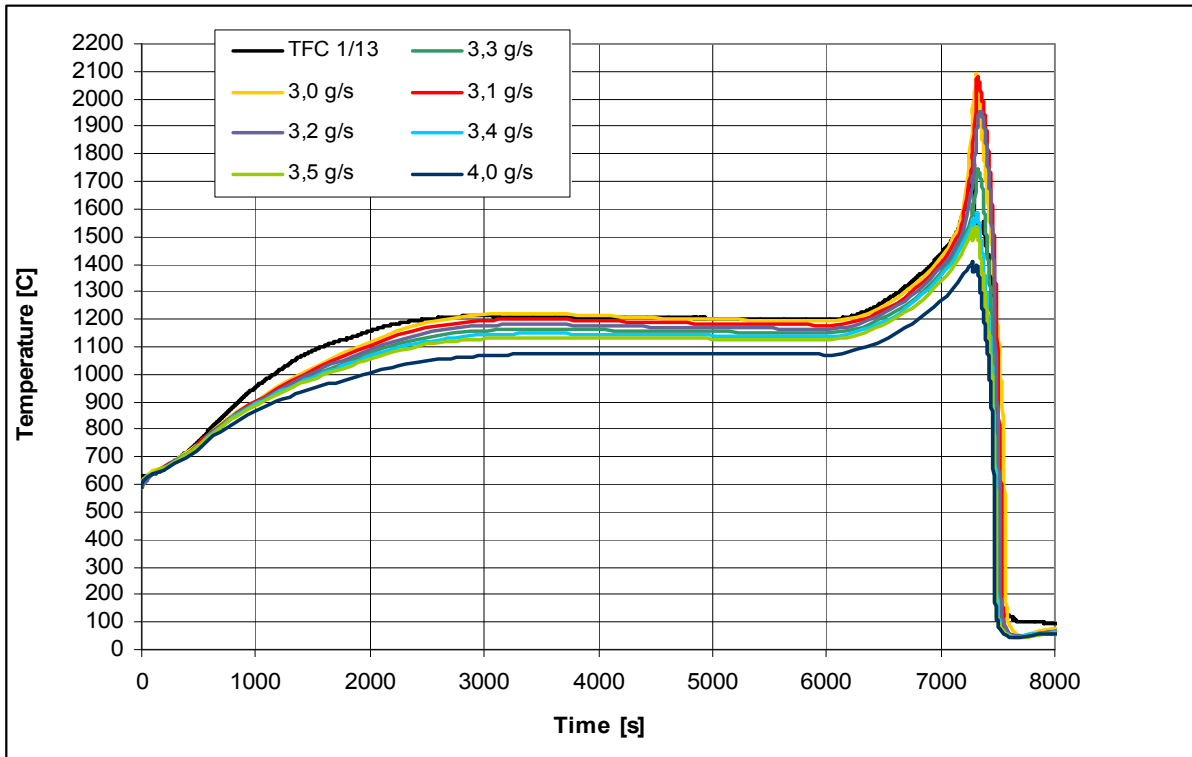
Figure A 1.1: Temperatures at the elevation 950 mm in the centre line of the central rod
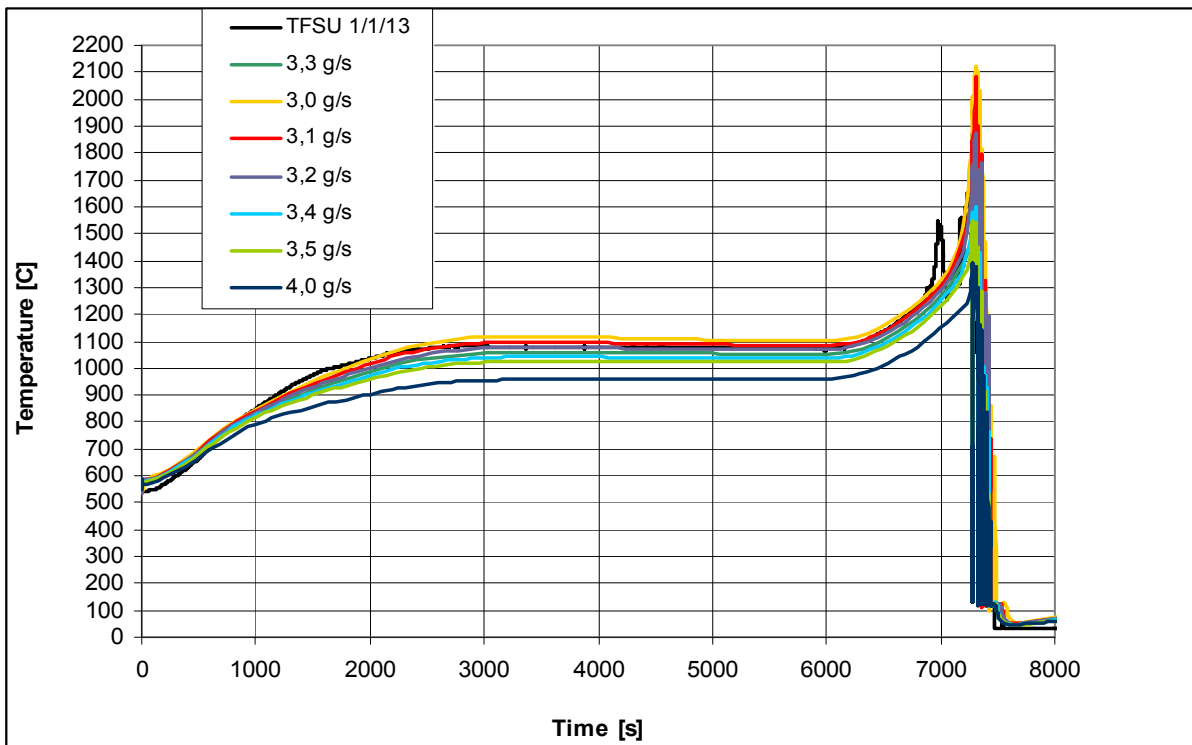
Figure A 1.2: Fluid temperatures at the elevation 950 mm in the bundle
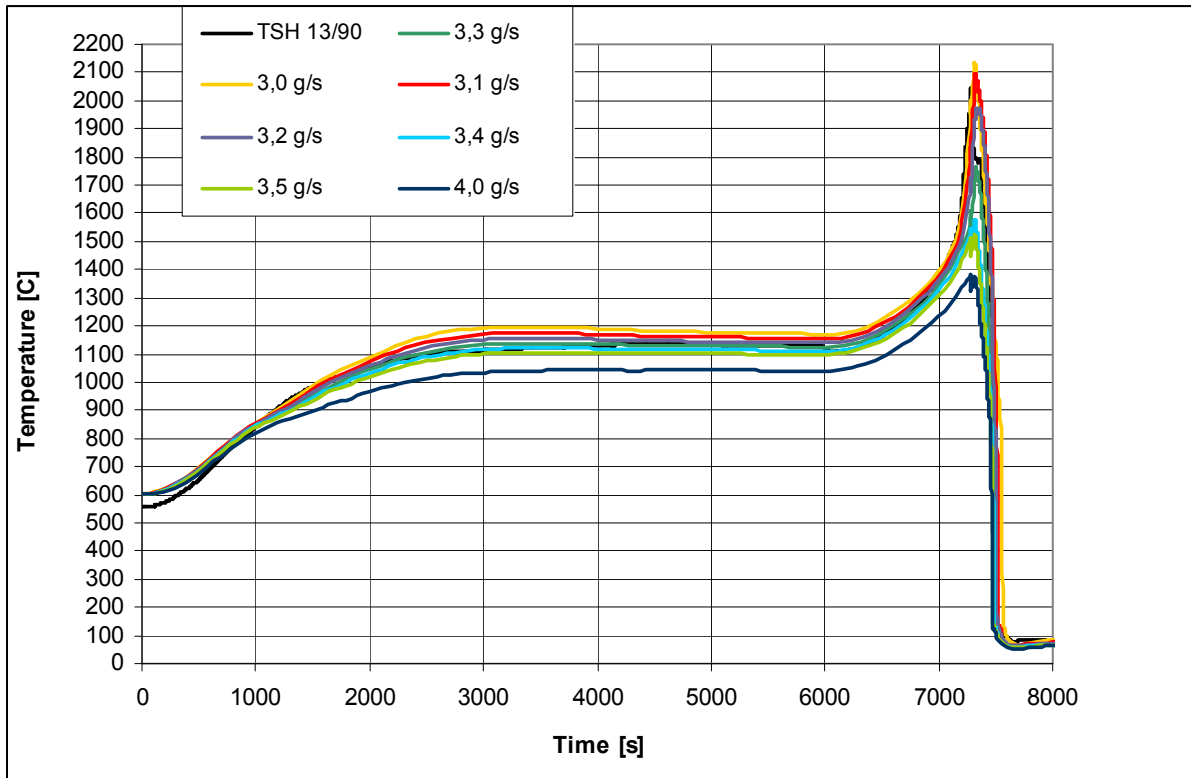
Figure A 1.3: Shroud temperature at the elevation 950 mm
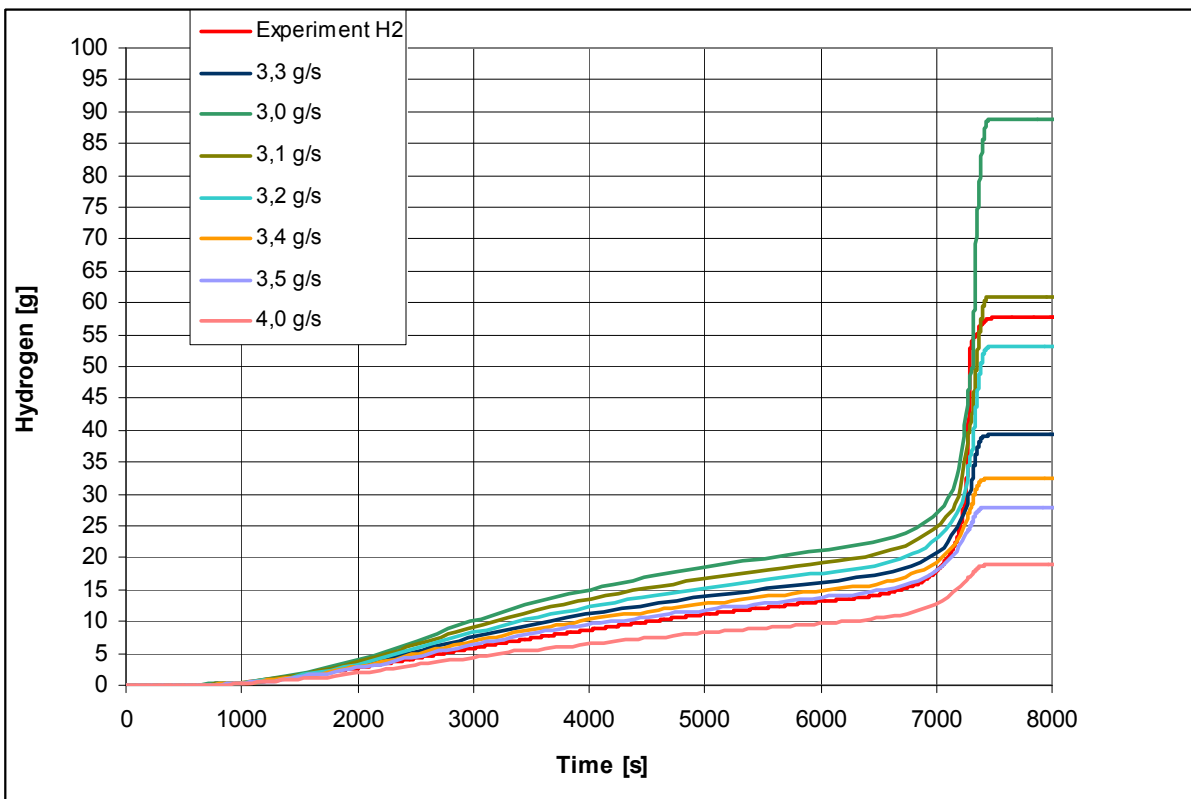
Figure A 1.4: Total hydrogen production: sensitivity analysis
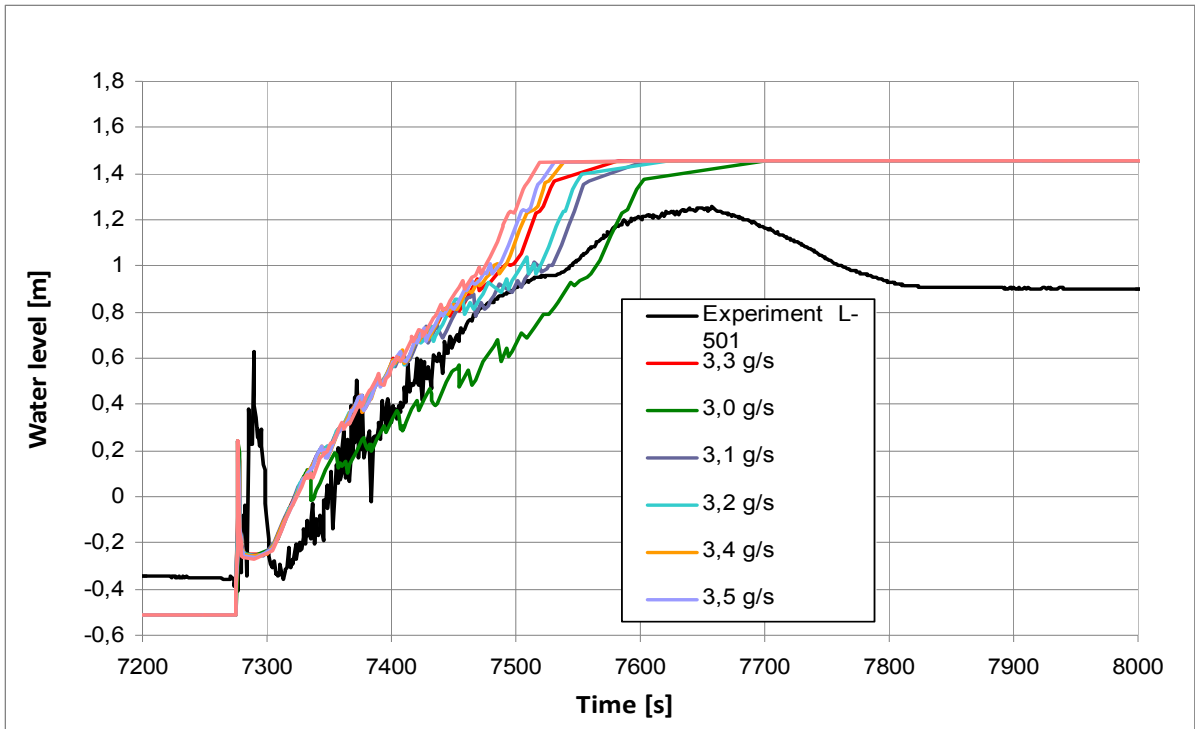
Figure A 1.5: Water level in the bundle

A 2. Reflood rates
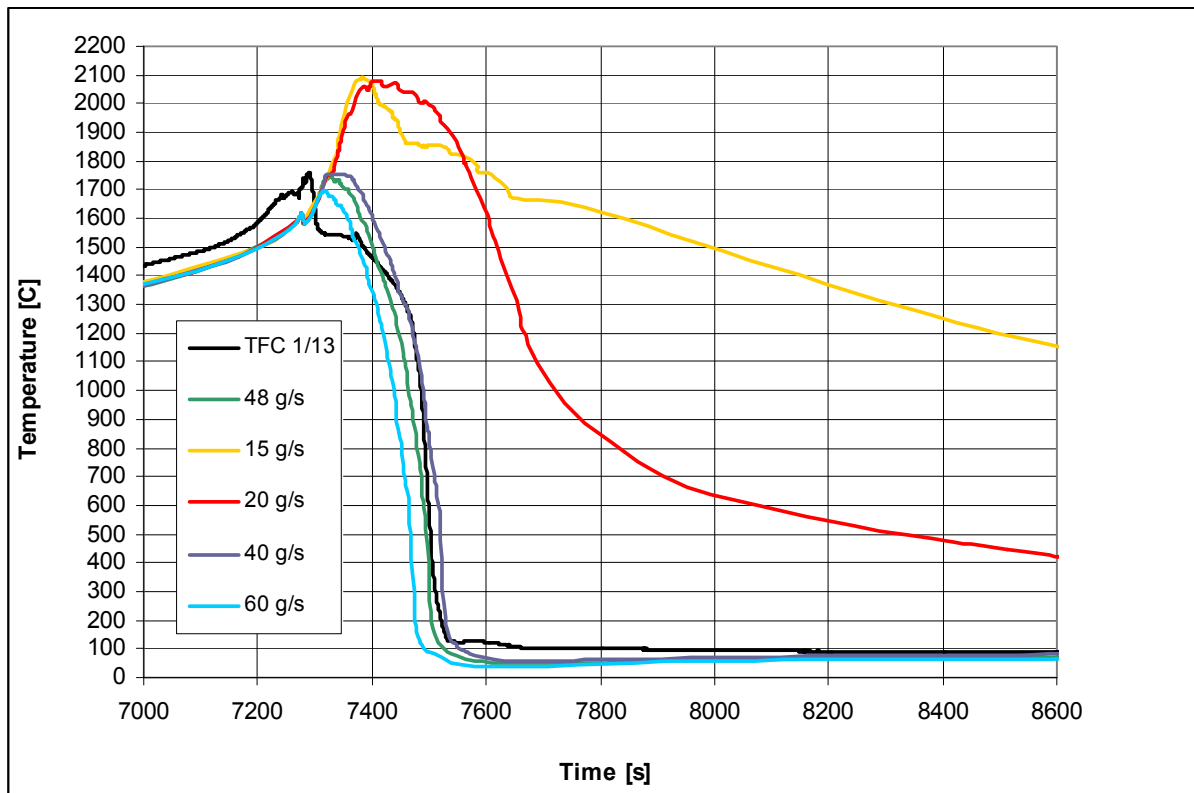
Figure A 2.1: Temperatures at the elevation 950 mm in the centre line of the central rod
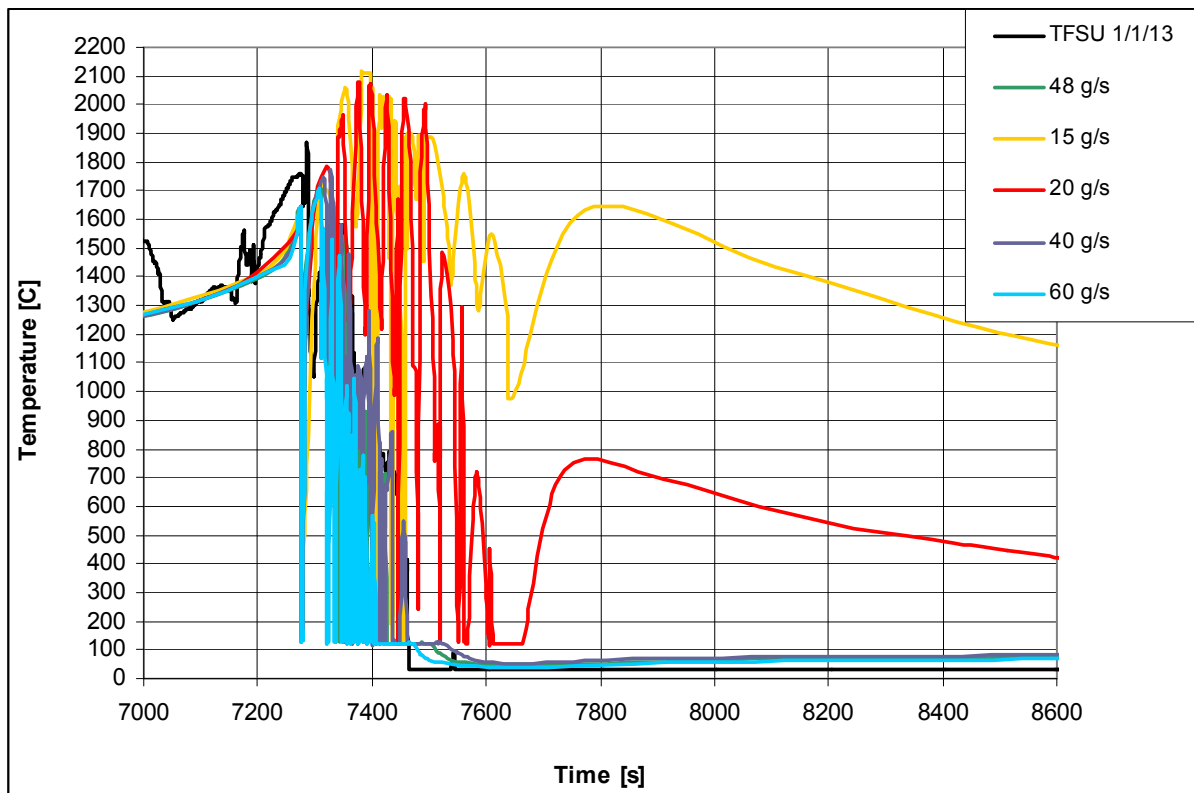
Figure A 2.2: Fluid temperatures at the elevation 950 mm in the bundle
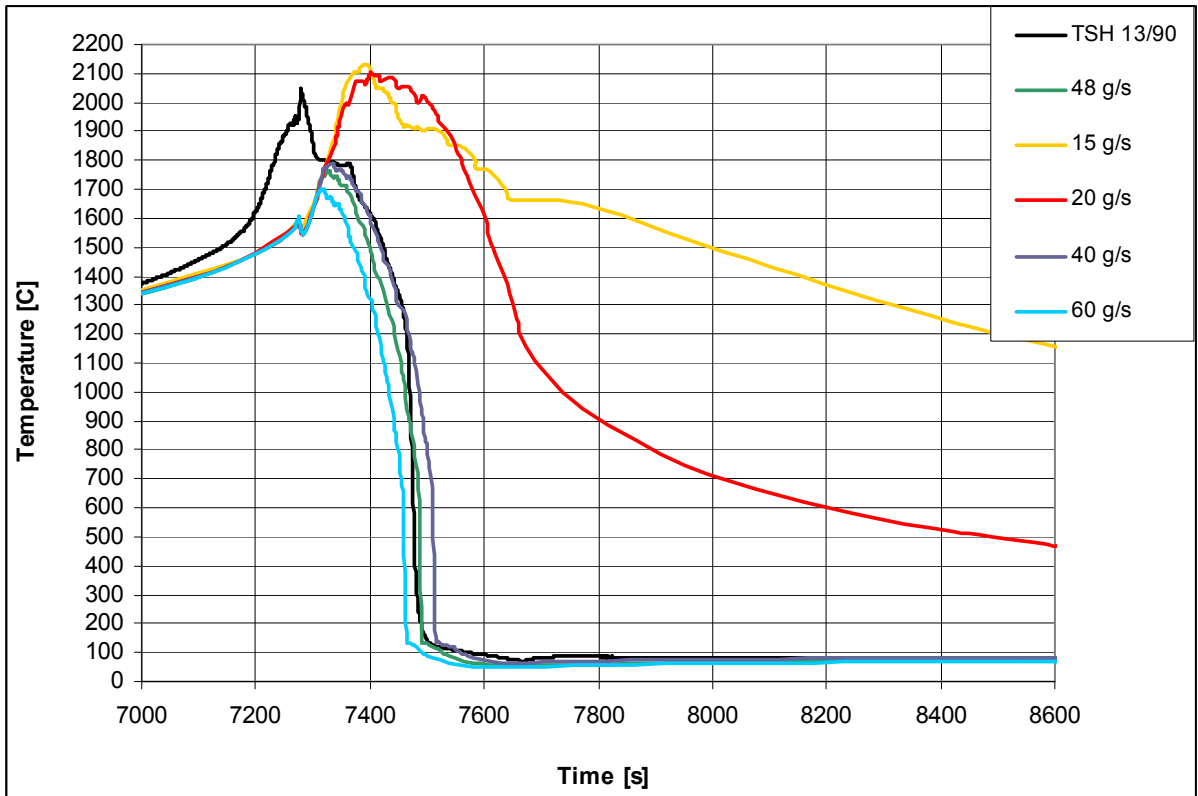
Figure A 2.3: Shroud temperature at the elevation 950 mm
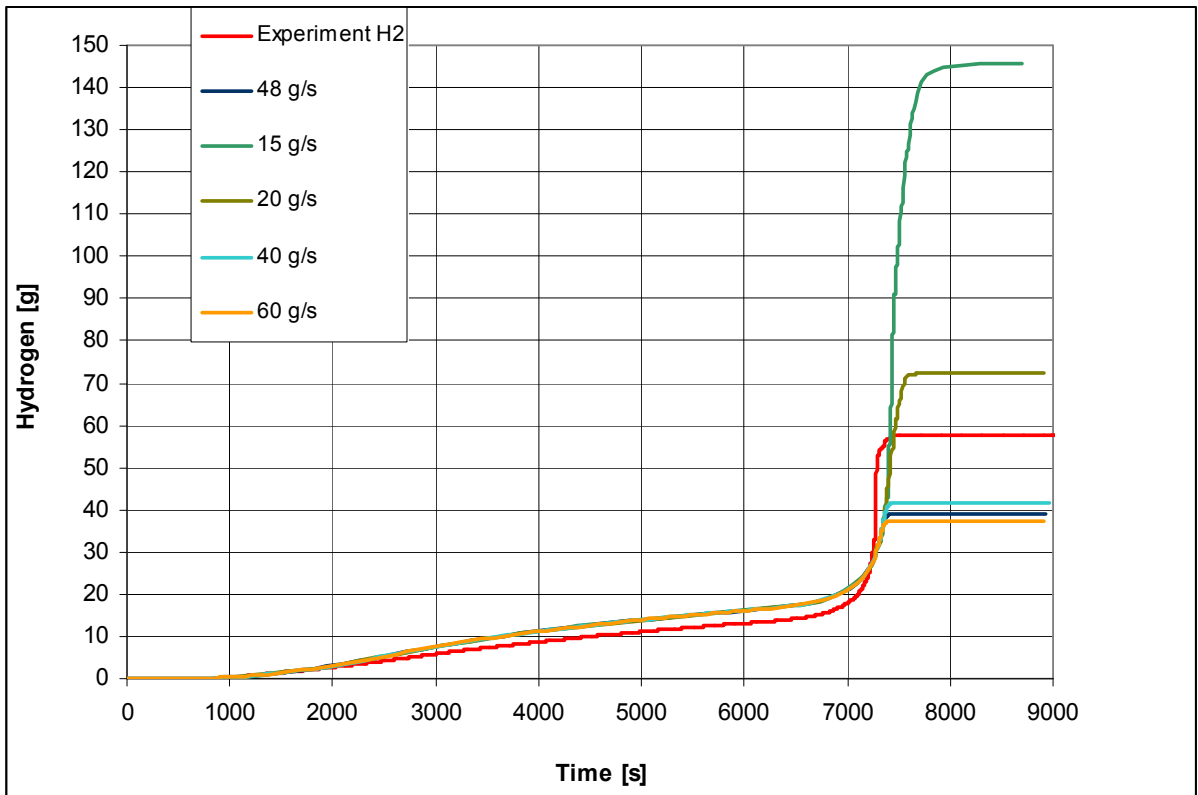
Figure A 2.4: Total hydrogen production during the QUENCH-12 experiment
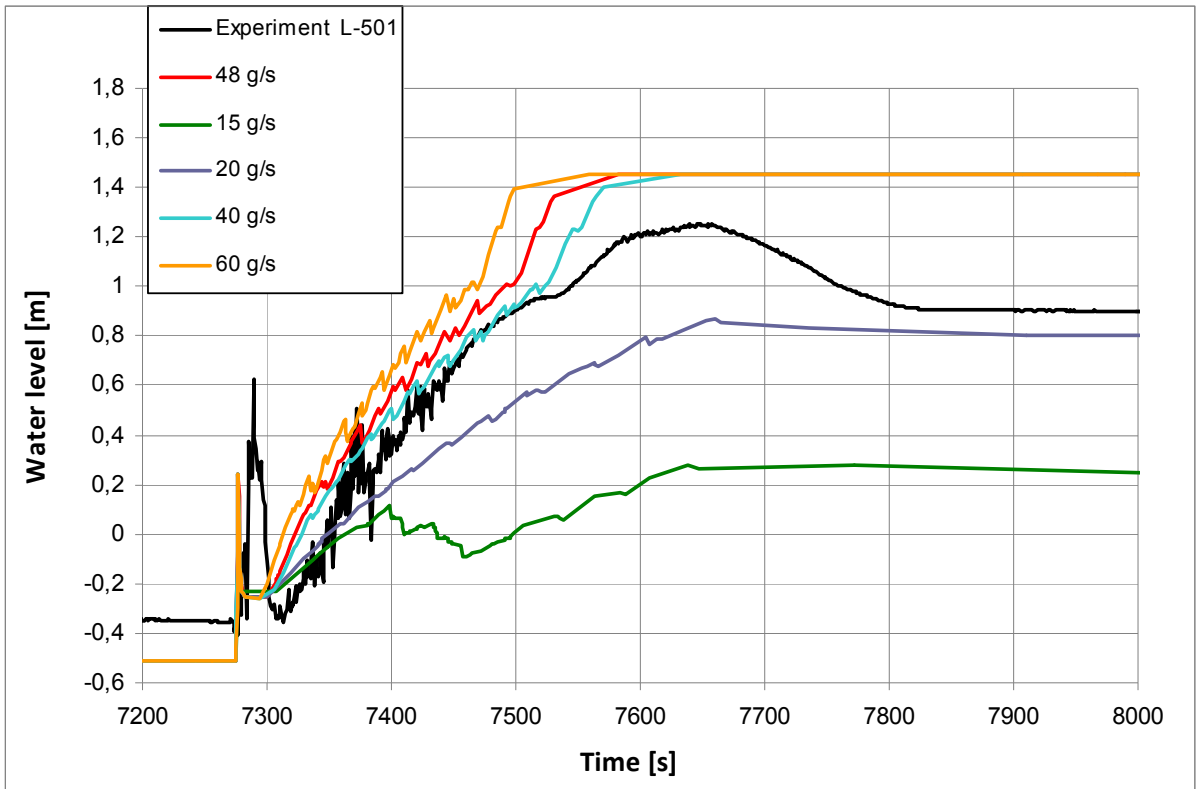
Figure A 2.5: Water level in the bundle

A 3. Argon flow rates
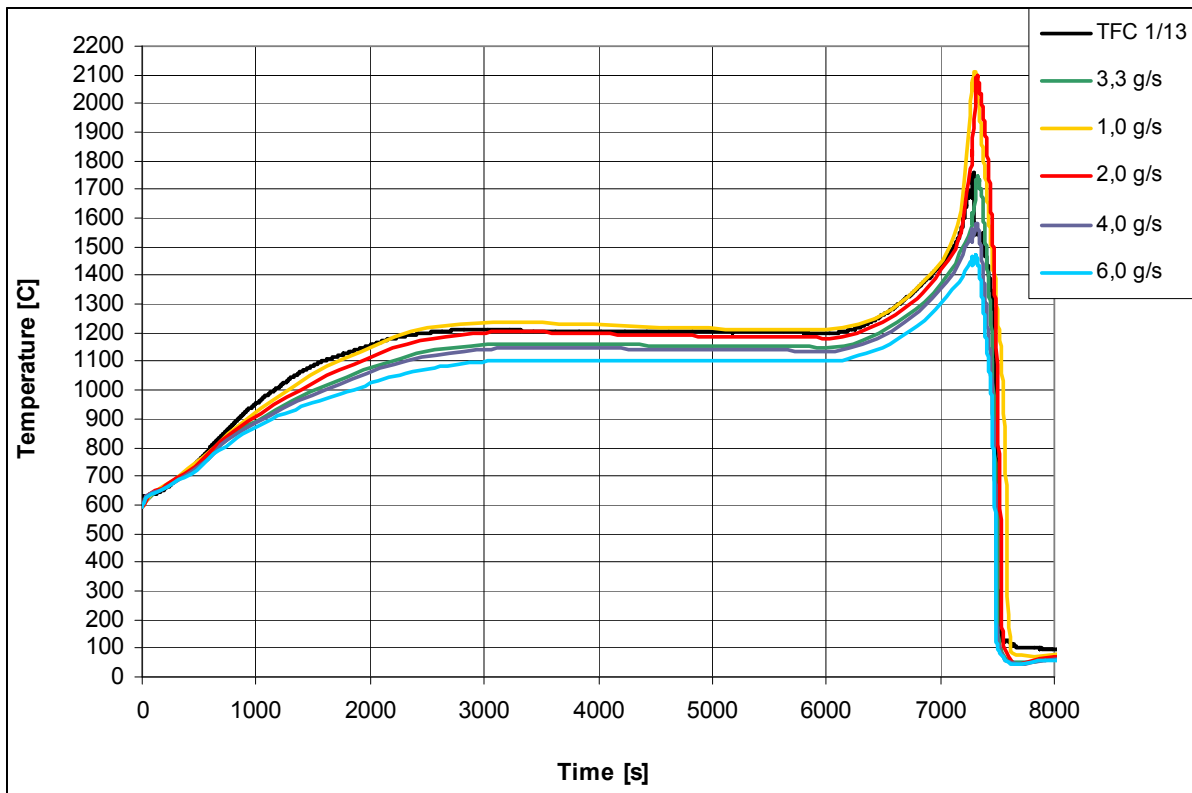
Figure A 3.1: Temperatures at the elevation 950 mm in the centre line of the central rod
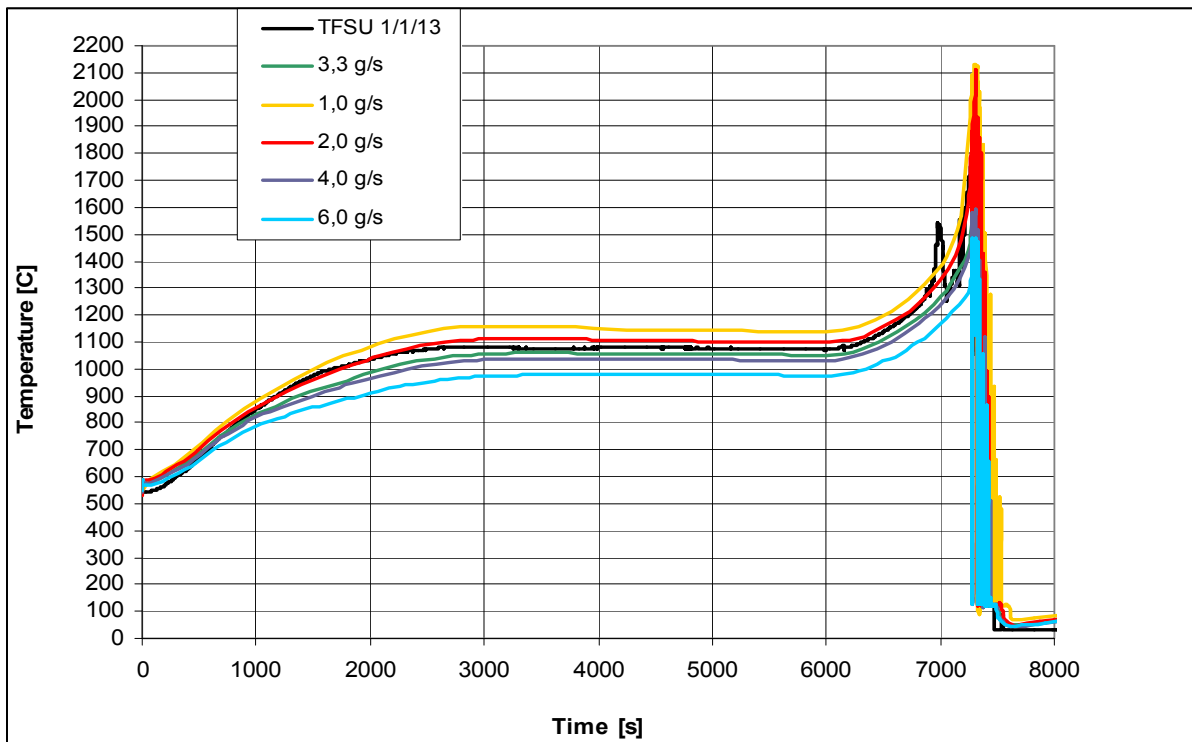
Figure A 3.2: Fluid temperatures at the elevation 950 mm in the bundle
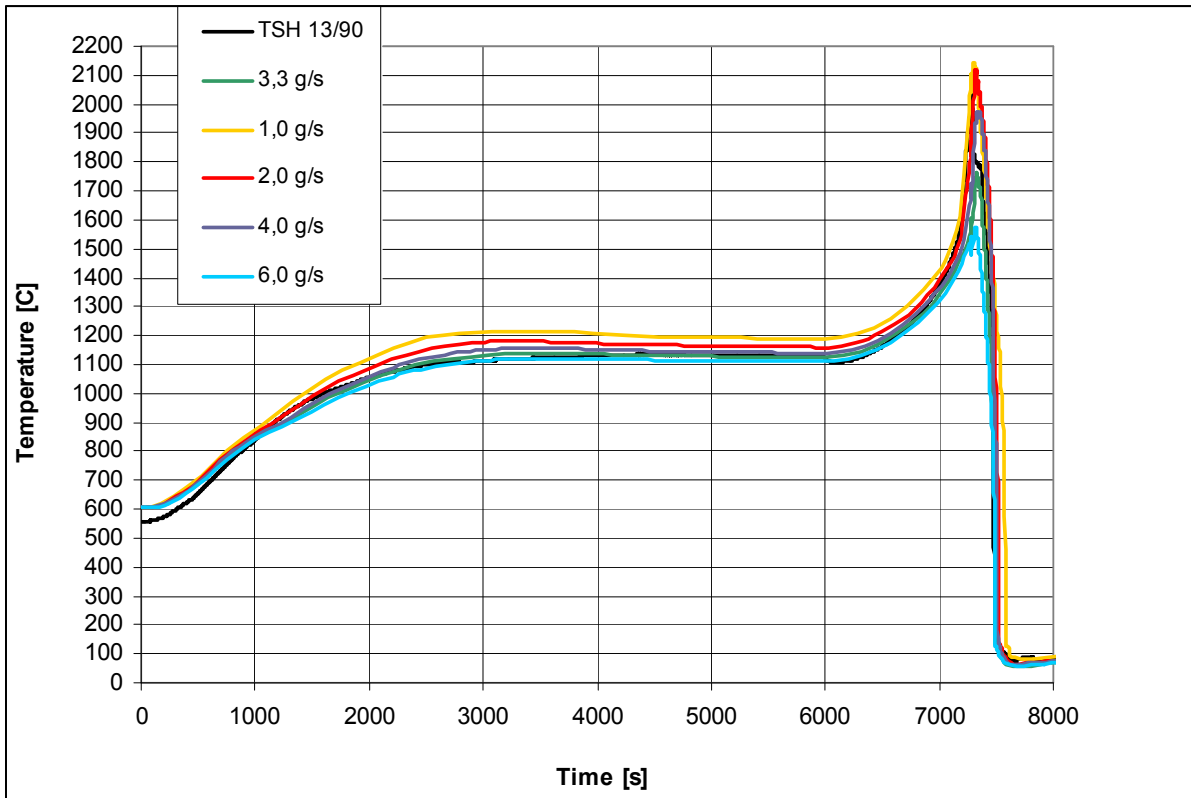
Figure A 3.3: Shroud temperature at the elevation 950 mm
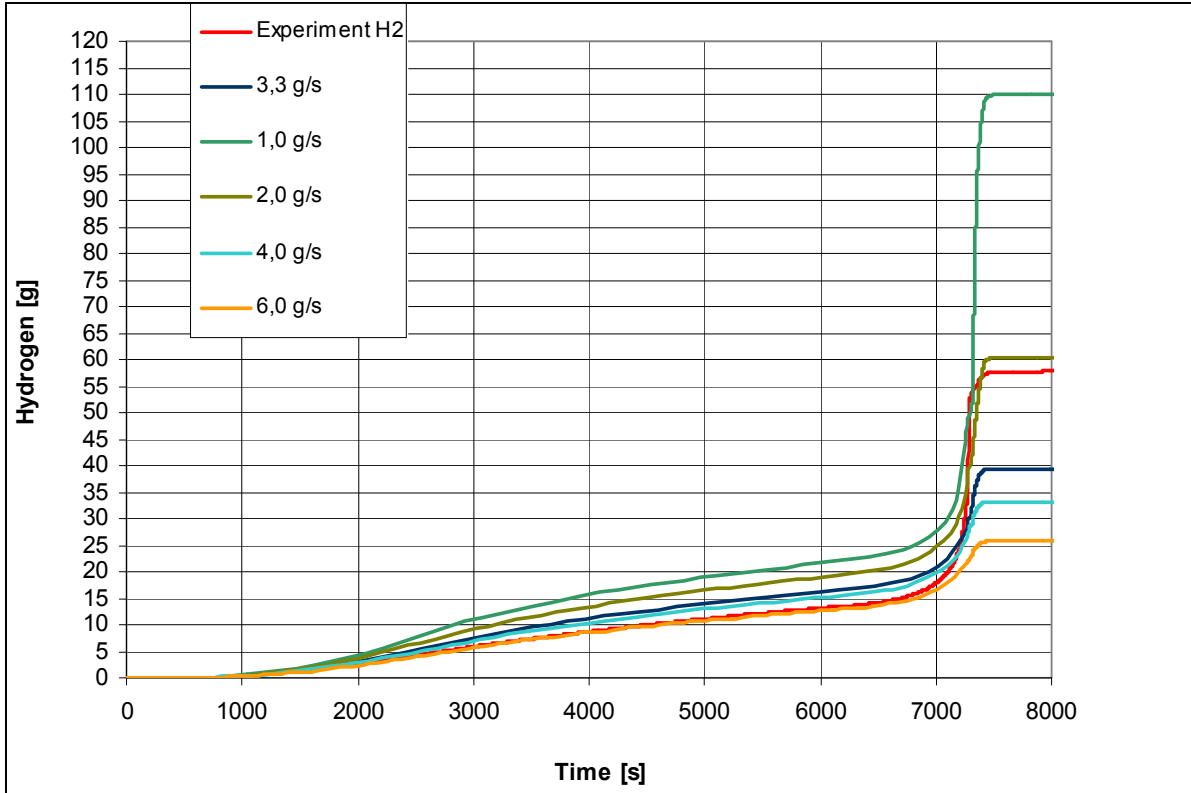
Figure A 3.4: Total hydrogen production: sensitivity analysis
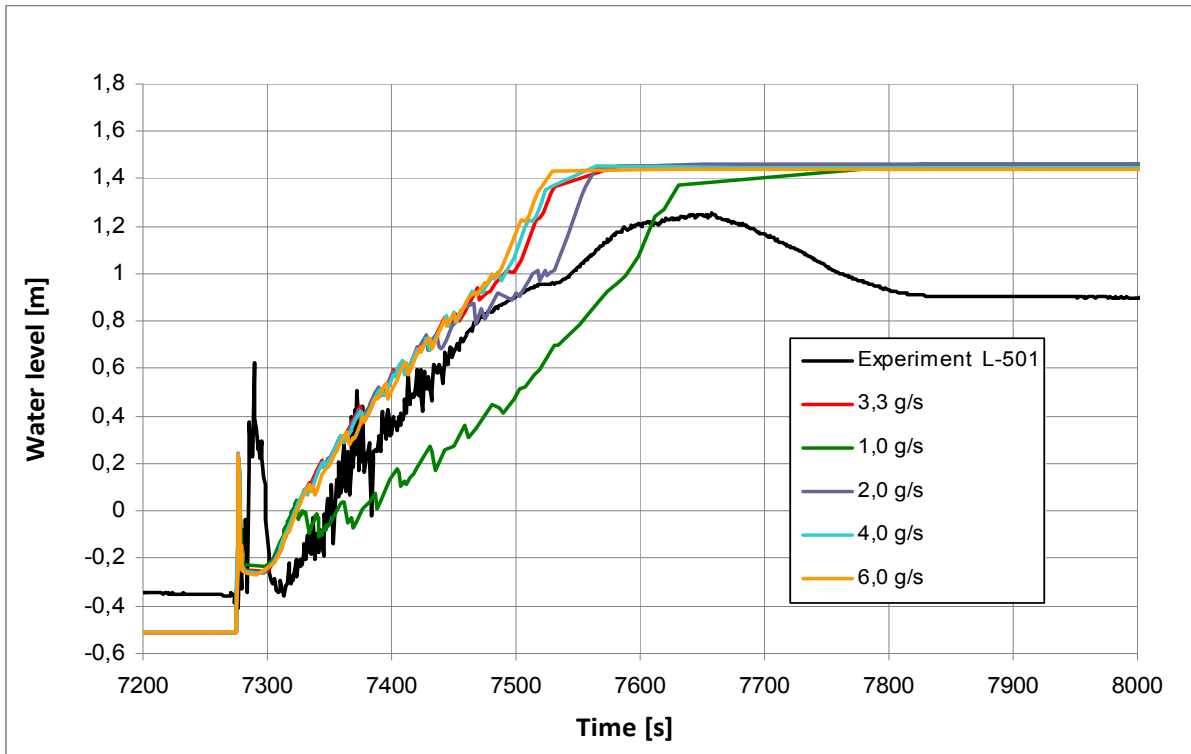
Figure A 3.5: Water level in the bundle: sensitivity analysis

A 4. External resistance per rod
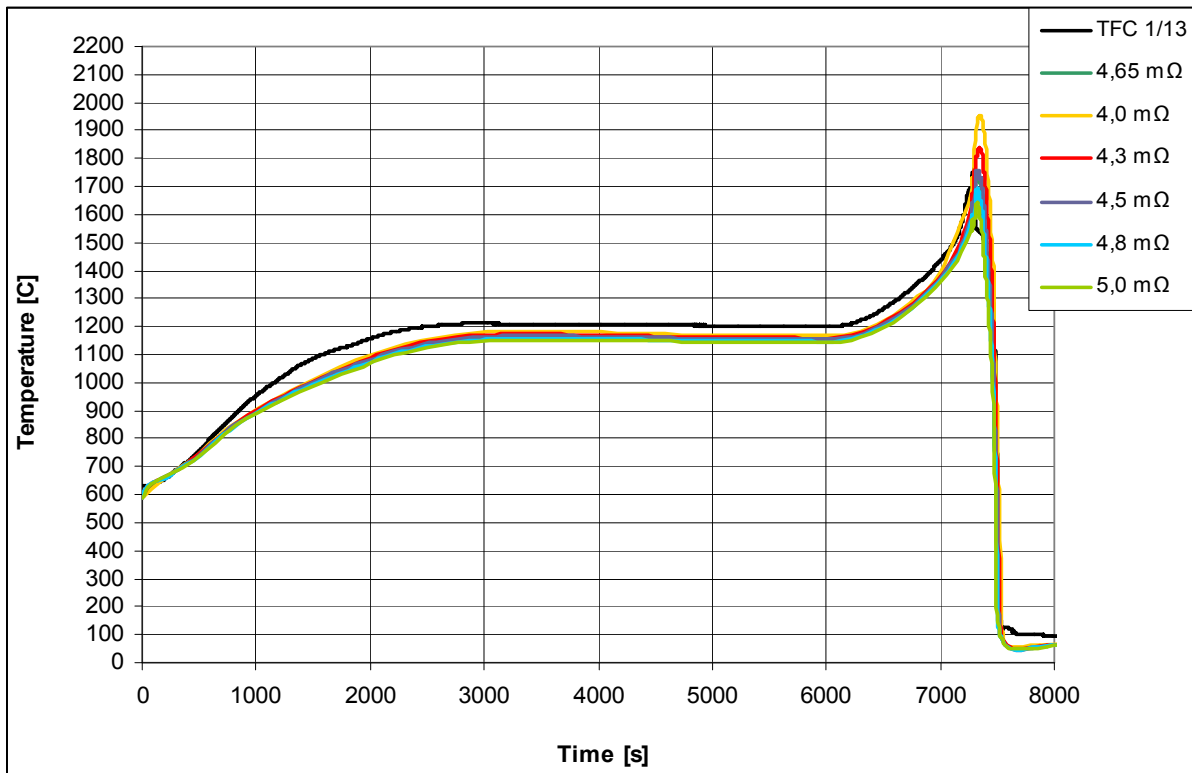
Figure A 4.1: Temperatures at the elevation 950 mm in the centre line of the central rod
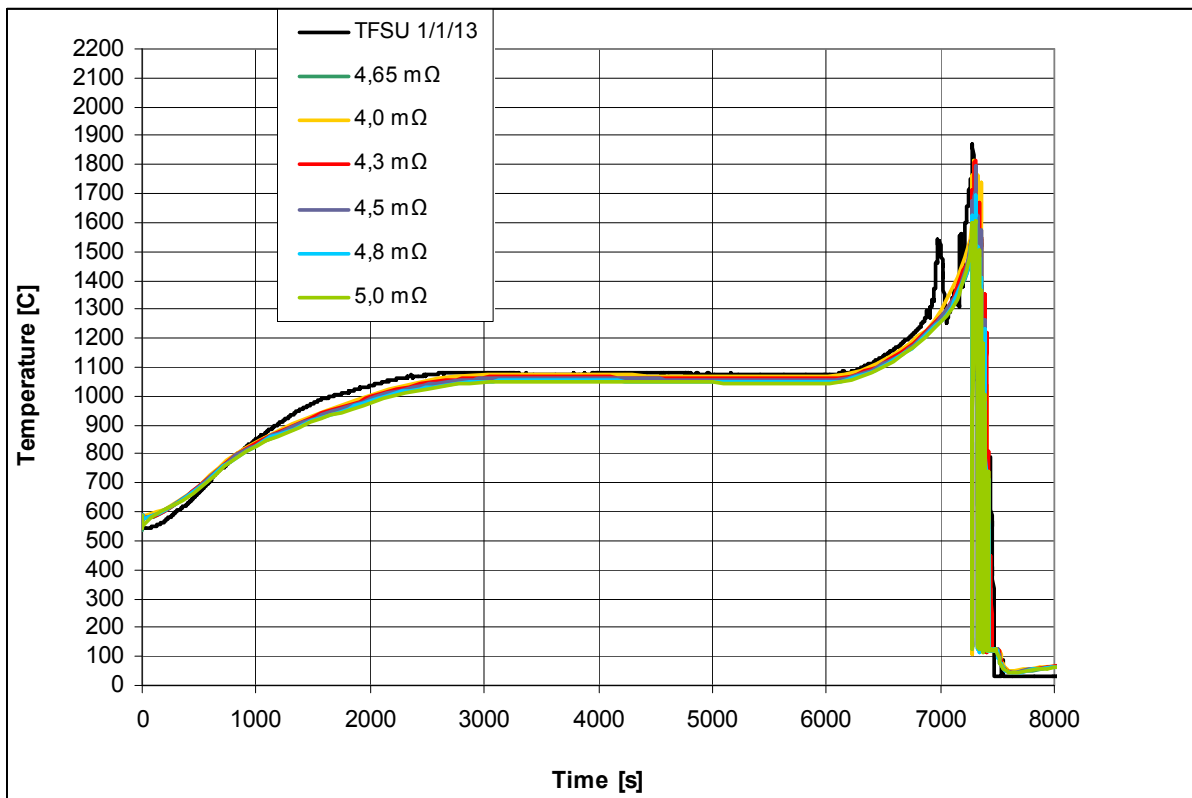
Figure A 4.2: Fluid temperatures at the elevation 950 mm in the bundle
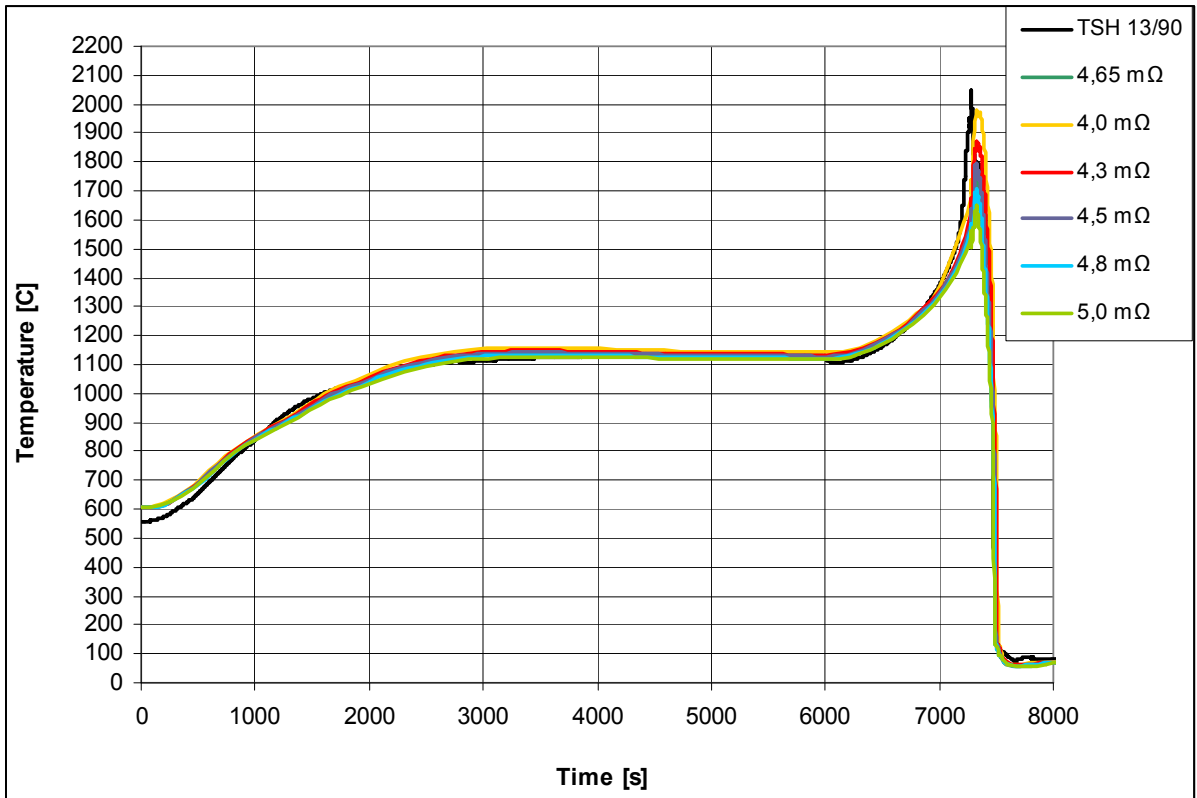
Figure A 4.3: Shroud temperature at the elevation 950 mm
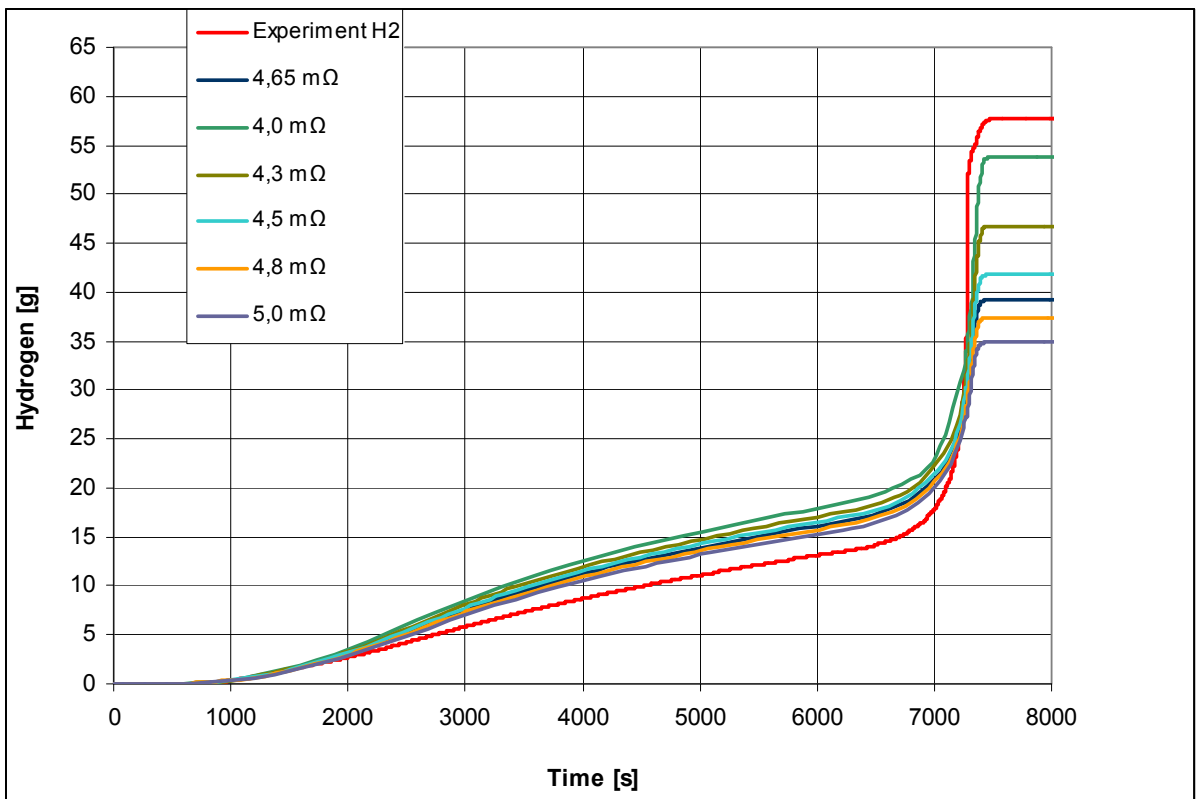
Figure A 4.4: Total hydrogen production: sensitivity analysis
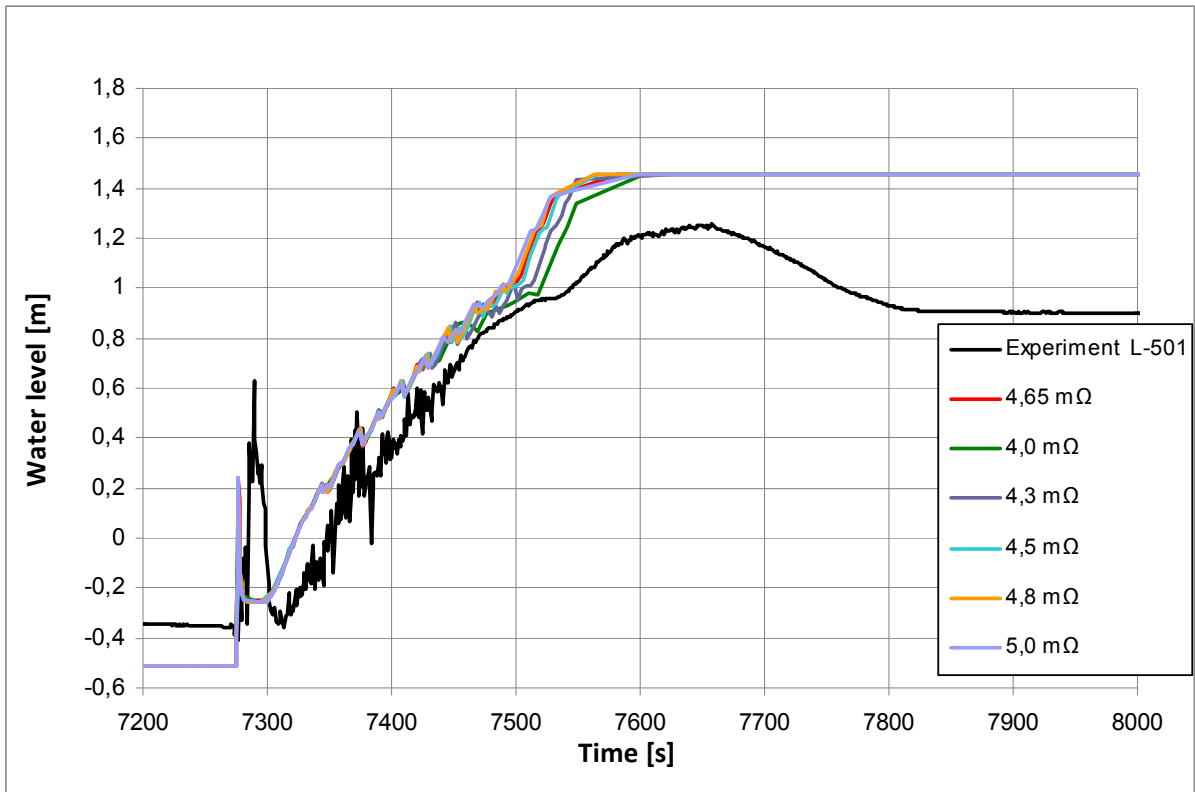
Figure A 4.5: Water level in the bundle: sensitivity analysis

A 5. Correlations for zirconium oxidation
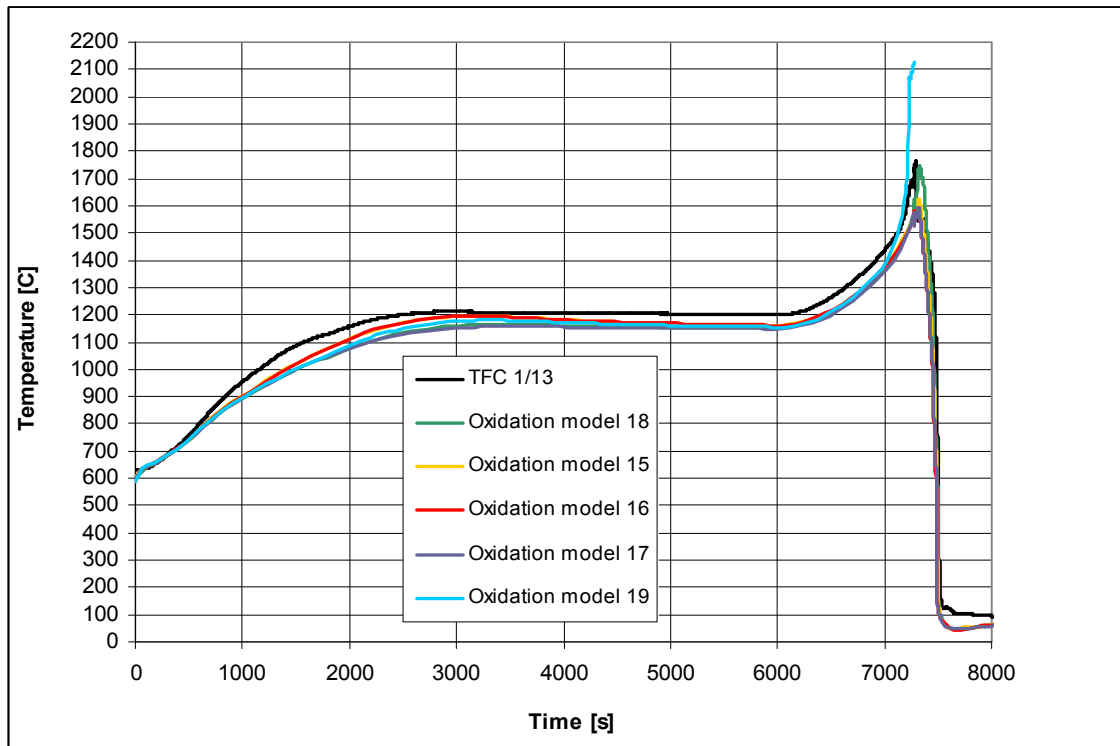
Figure A 5.1: Temperatures at the elevation 950 mm in the centre line of the central rod
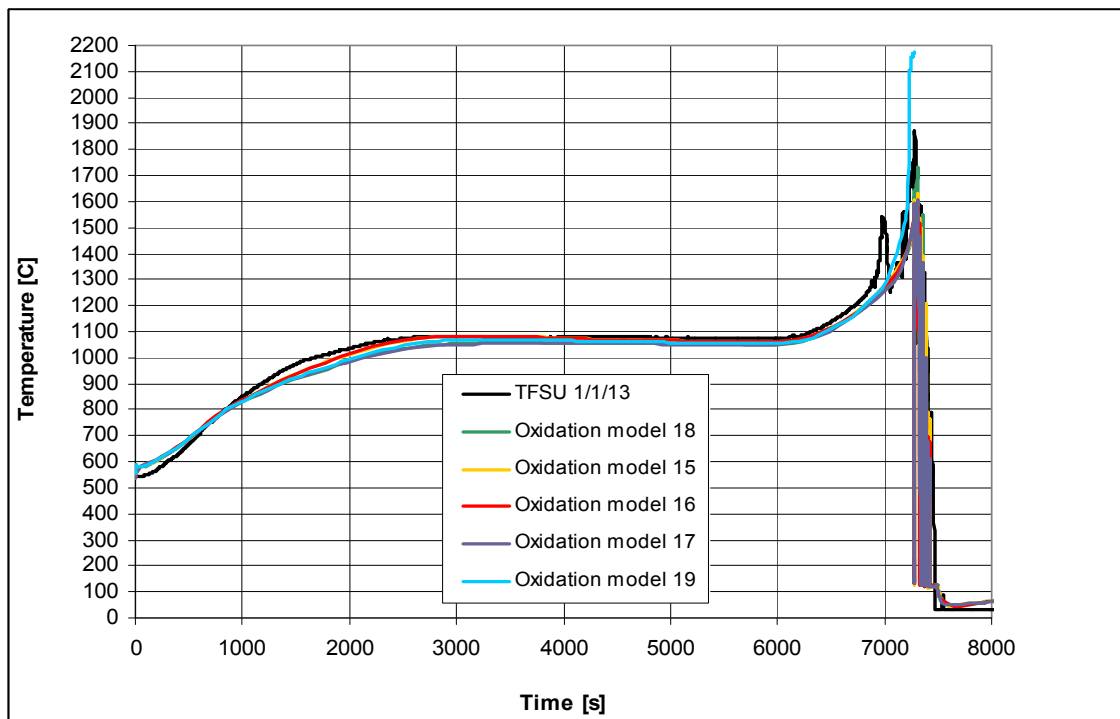
Figure A 5.2: Fluid temperatures at the elevation 950 mm in the bundle
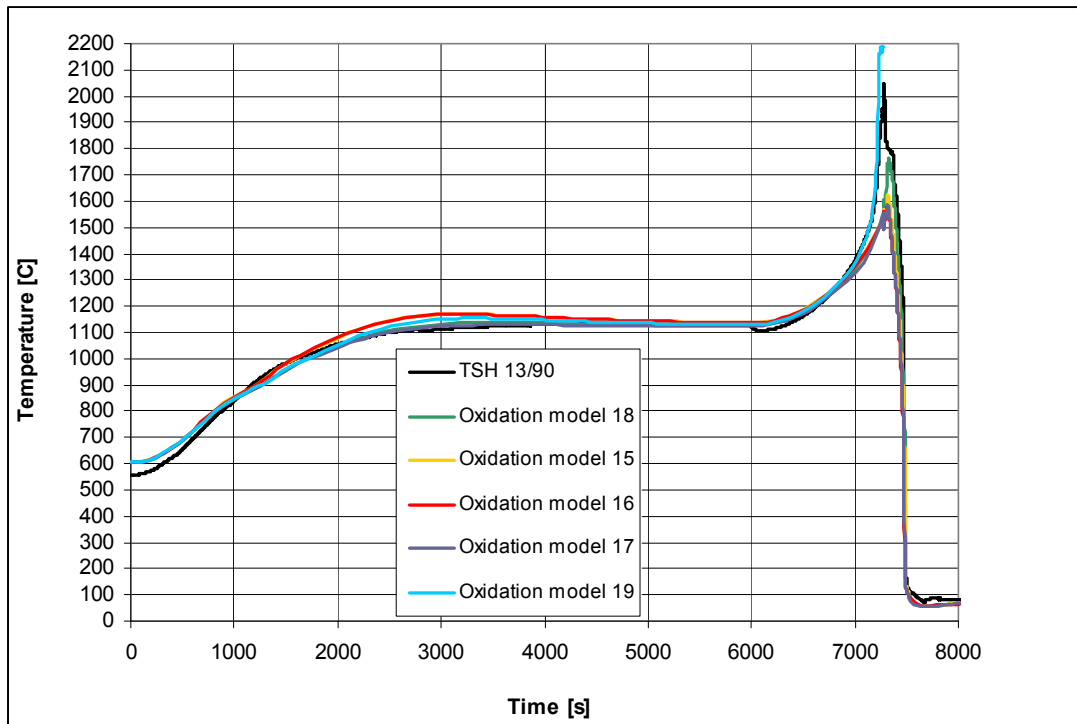
Figure A 5.3: Shroud temperature at the elevation 950 mm
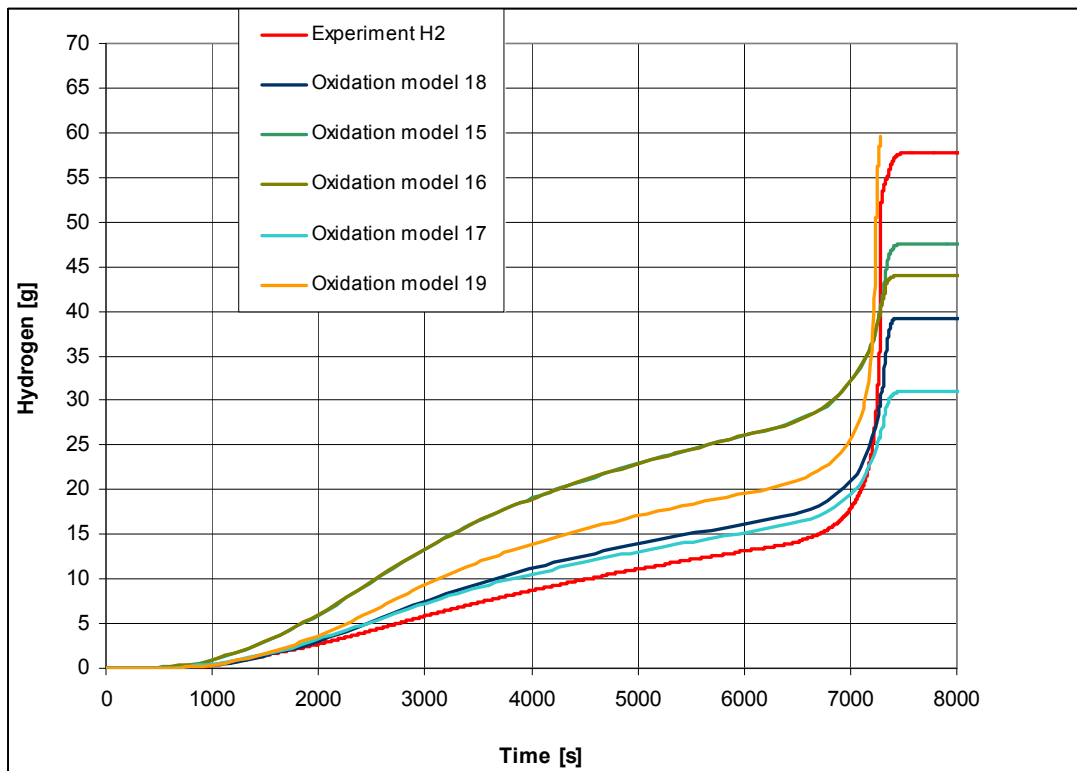
Figure A 5.4: Total hydrogen production: sensitivity analysis
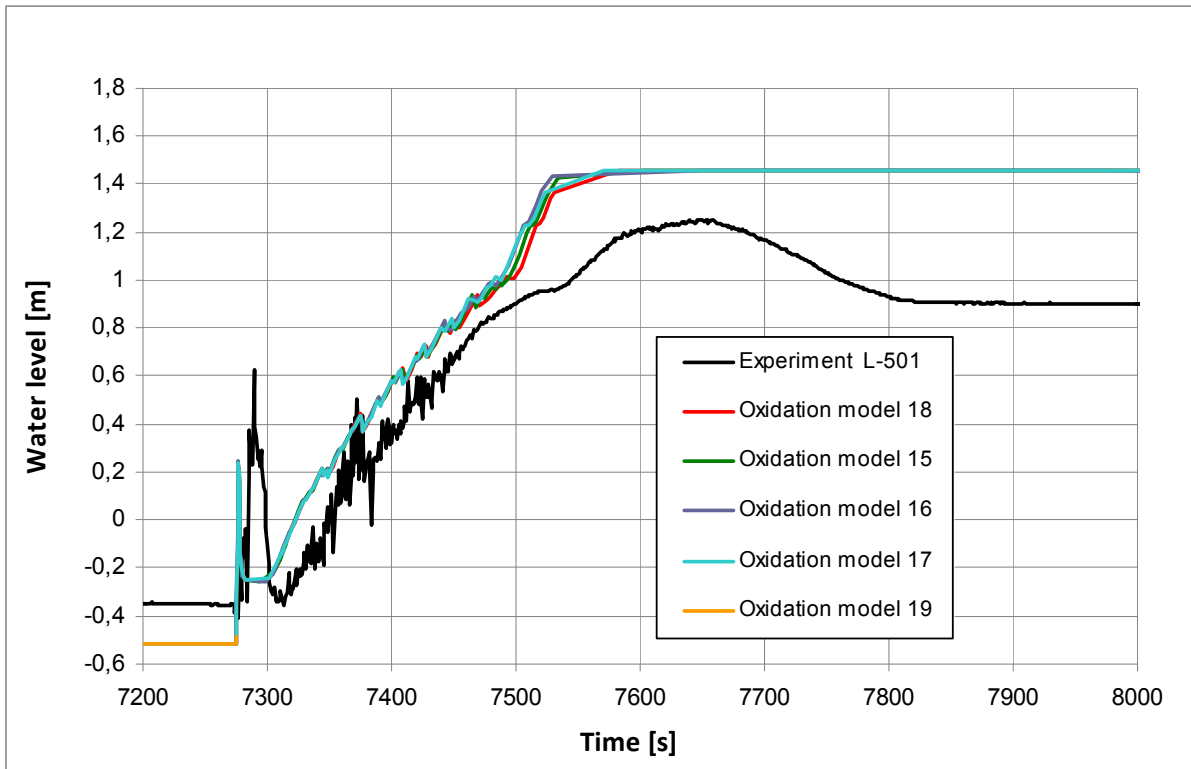
Figure A 5.5: Water level in the bundle: sensitivity analysis

A 6. Breakaway phenomena: oxide thickness threshold
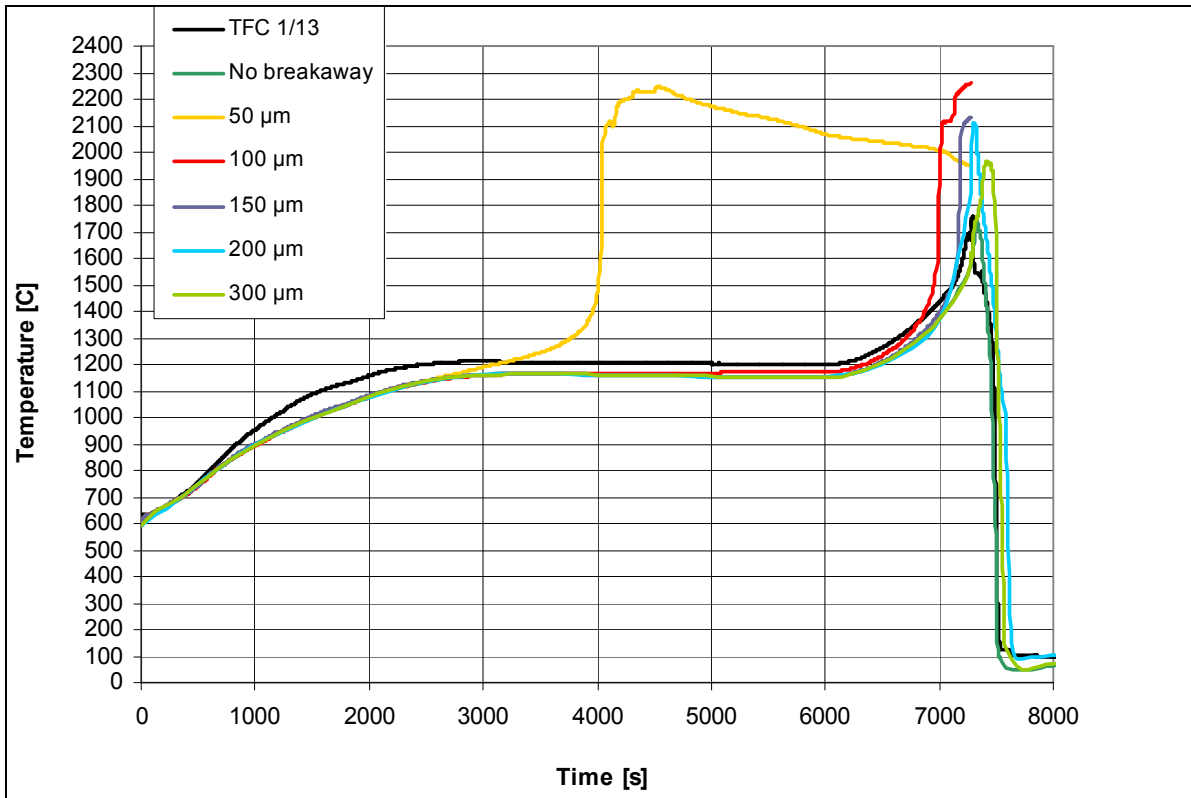
Figure A 6.1: Temperatures at the elevation 950 mm in the centre line of the central rod
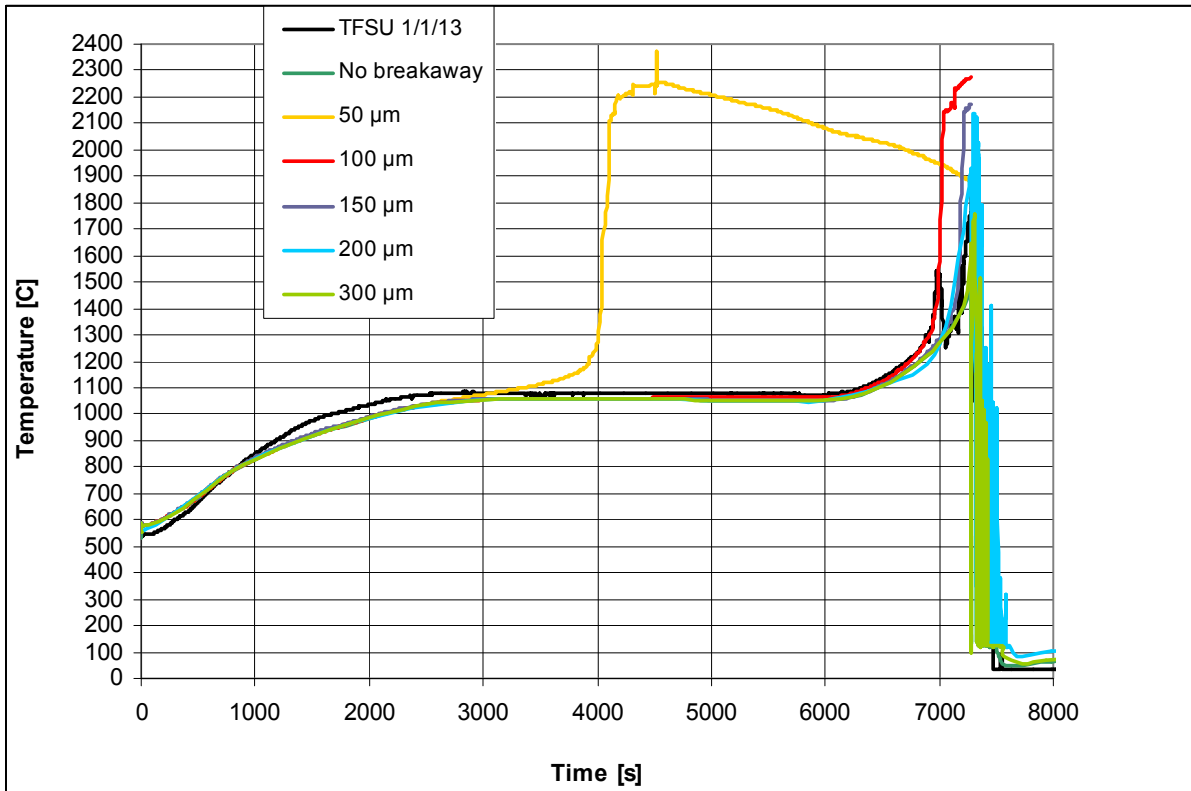
Figure A 6.2: Fluid temperatures at the elevation 950 mm in the bundle
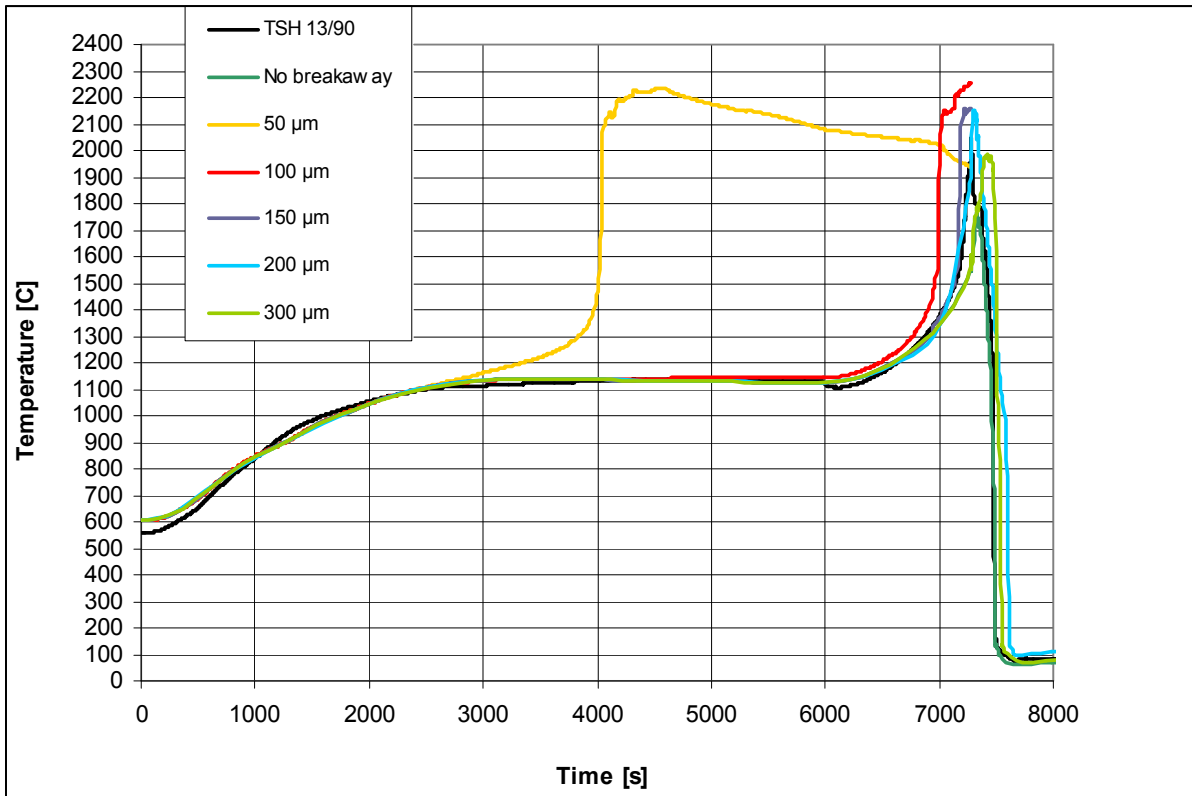
Figure A 6.3: Shroud temperature at the elevation 950 mm
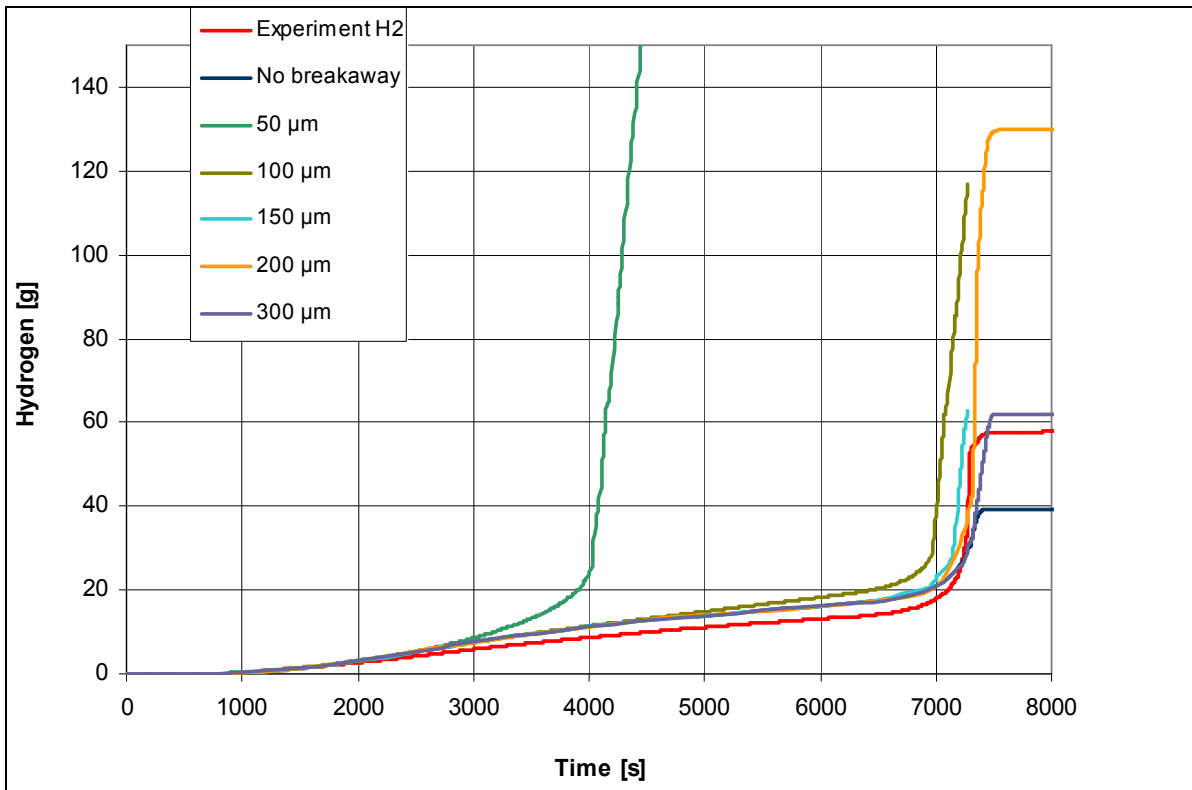
Figure A 6.4.1: Total hydrogen production: sensitivity analysis
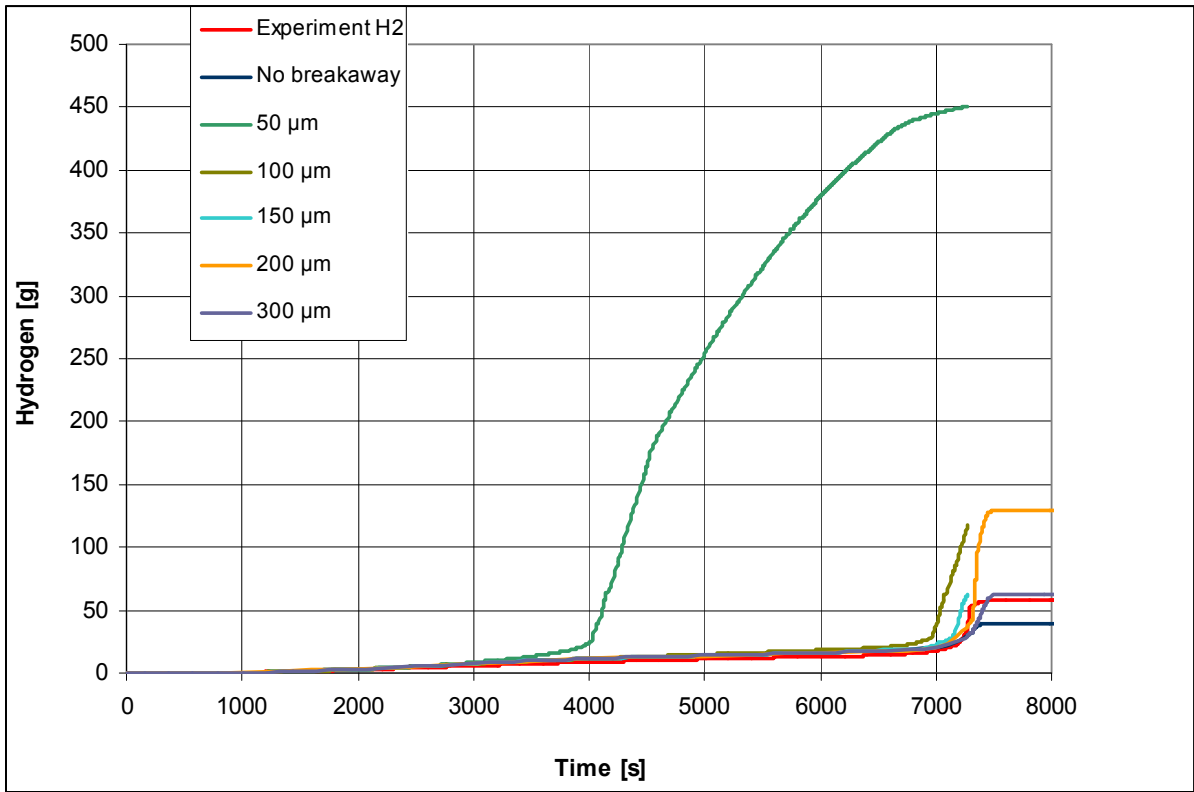
Figure A 6.4.2: Total hydrogen production: sensitivity analysis
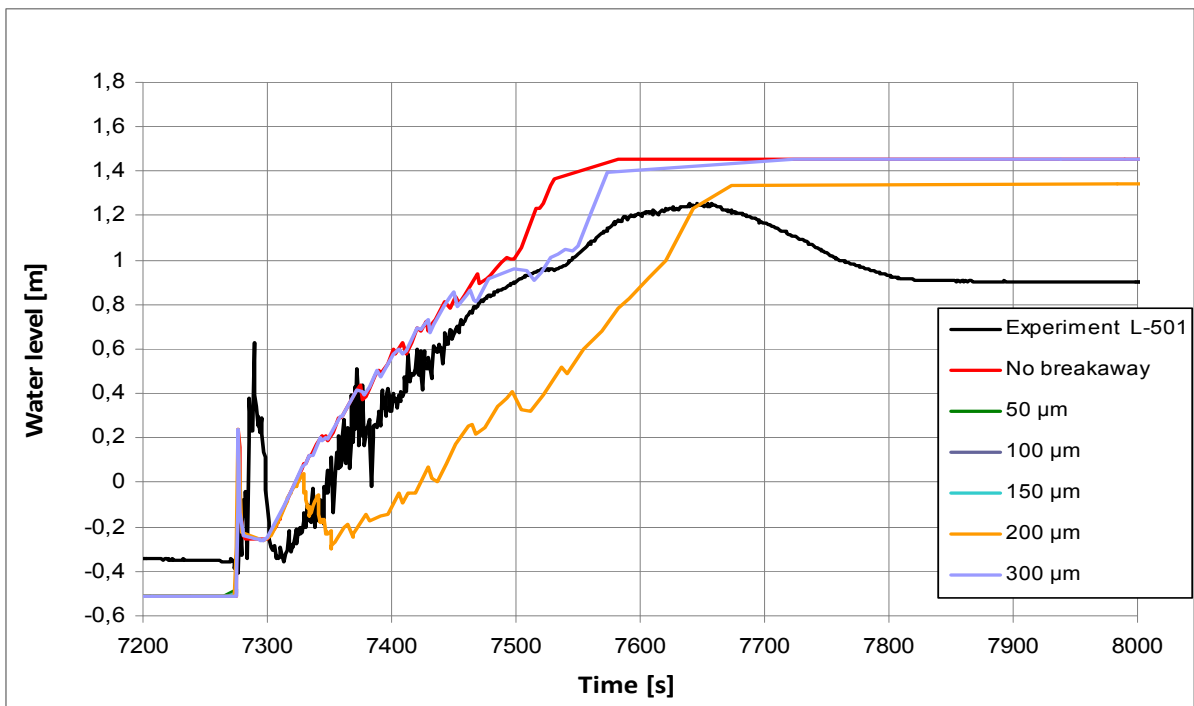
Figure A 6.5: Water level in the bundle: sensitivity analysis

A 7. Quench water temperature
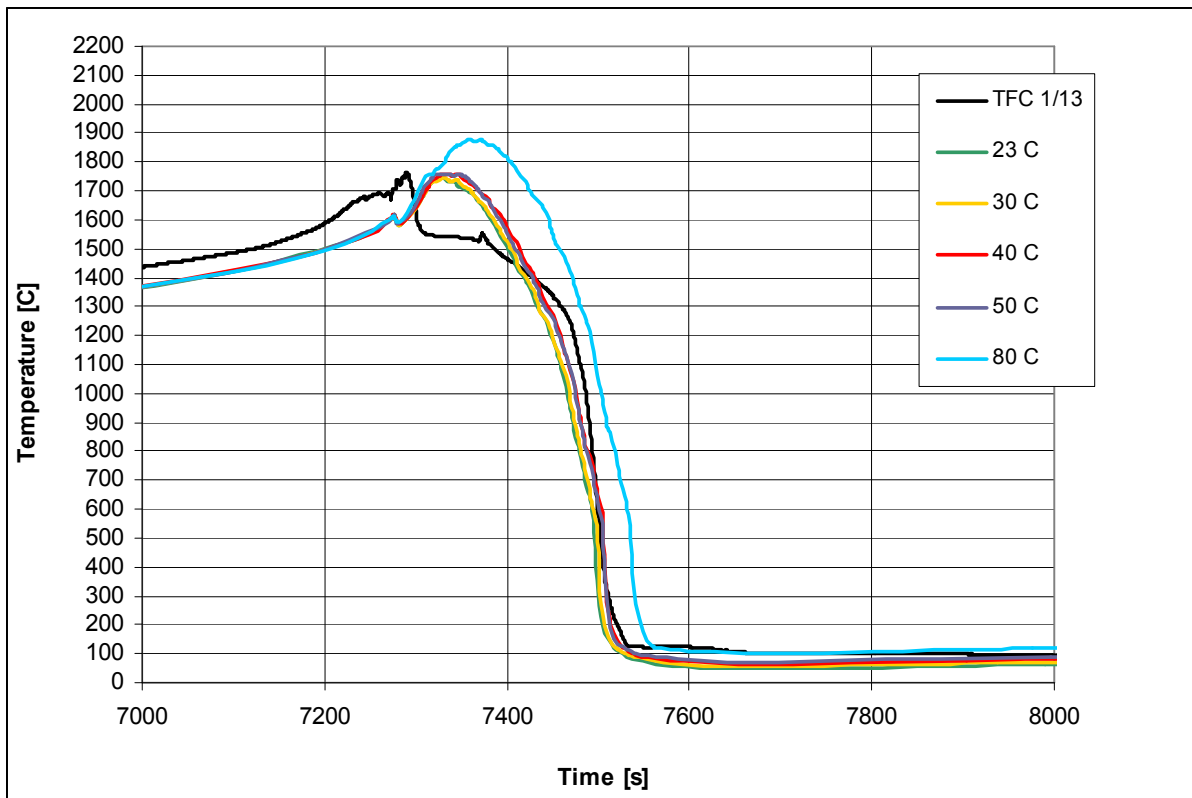
Figure A 7.1: Temperatures at the elevation 950 mm in the center line of the central rod
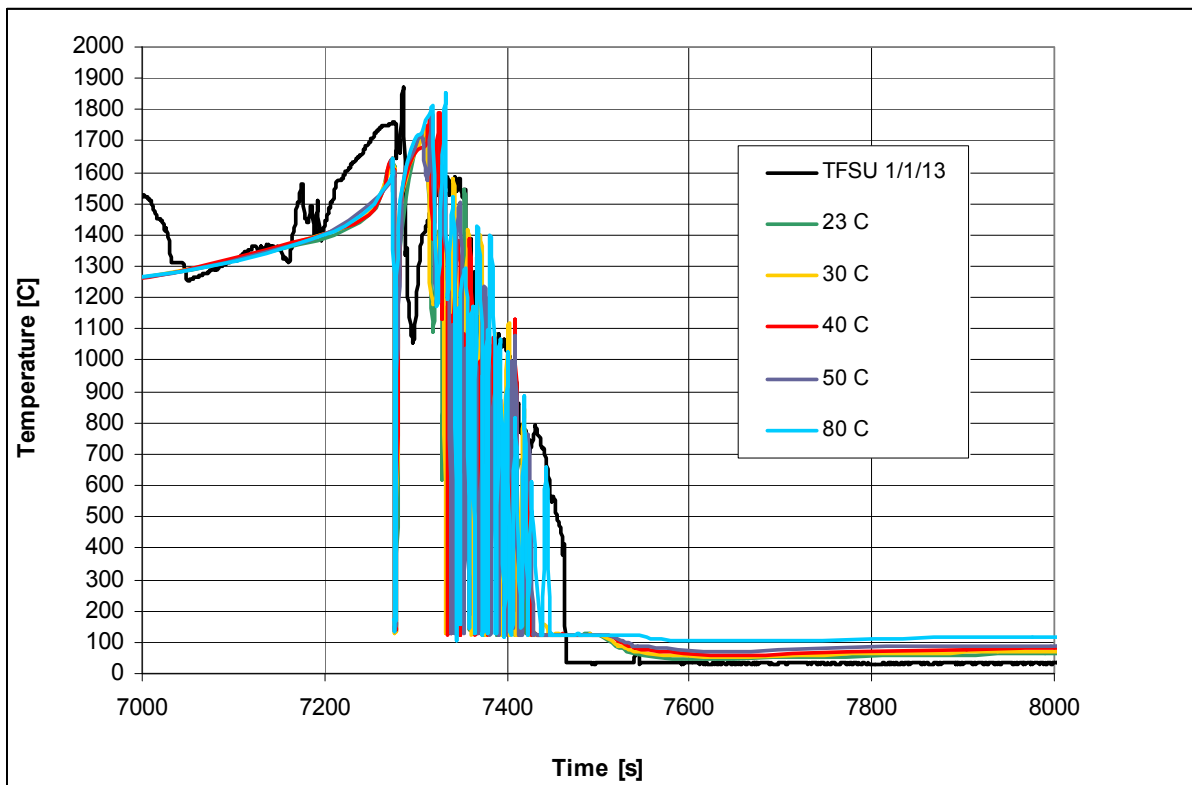
Figure A 7.2: Fluid temperatures at the elevation 950 mm in the bundle
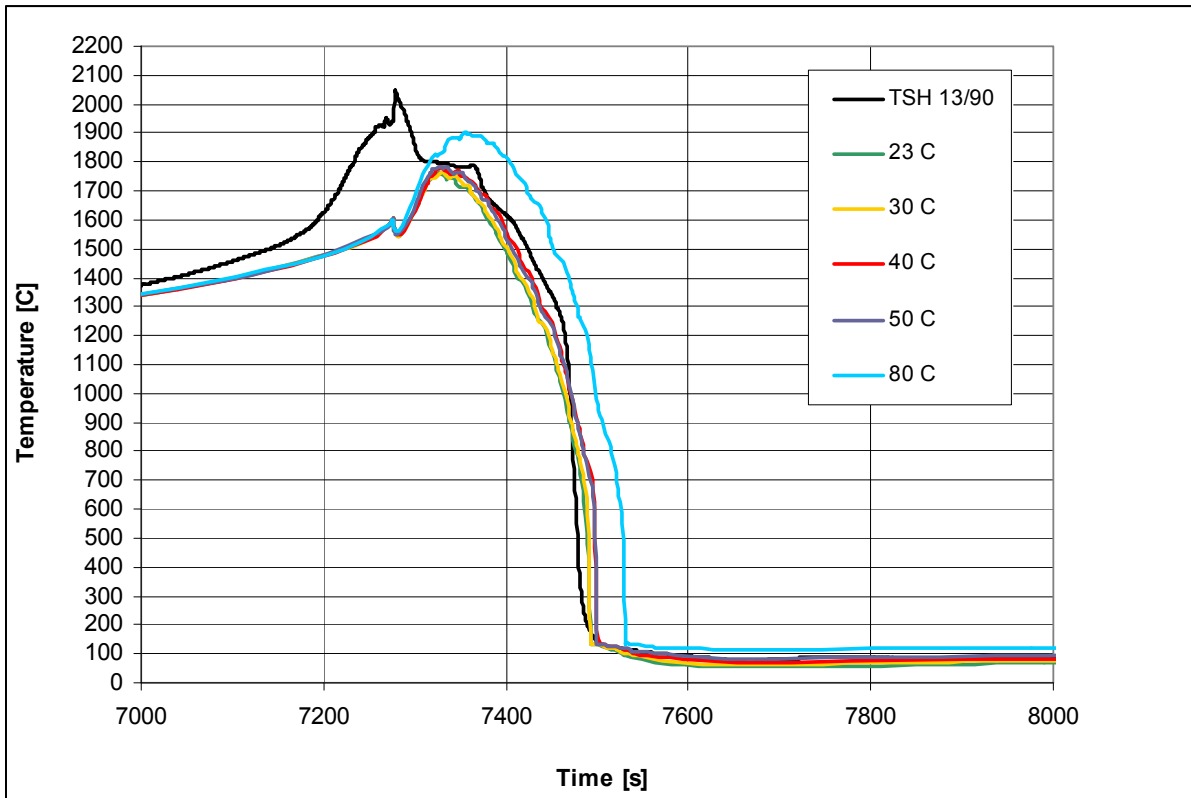
Figure A 7.3: Shroud temperature at the elevation 950 mm
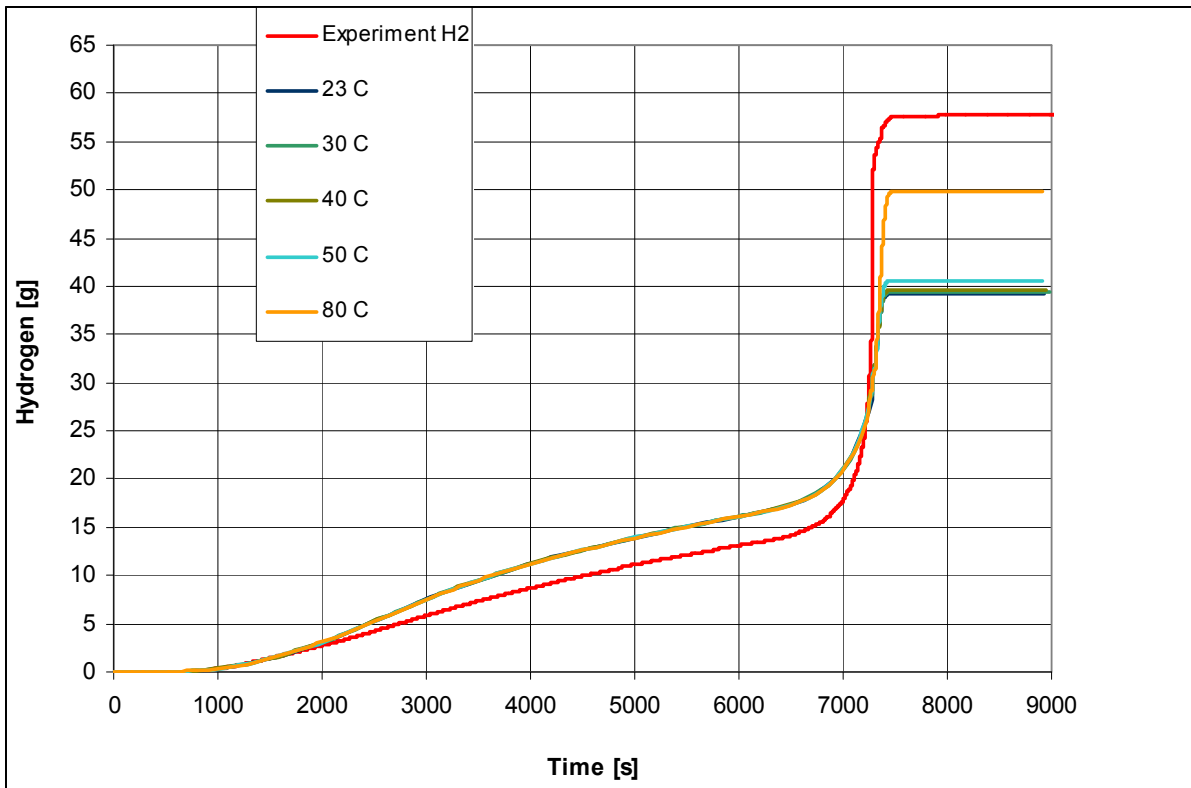
Figure A 7.4: Total hydrogen production: sensitivity analysis
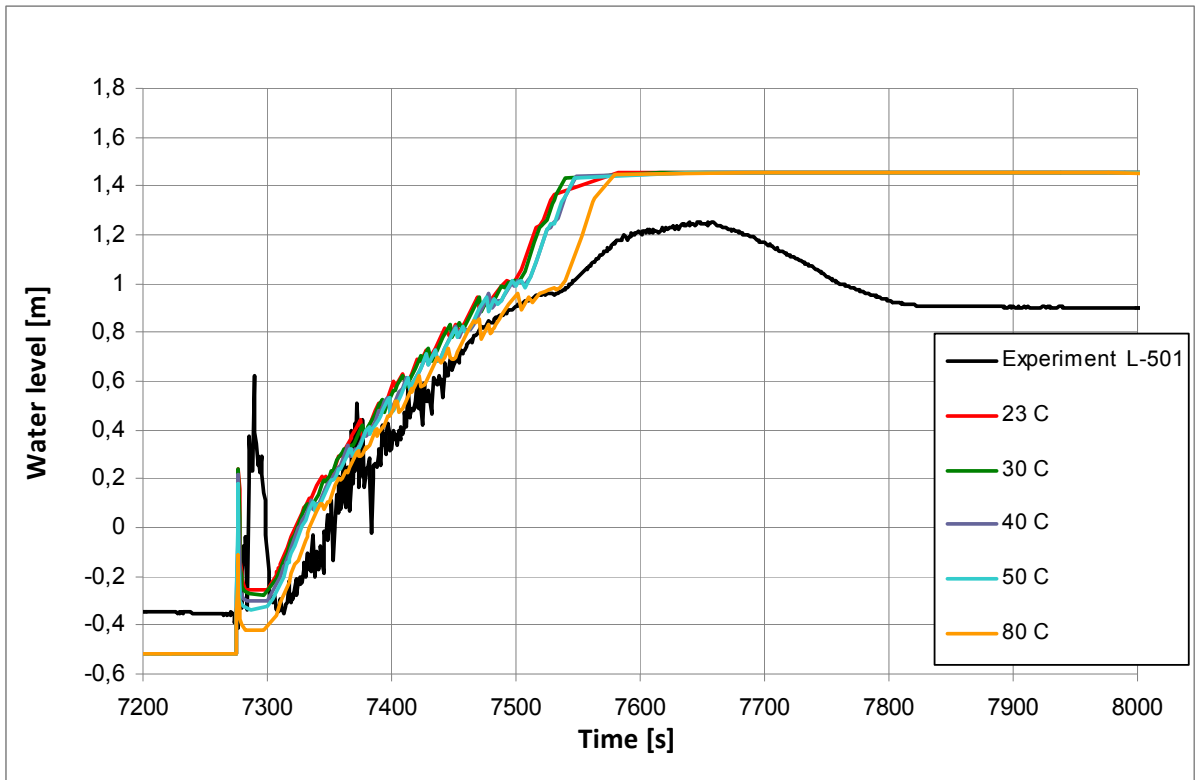
Figure A 7.5: Water level in the bundle: sensitivity analysis

A 8. Fast water injection flow rates
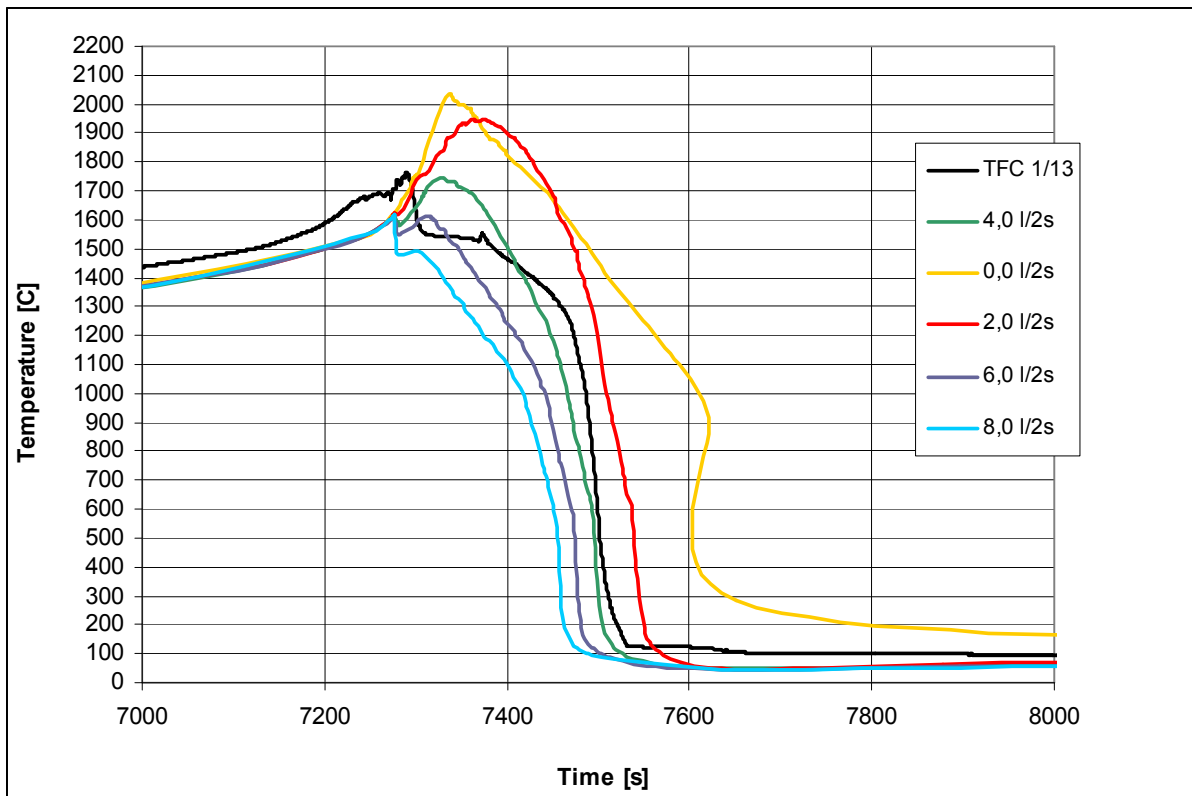
Figure A 8.1: Temperatures at the elevation 950 mm in the centre line of the central rod
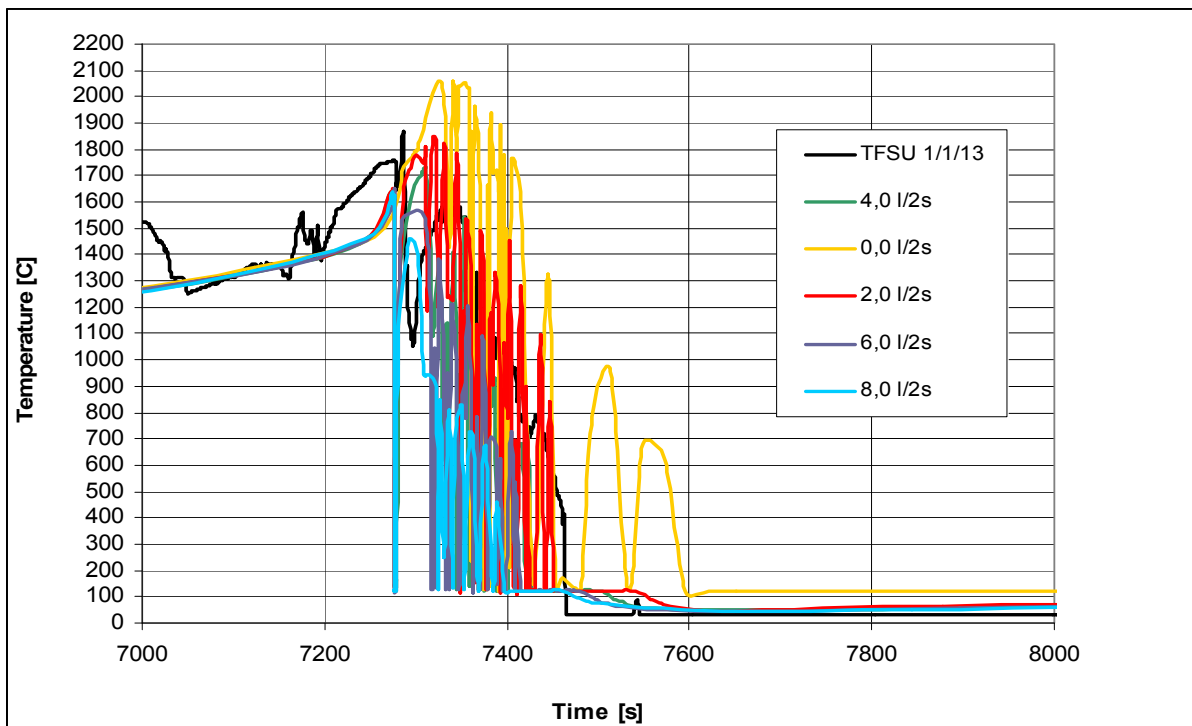
Figure A 8.2: Fluid temperatures at the elevation 950 mm in the bundle
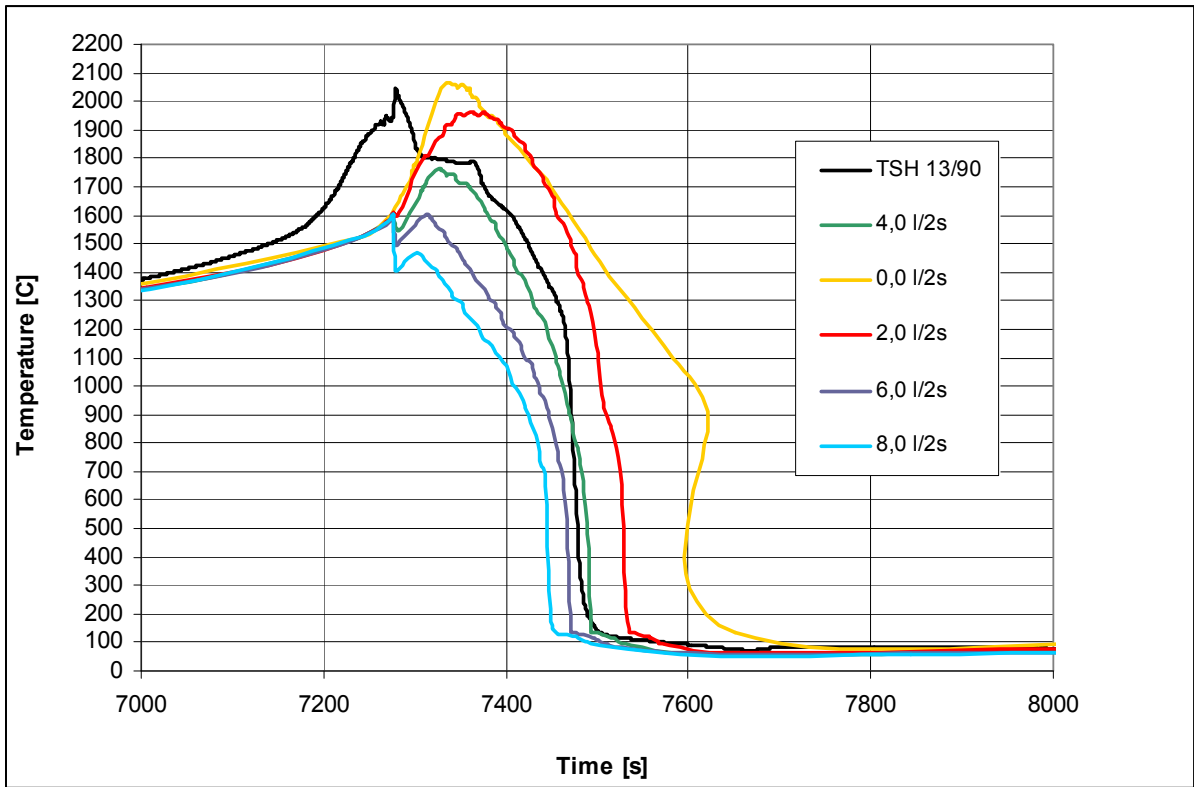
Figure A 8.3: Shroud temperature at the elevation 950 mm
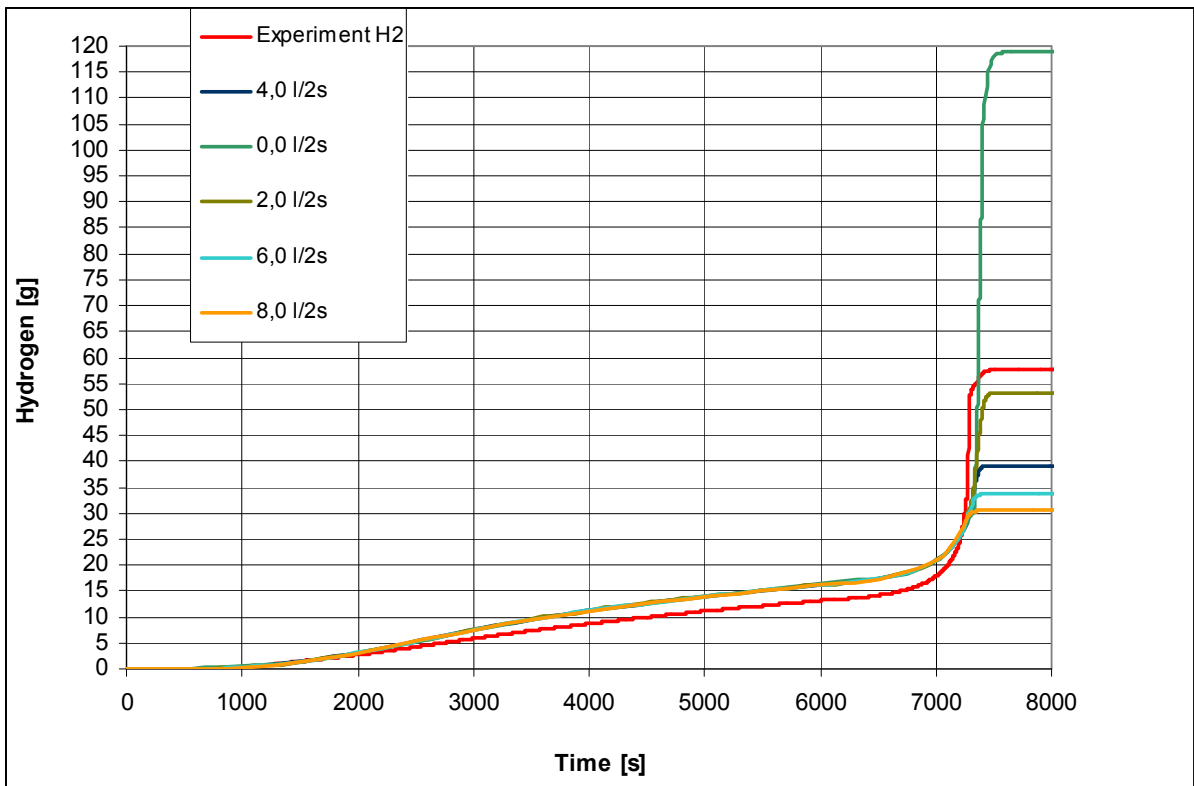
Figure A 8.4: Total hydrogen production: sensitivity analysis
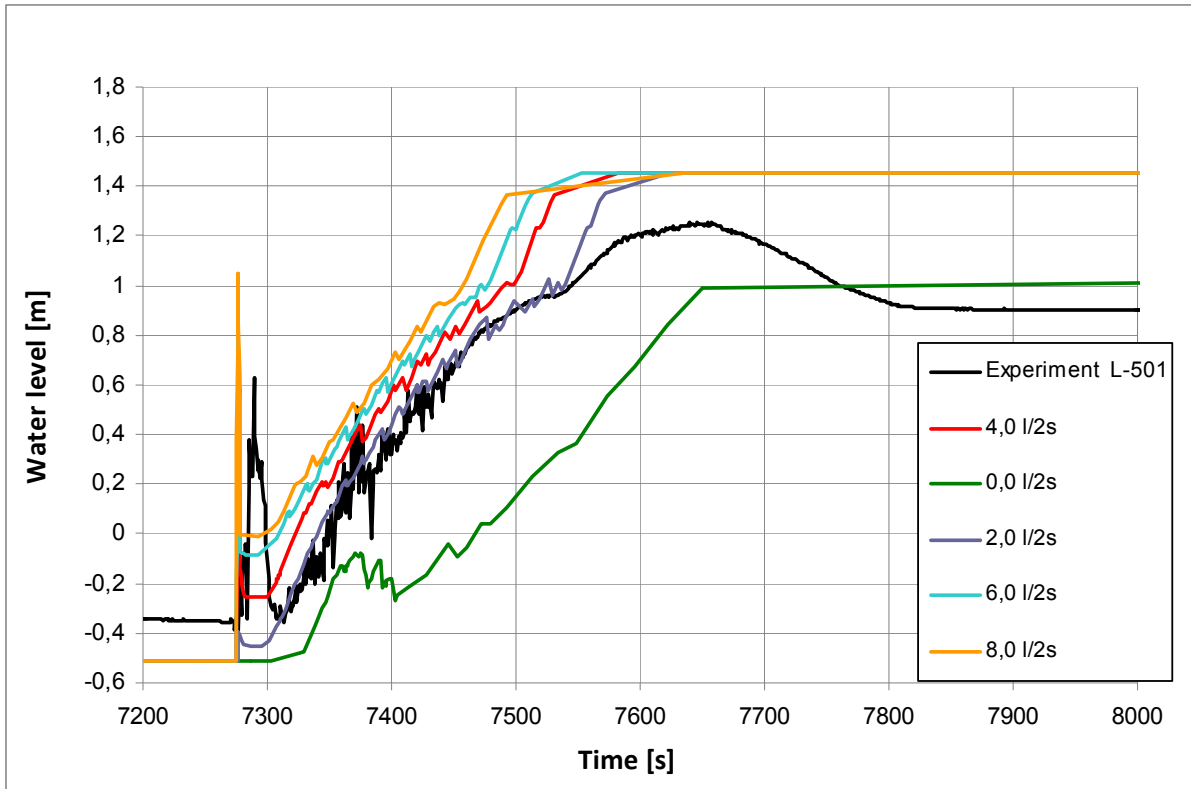
Figure A 8.5: Water level in the bundle: sensitivity analysis

A 9. Results with different nodalizations (variation of number of control volumes)
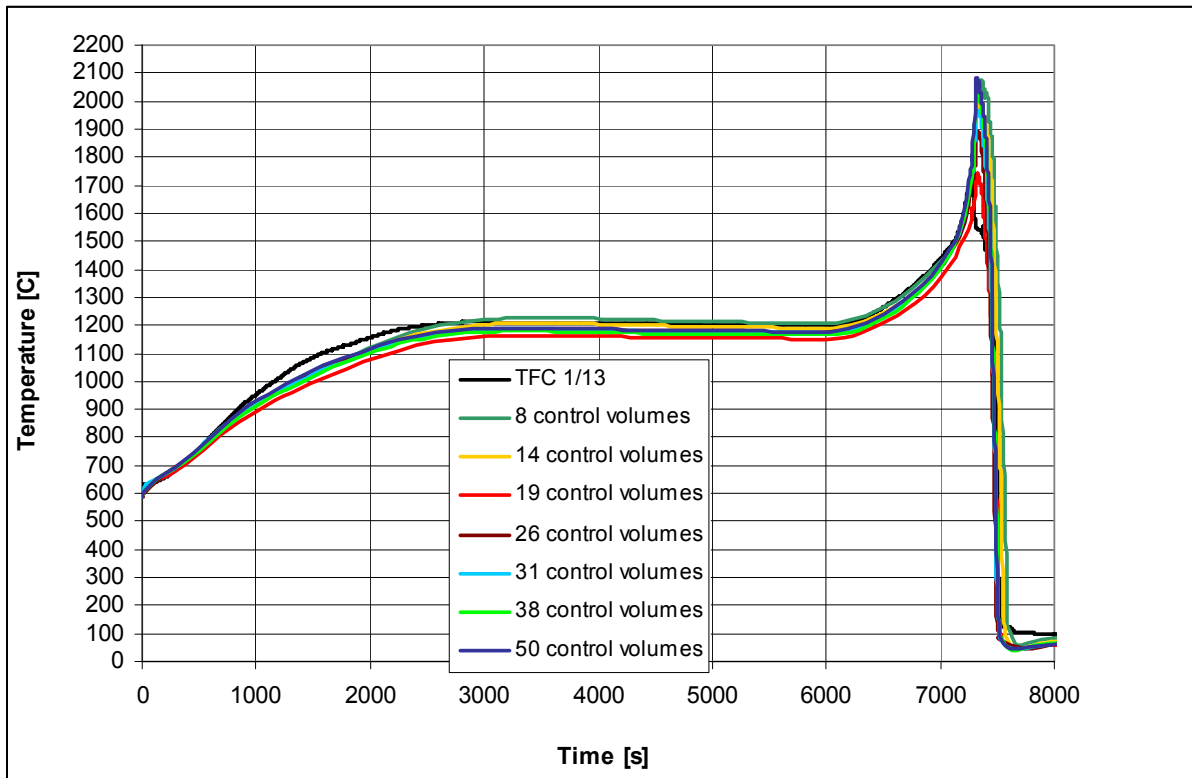
Figure A 9.1.1: Temperatures at the elevation 950 mm in the centre line of the central rod
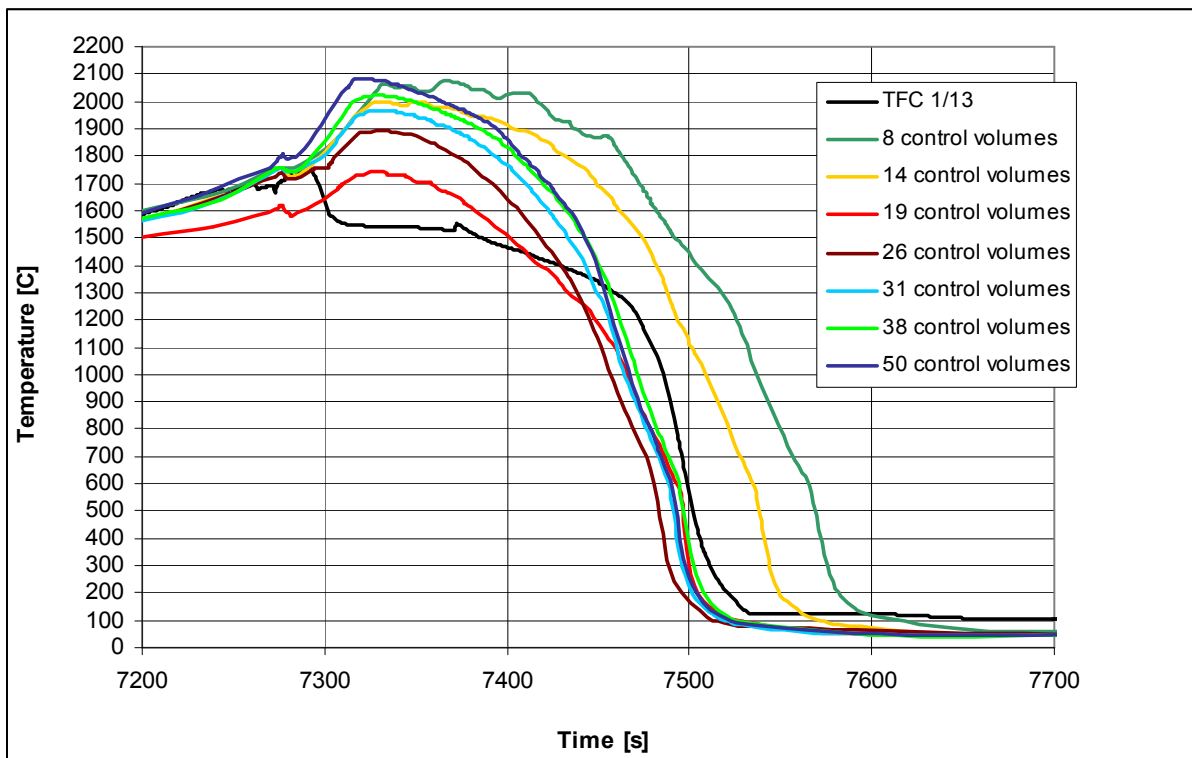
Figure A 9.1.2: Temperatures at the elevation 950 mm in the centre line of the central rod
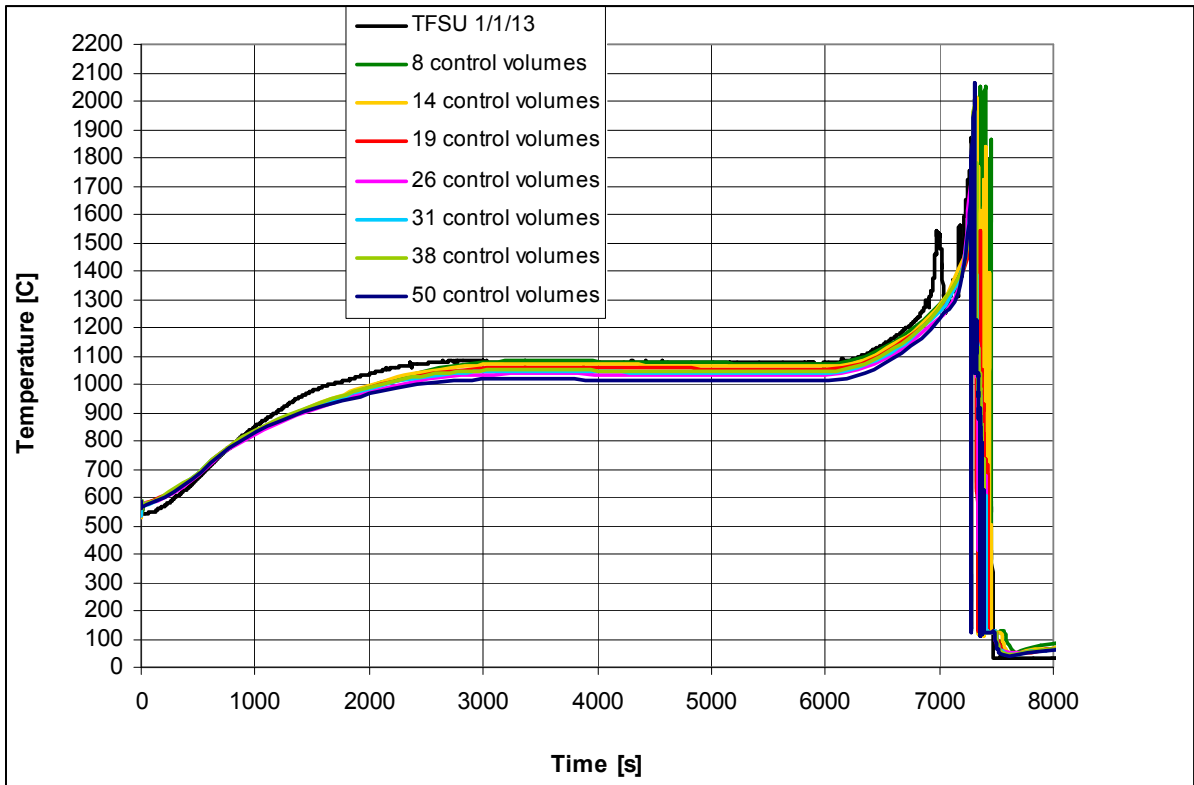
Figure A 9.2.1: Fluid temperatures at the elevation 950 mm in the bundle
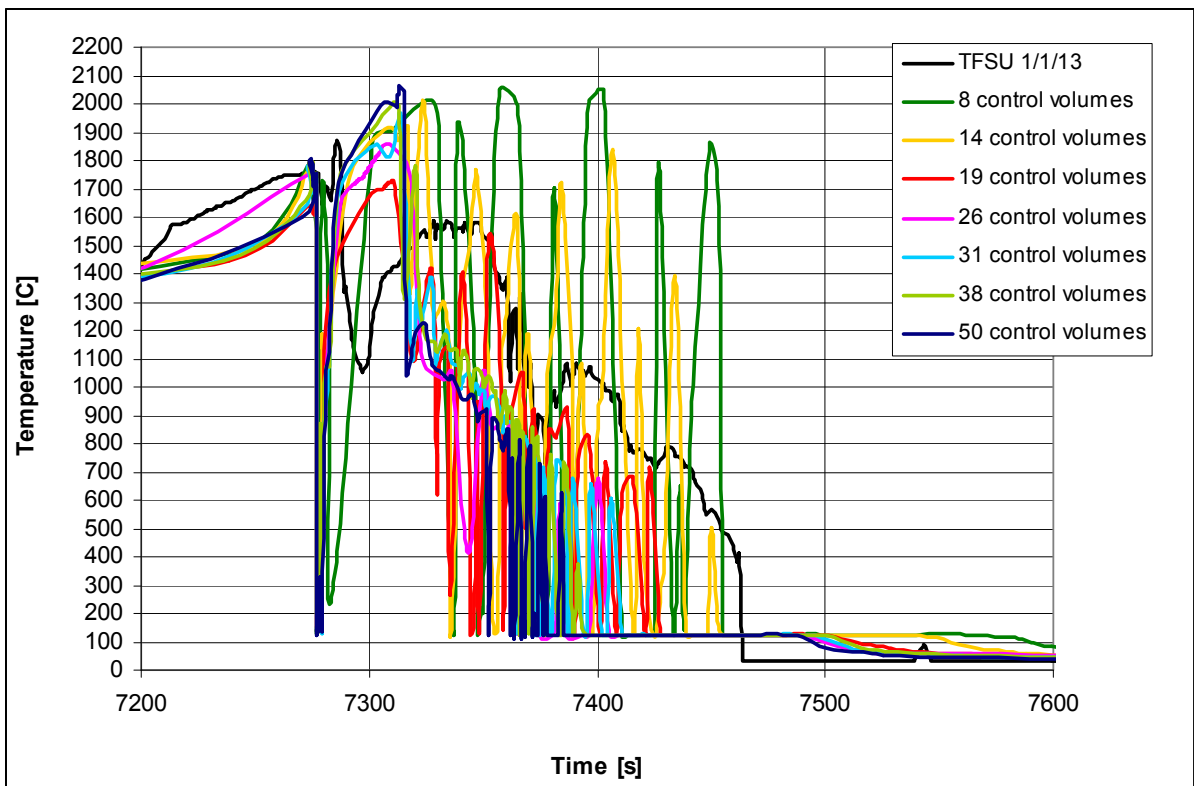
Figure A 9.2.2: Fluid temperatures at the elevation 950 mm in the bundle
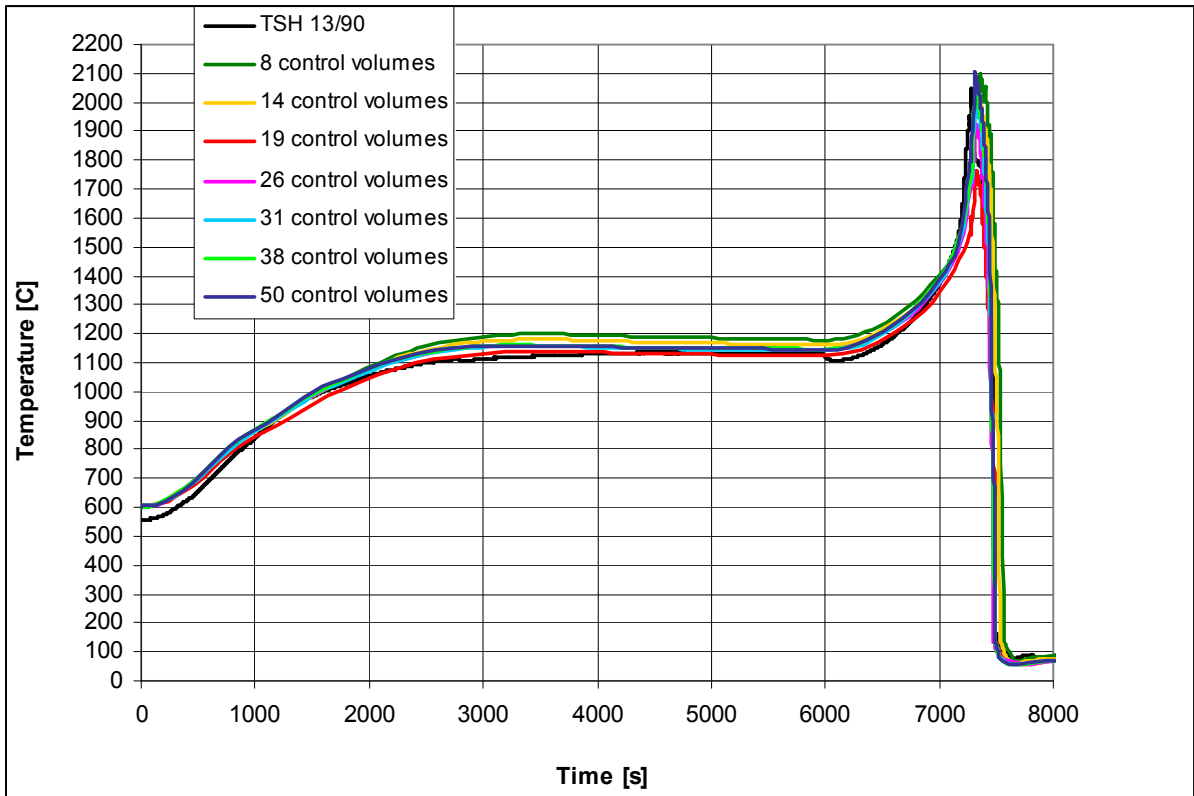
Figure A 9.3.1: Shroud temperature at the elevation 950 mm
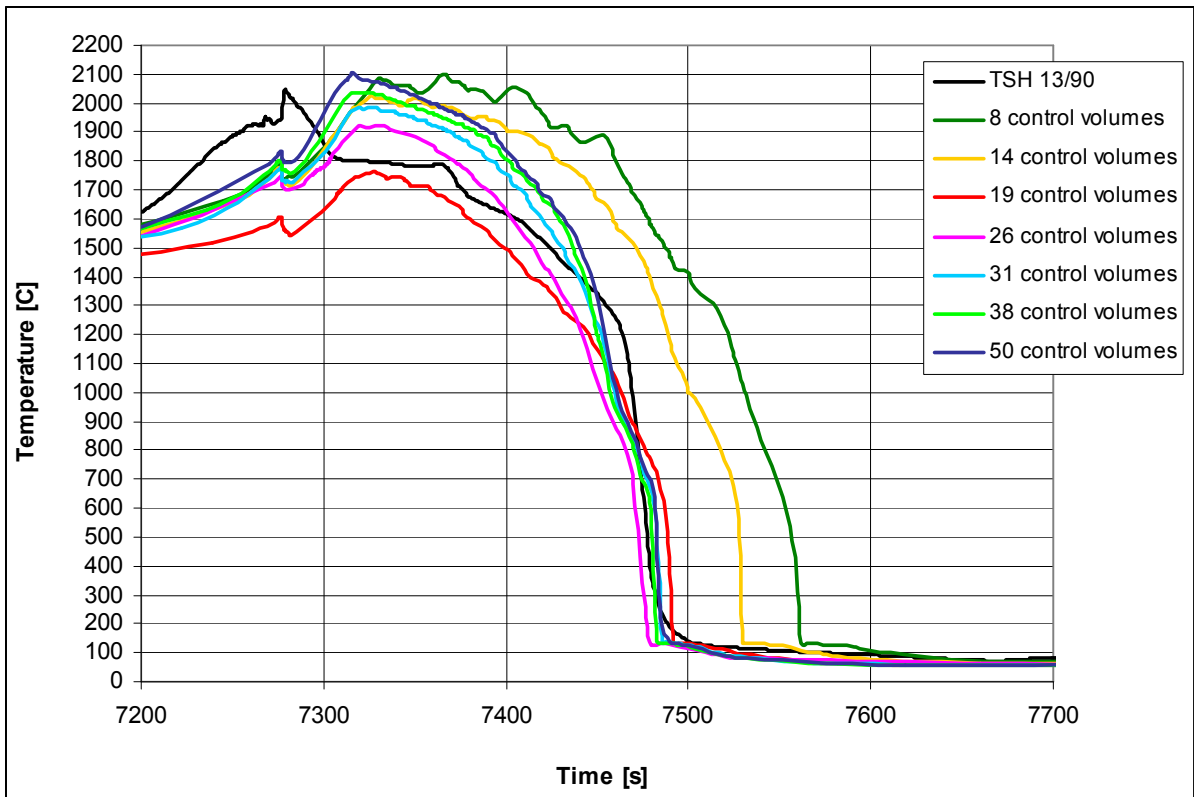
Figure A 9.3.2: Shroud temperature at the elevation 950 mm
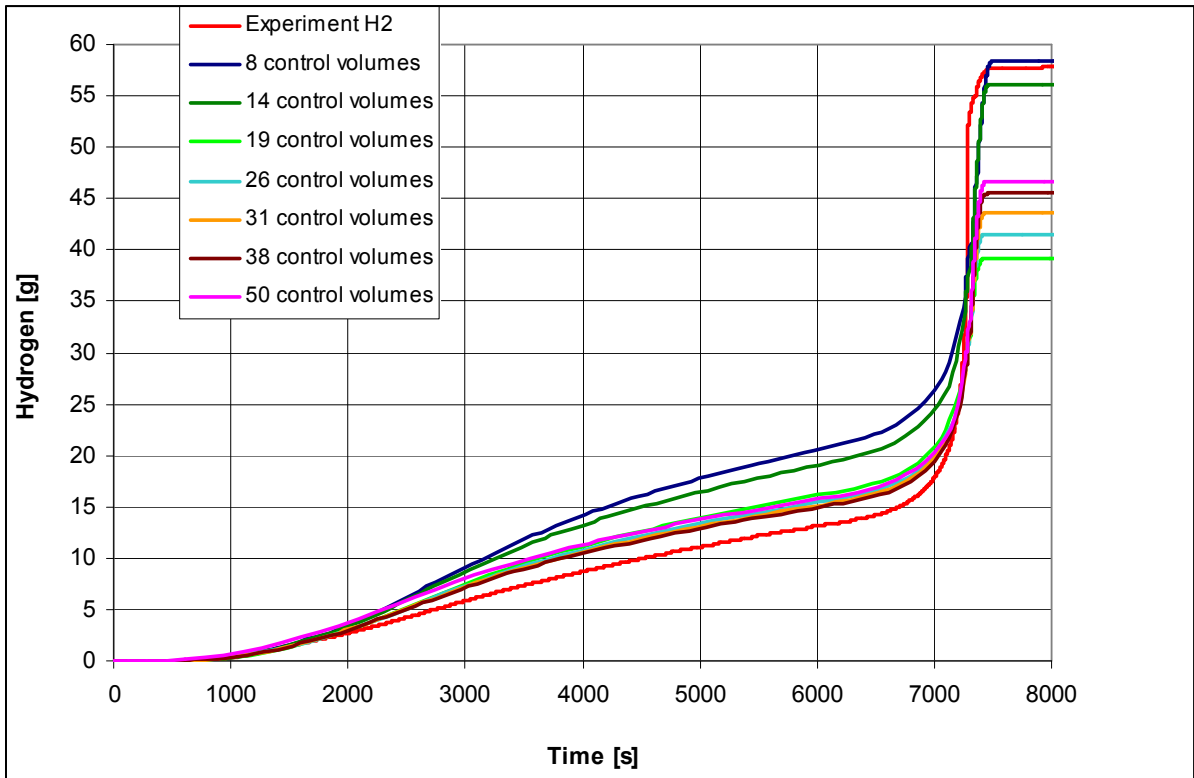
Figure A 9.4: Total hydrogen production: sensitivity analysis
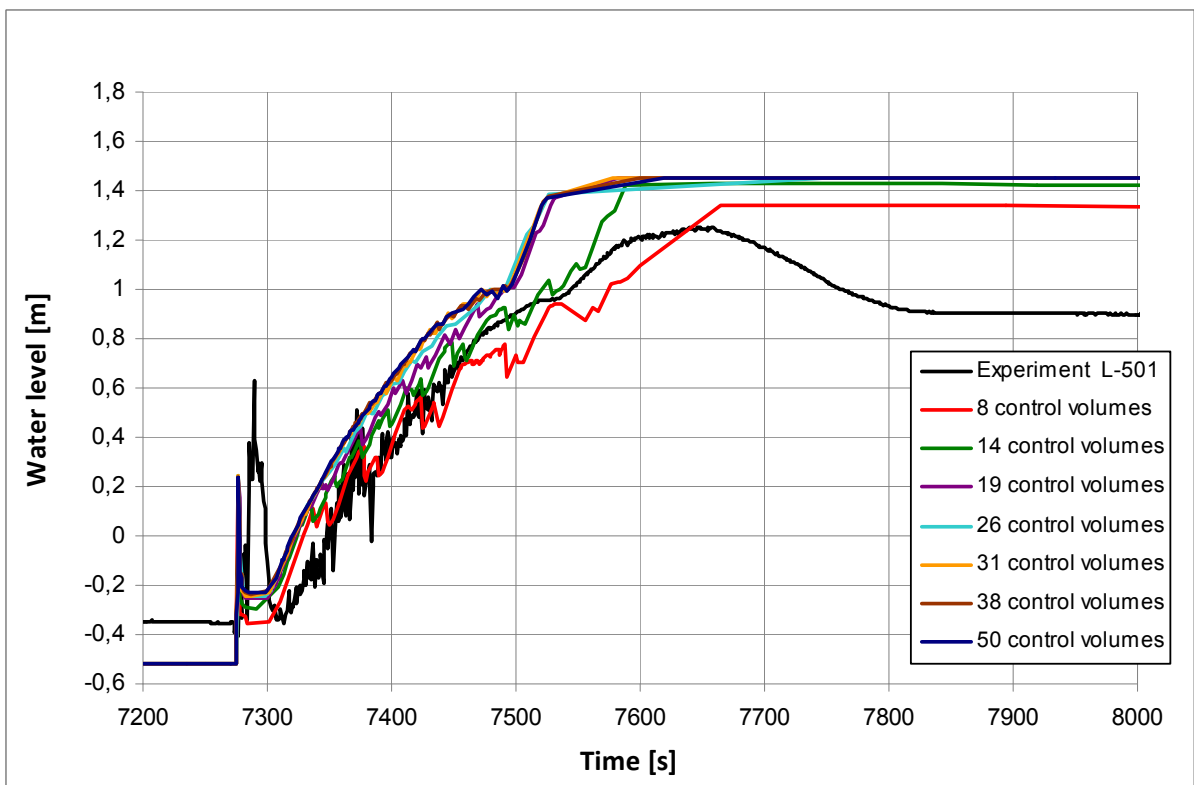
Figure A 9.5: Water level in the bundle: sensitivity analysis
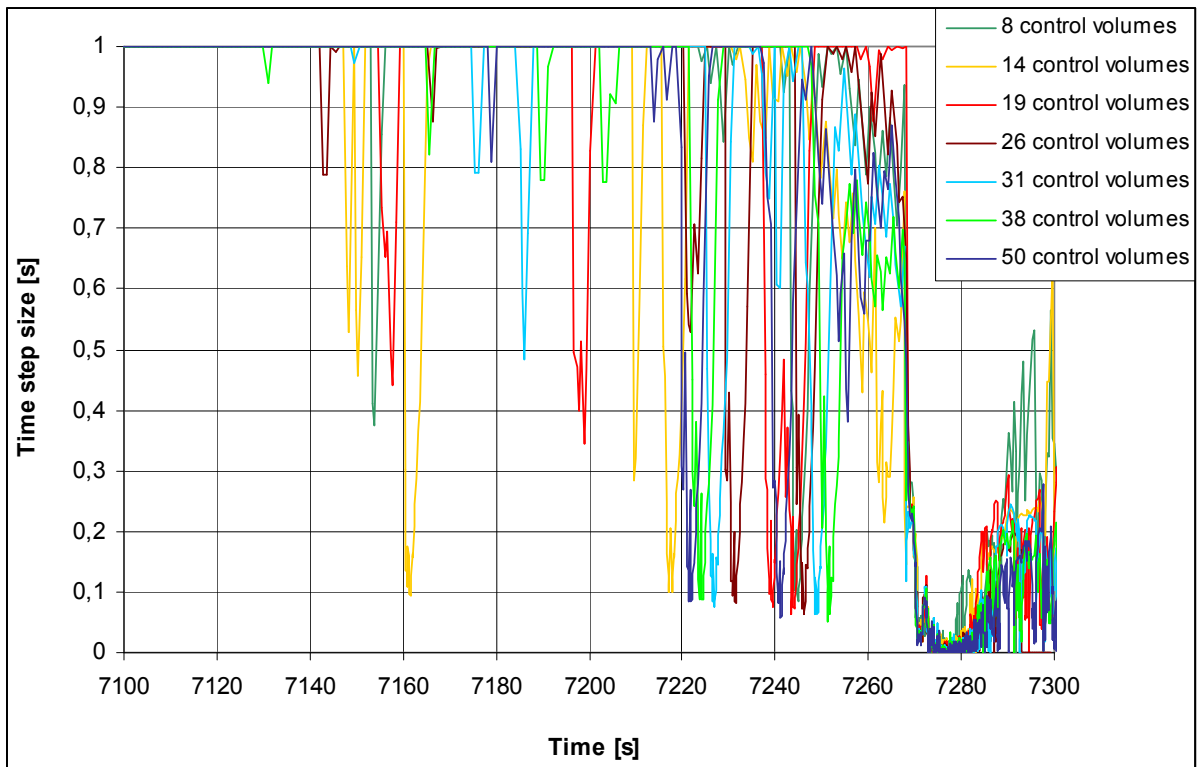
Figure A 9.6.1: Executed time step size in the transient phase
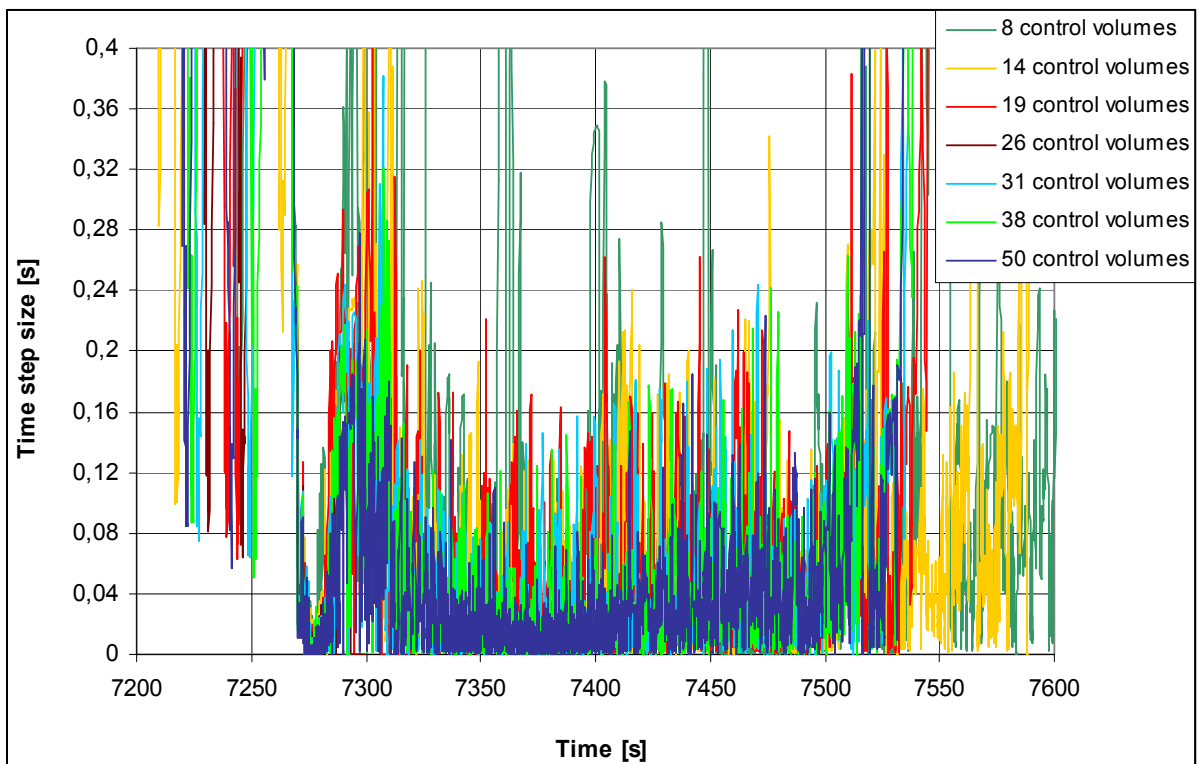
Figure A 9.6.2: Executed time step size in the quench phase
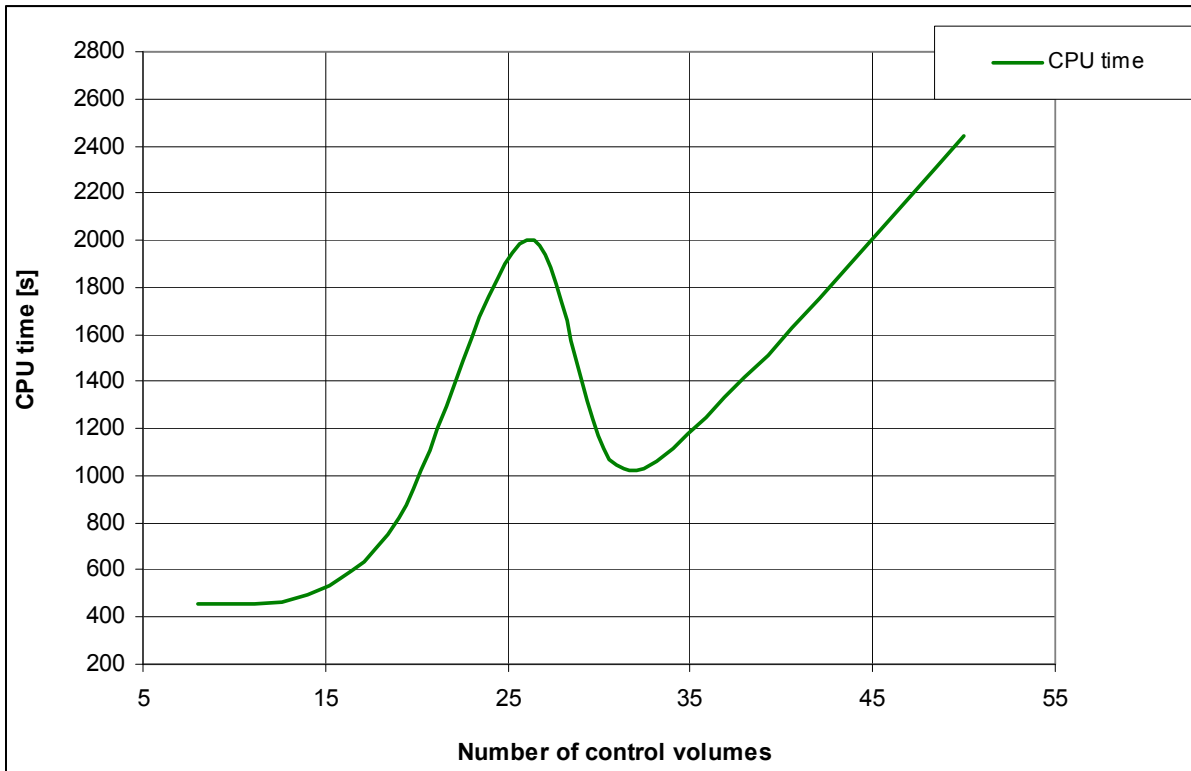
Figure A 9.7: CPU time as a function of the number of control volumes
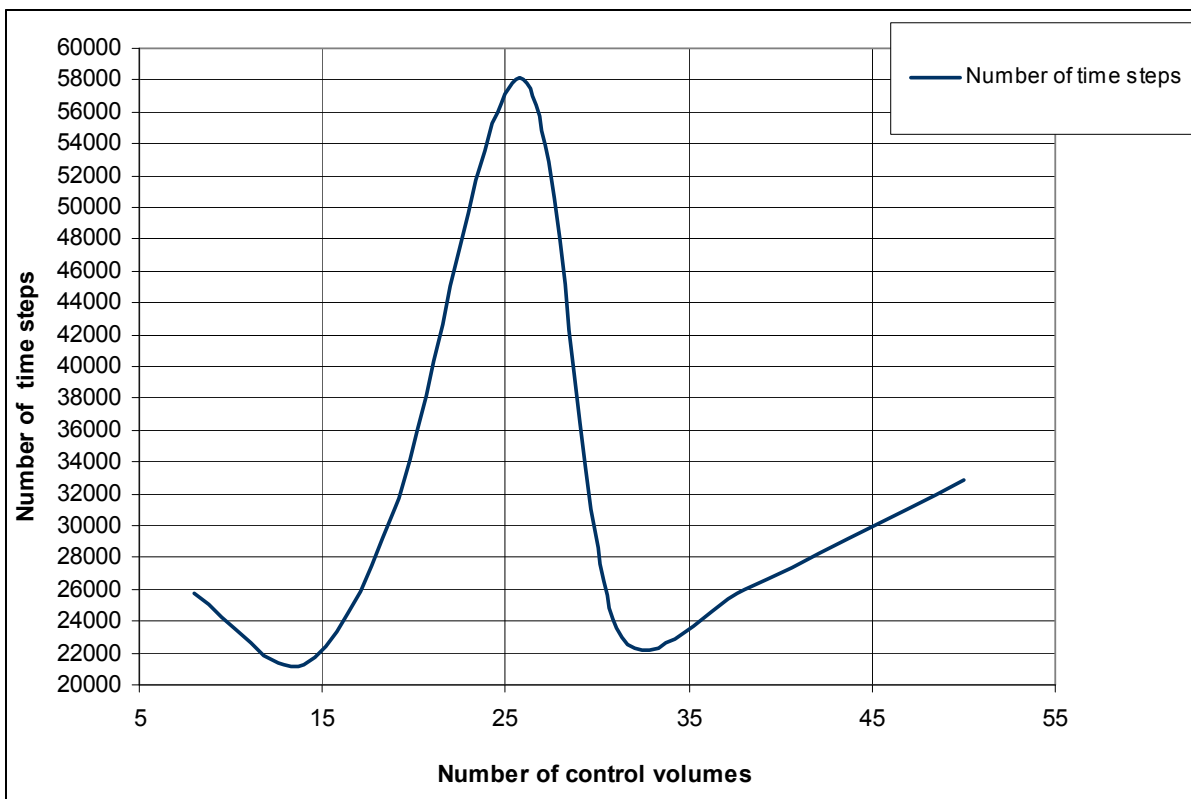
Figure A 9.8: Number of time step as a function of the number of control volumes

A post-test calculation of the QUENCH-12 experiment (reflood of a VVER test bundle), complemented by a sensitivity analysis, was performed with the system code ATHLET-CD2.2A. The calculated results showed a good overall agreement with the experimental results concerning the thermal-hydraulic behaviour of the test bundle. The performed simulations adequately reproduce temperature evolution at different elevations during the whole test with only small discrepancies.

Calculations show inadequate work of the code with respect to hydrogen production rate. The difference between experimental data and calculation results for the QUENCH-12 test is mainly due to breakaway oxidation of the bundle. Model for breakaway oxidation has not been yet fully developed in ATHLET-CD2.2A. Other reason for discrepancy in simulated hydrogen rate production is the fact that the hydrogen absorption by metal and its release actually cannot be simulated. The results of the simulations were affected also by the chosen nodalization schemes.

ISBN 978-3-86644-909-1